PHARMACOLOGICAL TARGETING OF GAIN-OF-FUNCTION KCNQ1 MUTATIONS PREDISPOSING TO ATRIAL FIBRILLATION

By

Courtney Michelle Campbell

Dissertation

Submitted to the Faculty of the

Graduate School of Vanderbilt University

in partial fulfillment of the requirements

for the degree of

DOCTOR OF PHILOSOPHY

in

Pharmacology

August, 2013

Nashville, Tennessee

Approved:

Dan M. Roden

Katherine T. Murray

L. Jackson Roberts

Chee Lim

Alfred L. George, Jr.

To my grandmother, Rosamond Maxine Hockett

ACKNOWLEDGEMENTS

This work would not have been possible without the financial support of the Greater Southeast Affiliate Predoctoral Fellowship 11PRE7610043 from the American Heart Association, Ruth L. Kirschstein National Research Service Award for Individual Predoctoral MD/PhD Fellows F30 HL107066 from the National Heart Lung and Blood Institute (NHLBI), Public Health Service Award T32 GM07347 from National Institute for General Medical Studies for the Vanderbilt Medical-Scientist Training Program, Cooperative Research Center grant U19-HL65962-10 from NHLBI, and a Vanderbilt University Graduate School Dissertation Enhancement Grant.

I am incredibly grateful to have had the opportunity to complete my dissertation under the direction of Dr. Al George. His mentorship over my project provided an excellent balance of both freedom to explore, as well as directed guidance when needed. He provided an outstanding model for how to communicate science skillfully, to assemble a supportive productive laboratory team, to develop collaborations, and to navigate a physician-scientist career. I appreciate that this relationship and his guidance will carry forward, as I continue on my own career path.

My colleagues in the George lab made completing my dissertation a fun, enjoyable experience. Their expertise, experimental skill, and willingness to troubleshoot any issue was critical to my success and development as a

scientist. Particularly, I would like to thank Dr. Carlos Vanoye, Dr. Chris Thompson, Dr. Christine Simmons, Rick Welch, and Jennifer Kunic.

Each member of my dissertation committee, Dr. Dan Roden, Dr. Chee Lim, Dr. Kathy Murray, and Dr. Jack Roberts, provided insight and guidance not only in our formal meetings, but whenever an issue or question arose. I am thankful for their continued support as my project developed.

The Vanderbilt Medical Scientist Training Program has been an incredible program and home to me over the course of my training. The leadership of Dr. Terry Dermody is unmatched as he continues to foster a dynamic, supportive, and engaging environment. The camaraderie within this program that is filled with such intelligent, passionate colleagues truly makes the Vanderbilt MSTP journey unique. I am indebted for the opportunity to be a part of this program.

Finally, I want to thank my family for their endless support as I pursue my career goals on this exciting, winding physician-scientist career path.

TABLE OF CONTENTS

Page

LIST OF TABLES

LIST OF FIGURES

CHAPTER I

INTRODUCTION

Atrial fibrillation is the most common sustained cardiac arrhythmia in adults with a rising incidence, and it is associated with significant increase in thromboembolic stroke risk and premature death.[1] Identification of the first causative familial AF mutation (S140G) in the potassium channel gene KCNQ1[2] has shed some light on the molecular etiology of AF, and provides an avenue for exploring AF mechanisms and therapeutic opportunities. This chapter provides an overview of KCNQ1 biophysical properties, KCNQ1 function in cardiac physiology, gain-of-function KCNQ1 mutations, and atrial fibrillation (AF).

Biophysical properties of KCNQ1

Voltage gated potassium (Kv) channels are transmembrane proteins that respond to alterations in membrane potential with conformational changes that allow potassium ions to move down their electrochemical gradient. The pore-forming (α) subunit is the minimal functional unit of a Kv channel. Each six transmembrane domain α-subunit monomer has an intracellular N-terminus, four transmembrane segments (S1-S4) with S4 as the primary voltage-sensing domain, then a pore domain consisting of two transmembrane segments (S5 and S6) linked by the pore-loop, and a long intracellular C-terminus. Fully assembled channels are formed by homo- or heterotetramers of these α-subunits. α-

subunits are grouped into 12 subfamilies (Kv1-12) each with unique characteristics.

The Kv7 family channels are responsible for neuronal and muscular membrane excitability, and salt and water homeostasis. There are five members of this family, KCNQ1-5. KCNQ2-5 are primarily found in the central nervous system. KCNQ1, our focus, is expressed throughout the body in excitable and epithelial tissues, and is notably absent from the CNS. KCNQ1 is the only Kv7 member that assembles only into homo-tetrameters. Expressed alone, KCNQ1 produces a rapidly activating outward current with increasing current density in response to depolarizing voltage steps (Figure 1). When the membrane is repolarized to -30 mV, KCNQ1 partially inactivates and its recovery forms a hook in the tail current reflecting recovery from the inactivated state before deactivation takes place. At -80 mV, the channel fully deactivates.

With functions in both excitable and non-excitable tissues, the KCNQ1 activity is diversified extensively through its interactions with auxiliary subunits and other factors. One class of auxiliary subunits is the single transmembrane domain KCNE family (1-5). The KCNEs are promiscuous, interacting with many Kv channels, and are differentially expressed in human tissue (Figure 2).[3, 4] When expressed alone, the KCNEs do not generate any current. Yet when co-expressed with KCNQ1, each KCNE differentially modulates the channel current (Figure 3). KCNE1 increases current amplitude, slows activation and

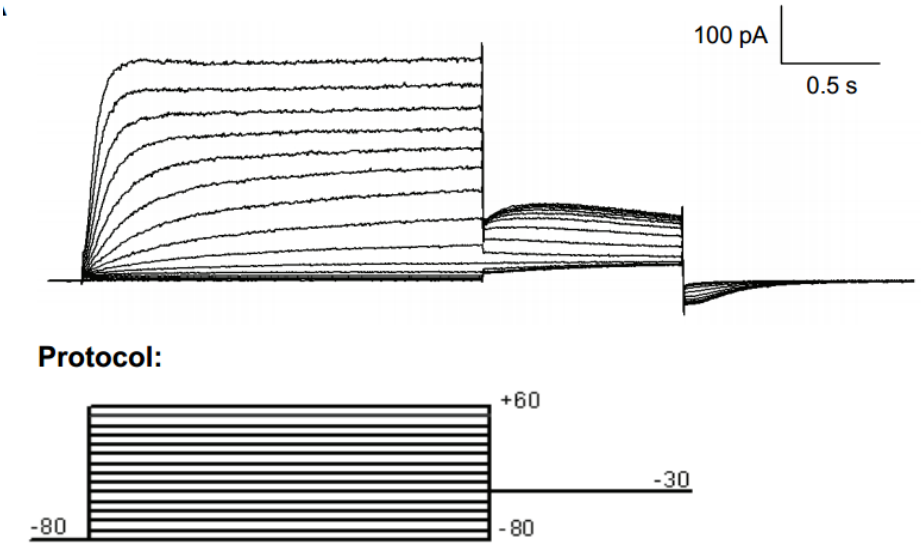

Figure 1. Biophysical properties of KCNQ1 current. Representative whole-cell currents elicited in CHO cells transiently transfected with KCNQ1 upon applying series of test potentials as illustrated in voltage-clamp protocols (membrane voltage indicated in mV). Modified from Ciampa, EJ, 2011.[5]

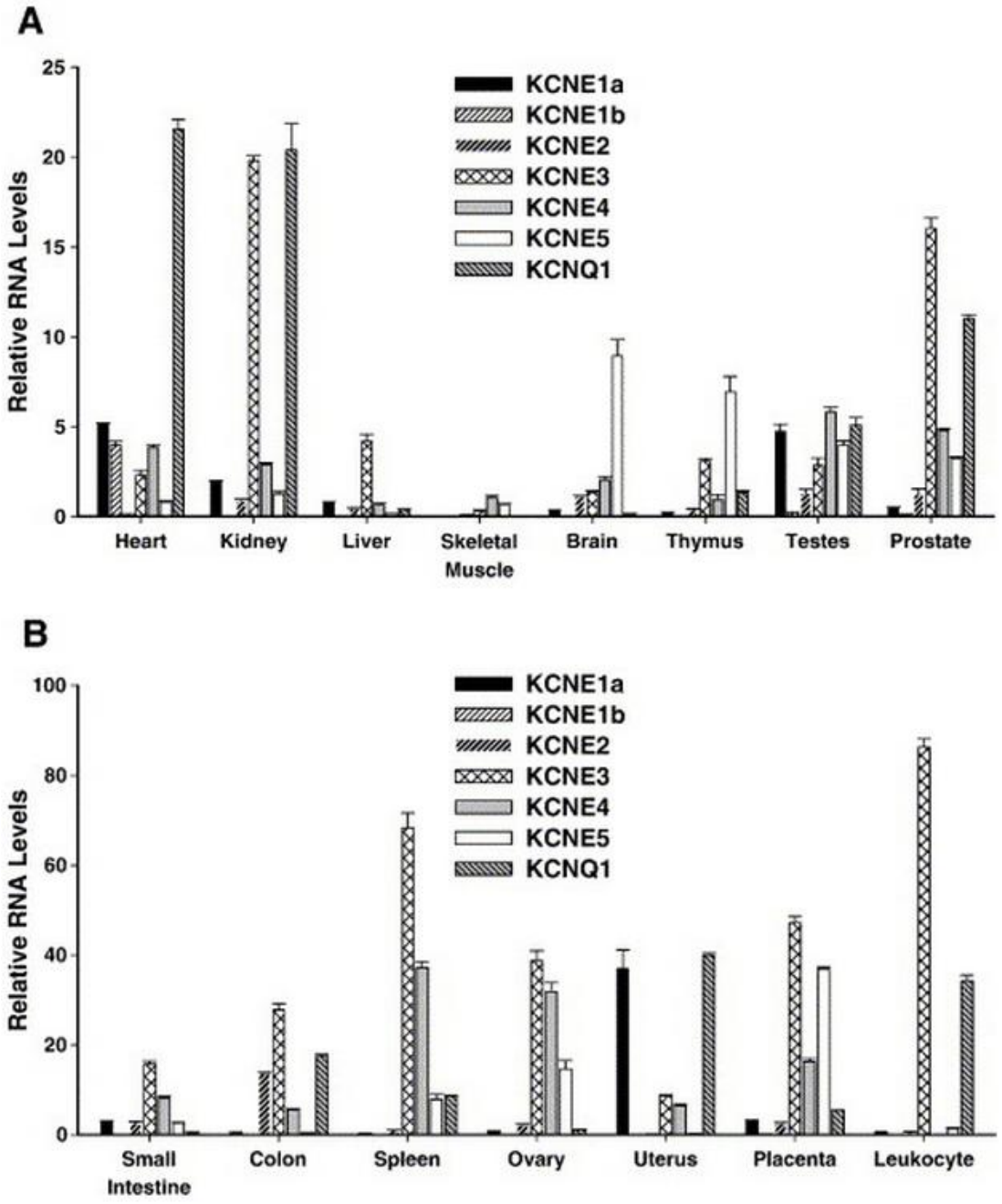

Figure 2. Relative expression of KCNQ1 and KCNE genes in human tissues. Several human tissues were examined by real-time quantitative RT-PCR. Tissues were grouped by low (A) and high (B) overall expression for display purposes (note differences in the y-axis scale). All data were quantified by gene specific standard curves and results were normalized by GAPDH expression. Data are presented as mean ± SEM for at least 6 replicates from 2 different pooled (2 or more individuals) cDNA samples isolated from healthy individuals. From Lundquist et al. 2006[4]

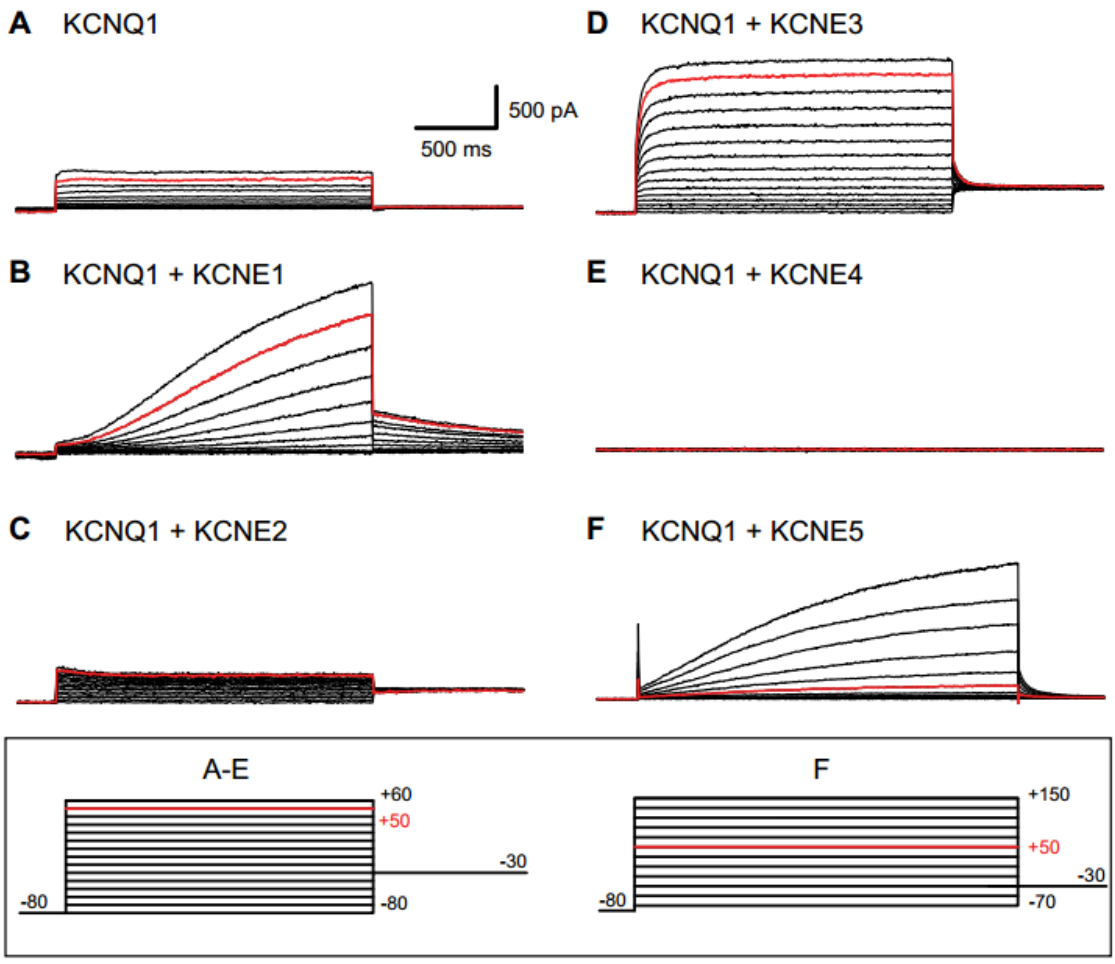

Figure 3. Whole-cell currents recorded in CHO cells co-transfected with KCNQ1 and KCNE1-5. Each set of traces recorded using voltage-clamp protocol as indicated in box. Currents recorded upon +50 mV test depolarization illustrated in red for reference. Adapted from Ciampa, EJ 2011.[5]

deactivation rates, and positively shifts the voltage-dependence of activation. KCNE2 decreases current amplitude but results in constitutive channel activity. KCNE3 increases current amplitude and results in near-instantaneous channel activation. KCNE4 and KCNE5 dramatically inhibit channel activation. With KCNE5, supra-physiologic depolarization yields a slowly activating current. This diverse biophysical modulation contributes to the variable functions of KCNQ1.

The slowly activating current produced by KCNQ1-KCNE1 channel complex, known as I_{Ks}, is further regulated by other factors in the cell (Figure 4). Adrenergic agonists stimulate cyclic AMP (cAMP) activation of protein kinase A (PKA), which phosphorylates Ser^{27} of KCNQ1.[6] Critical to this phosphorylation event is the A-kinase anchor protein (AKAP) known as yotiao.[6] With KCNE1 and yotiao co-expression, I_{Ks} current density is augmented in response to adrenergic stimulation. Another regulator of I_{Ks} is phosphaditylinositol-4,5-bisphosphate (PIP_2).[7, 8] PIP_2 is a minor acidic membrane lipid found primarily on the inner leaflet of the plasma membrane. PIP_2 stabilizes the open state, increases current amplitude and slows deactivation of I_{Ks}. These examples emphasize the complexity of regulation of I_{Ks} within the cell.

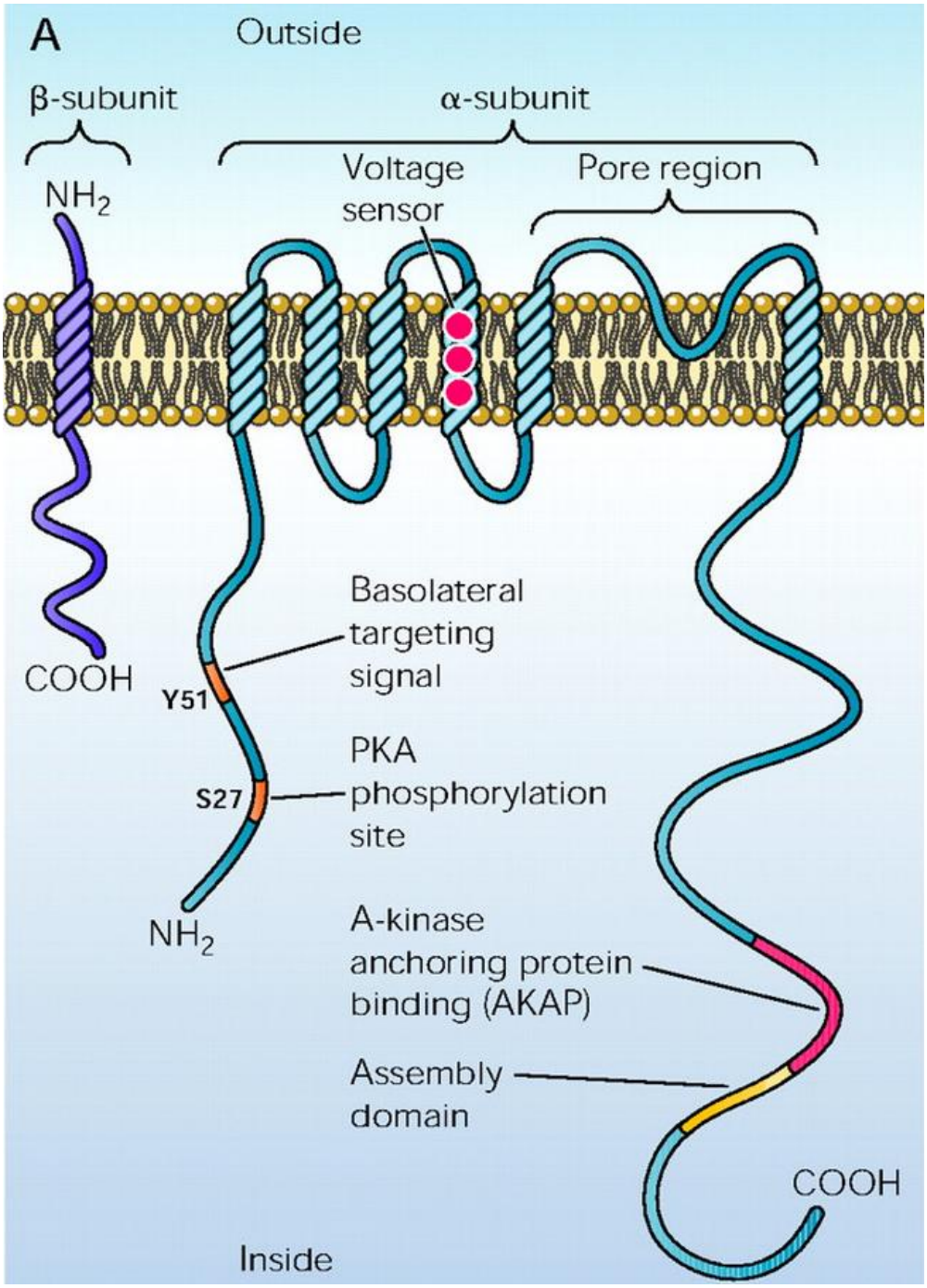

Figure 4. Topology and channel architecture of KCNE(purple) and KCNQ1 (blue) proteins. Topology of KCNE proteins as well as the delayed rectifier potassium channel KCNQ1 with indications of some of the domains important for regulation of the channel. Adapted from Jespersen *et al,* 2005.[9]

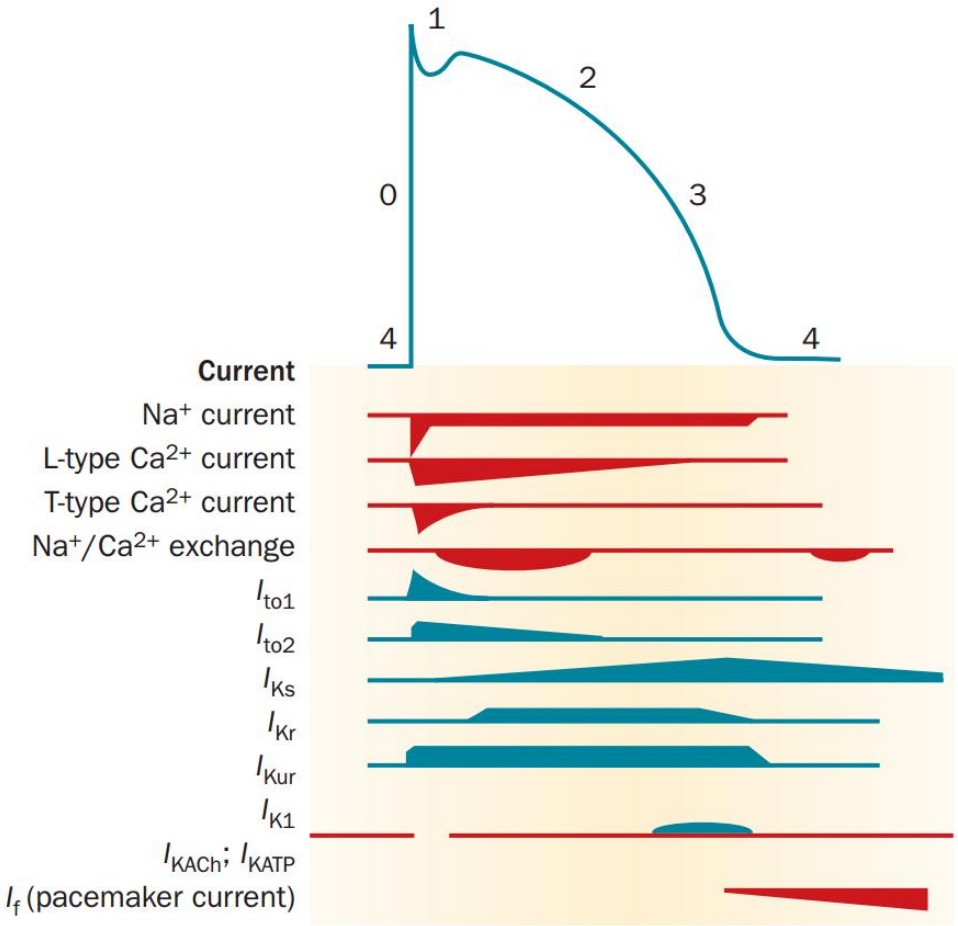

Figure 5. The relationship between ionic currents and the duration of the atrial action potential. The action potential is initiated by a rapid influx of Na+ ions (phase 0), followed by early (phases 1 and 2) and late (phase 3) stages of repolarization, before returning to the resting membrane potential (phase 4). Repolarization is controlled by a balance between inward (red) and outward (blue) currents. Adapted from Darbar and Roden, 2013.[10]

KCNQ1 in cardiac physiology

I_{Ks} is the slow component of the delayed rectifier potassium current in the heart. The heterologously expressed KCNQ1-KCNE1 complex recapitulates the key kinetics of the native cardiac I_{Ks}.[11, 12] This current is a critical component of cardiac repolarization within the action potential (Figure 5). The action potential generation is dependent on the finely tuned interaction between ion channels through the phases of rapid depolarization (phase 0), early repolarization (phase 1), plateau phase (phase 2), late repolarization (Phase 3), and return to the resting membrane potential (phase 4). The action potential is initiated (phase 0) when a change in the membrane potential across the cell is sensed by sodium channel proteins, which alter their confirmation to open, allowing a large, rapid sodium influx. This current, I_{Na}, is mediated by ion channels composed of SCN5A ($Na_v1.5$) and its ancillary subunits SCN1B (β1) and SCN2B (β2). During *phases 0, 1 & 2* L-type calcium channels are open, producing the depolarizing I_{CaL} current. The interplay between calcium and the repolarizing potassium currents characterize the phases of repolarization. Early, rapid repolarization (phase 1) is due to outward movement of potassium ions from the transient outward current (I_{TO}), composed of pore-forming Kv4.3 and β-subunit KChIP2. The plateau phase of the AP (phase 2) typically is a dome shape, representing the depolarizing effect of I_{CaL} counteracting initial activation of the later repolarizing potassium currents (I_{Kr}, I_{Ks}, I_{Kur}). Late repolarization (phase 3) occurs as the balance shifts to the potassium currents and the calcium channels inactivate. The delayed rectifiers, with both a fast (I_{Kr} produced by HERG ($K_v11.1$)) and slow component

(I_{Ks}), are critical determinants of this phase. Final repolarization in this phase is accomplished by movement of potassium through inward rectifier channels KCNJ2 (K_{ir}2.1), composing the I_{K1} current. I_{K1} also helps establish the resting membrane potential in *Phase 4.* Other ionic transporters (NCX, Na/K ATPase) help maintain ionic homeostasis during the large fluxes of the action potential. In addition to maintaining the repolarization of the normal cardiac action potential, the response of I_{Ks} to adrenergic stimulation is crucial. During stress or exercise, the sympathetic nervous system (α- and β-adrenergic stimulation) is activated. The augmentation of I_{Ks} from this stimulation aids in the shortening of the action potential with faster repolarization, required during heart rate acceleration. Importantly, the KCNE subunits are differentially expressed within the cardiac chambers suggesting a rather nuanced function of KCNQ1 within specific regions of the heart (Figure 6).

Gain-of function KCNQ1 mutations in cardiac arrhythmias

The importance of I_{Ks} is emphasized by the functional impact of mutations in these proteins or in relevant regulatory proteins that predispose to arrhythmias. Mutations in KCNQ1 causing dysfunction by defective trafficking, assembly, or regulation can lead to prolonged action potentials.[13,14] During long action potentials, the calcium channels may be reactivated causing early after-depolarizations. Delayed repolarization, as a consequence of KCNQ1 mutations, is reflected directly by a prolongation of the time interval between the initiation of

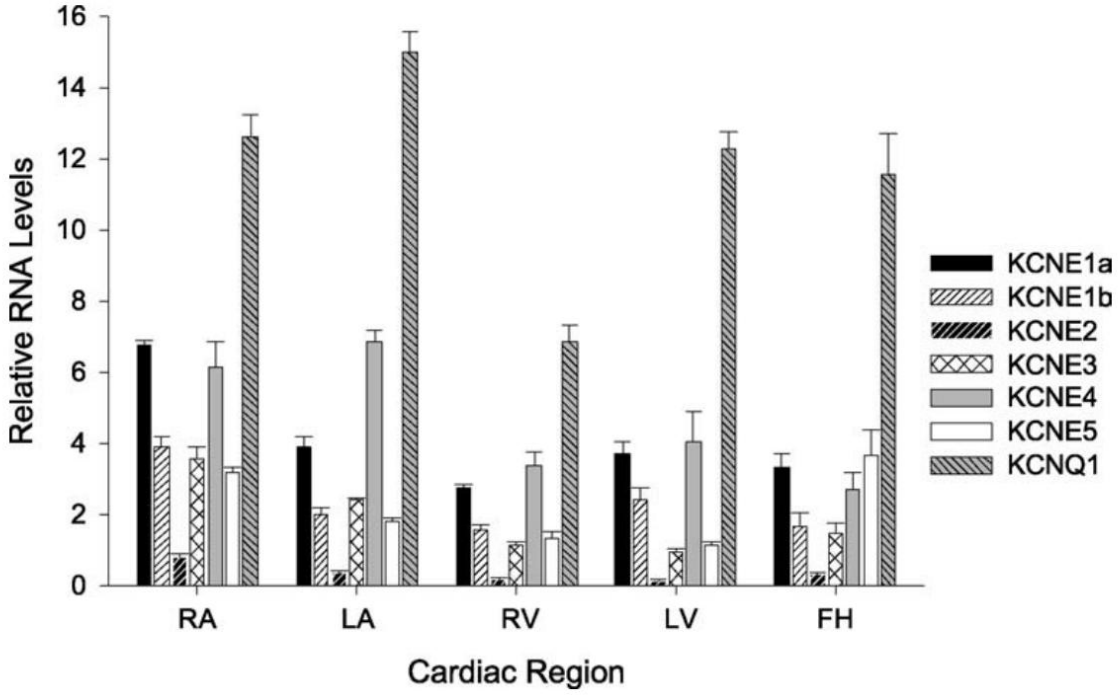

Figure 6. Relative expression of KCNQ1 and KCNE genes in human heart. Five human cardiac tissues were examined by real-time quantitative RT-PCR: right atrium (RA), left atrium (LA), right ventricle (RV), left ventricle (LV), and fetal heart (FH). All data were quantified by gene-specific standard curves and values were normalized to GAPDH expression. Data were presented as mean ± S.E.M. of at least six replicates from two different pooled cDNA samples derived from multiple individuals. From Lundquist *et al*. 2005.[3]

the QRS complex (ventricular depolarization) and the end of the T-wave (ventricular repolarization) recorded by a surface electrocardiogram (ECG). This prolonged QT interval caused by dysfunction in KCNQ1 characterizes one form of the long QT syndrome 1 (LQT1). A long QT interval can predispose to torsade-de-pointes arrhythmia, ventricular fibrillation, and sudden cardiac death, particularly under conditions of adrenergic stimulation such as exercise or stress. Indeed, linkage analysis of LQT1 patients led to the identification of the KCNQ1 gene and its original designation as KvLQT1 in 1996.[13, 14] These loss of function mutations are the most common cause of inherited LQTS.

While the KCNQ1 loss-of-function link to LQTS1 is well established, gain-of-function KCNQ1 mutations have been more recently identified and are associated with increased AF susceptibility. The first identified gain-of-function KCNQ1 mutation was KCNQ1-S140G,[2] and this mutation is the primary focus of this dissertation (Figure 7). The missense mutation was later identified as the causative mutation in a large Chinese family with autosomal-dominant early-onset persistent AF (Figure 8).[2] A neighboring mutation, V141M, was identified as a de novo KCNQ1 mutation responsible for AF.[15] These two mutations are located near the extracellular end of the S1 transmembrane domain. When these mutant KCNQ1 subunits are expressed alone, the potassium currents are largely similar. However, when these mutant subunits are co-expressed with the KCNE1 subunit, the outward currents generated were larger with more instantaneous

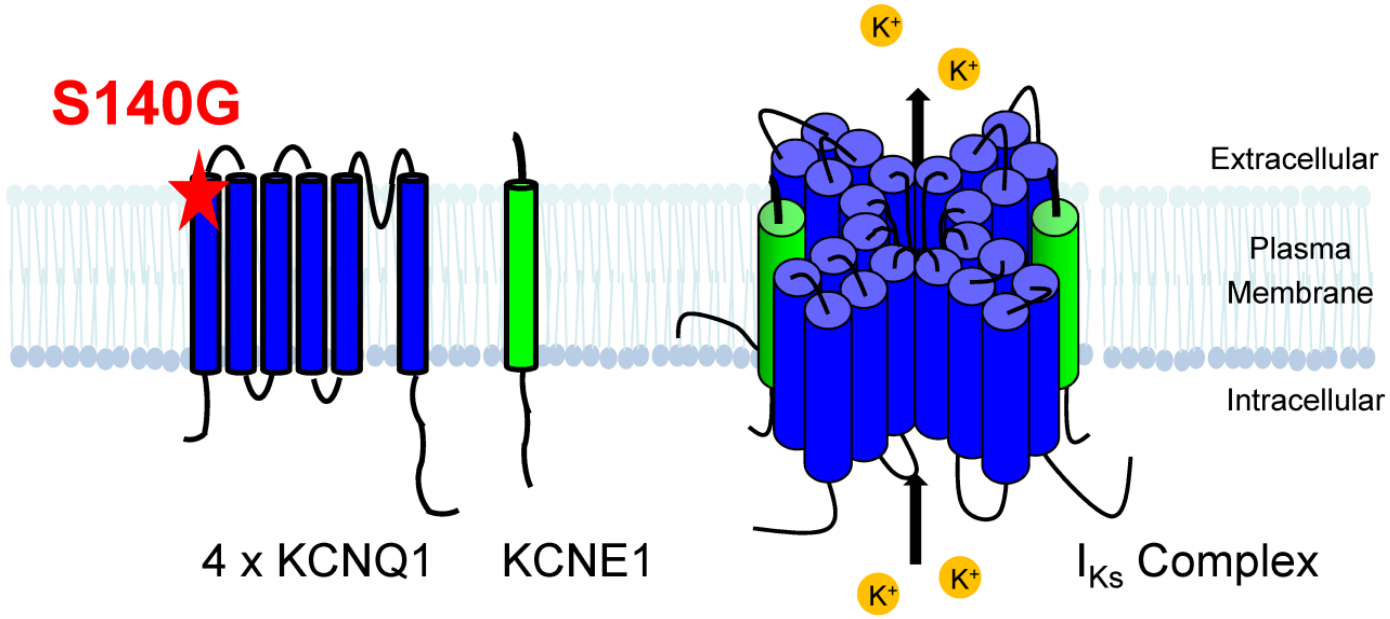

Figure 7. Representative topology of the voltage-gated potassium channel complex that forms the slow delayed rectifier potassium current, I_{Ks}. 6-transmembrane domain KCNQ1 (blue) with mutation S140G location indicated with the red star, single transmembrane domain KCNE1 (green). The I_{Ks} channel complex (right) is composed of 4 KCNQ1 subunits to form the K^+ selective pore and is flanked by KCNE1.

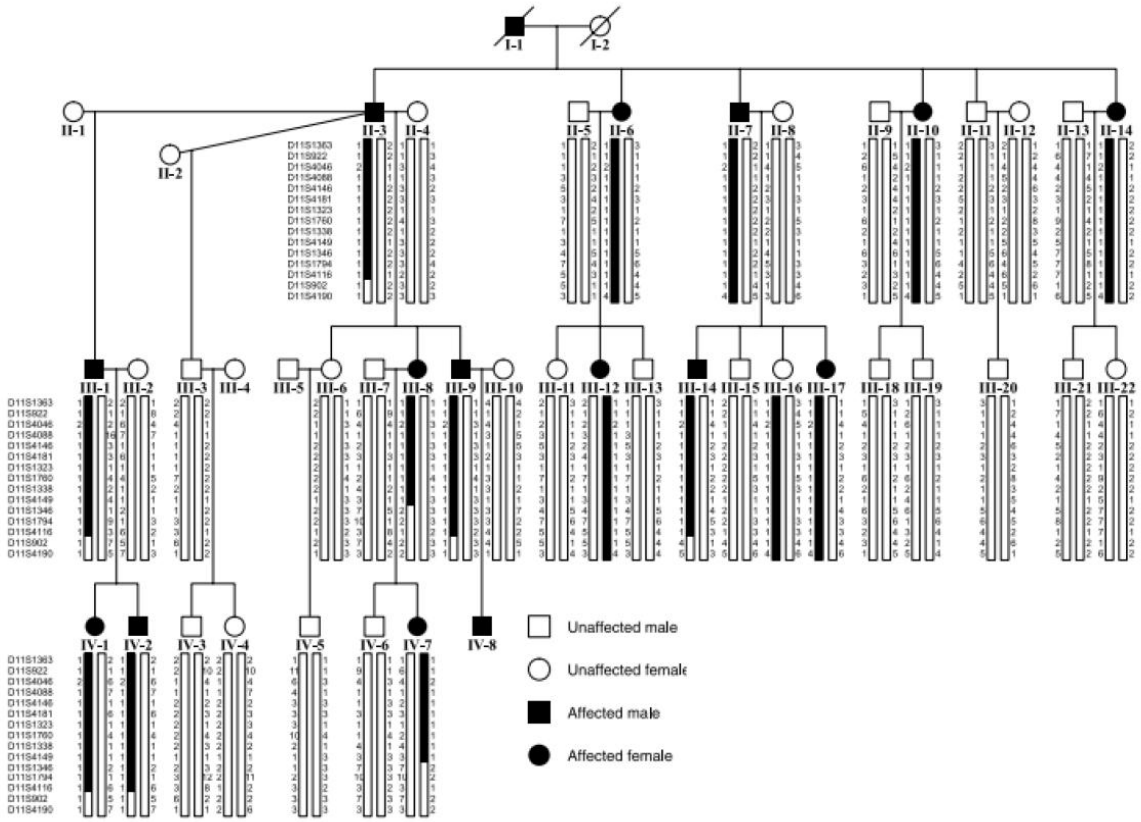

Figure 8. Mapping analysis of the familial AF family with mutation KCNQ1-S140G. Diagonal lines through the symbols indicate deceased individuals. Each individuals ID number is listed below the pedigree symbol. Vertical bar represents chromosome segment. Selected markers spanning the 11p15.5 region are shown to the left of the pedigree, with each individual's allele shown next to the chromosome bar. The chromosome segment originating from the mutation carrying chromosome of the affected individual in the first generation (I-1) is represented by filled bars. Adapted from Chen, *et al.* 2003.[2]

current activation (Figure 9). Although these channels appear constitutively active, Restier *et al* elucidated that S140G-I_{Ks} and V141M-I_{Ks} actually had a markedly slowed rate of deactivation compared to WT-I_{Ks}.[17] With a long enough interval between pulses to allow for complete deactivation, the slowly activating gating kinetics of I_{Ks} could be restored to the mutant I_{Ks}. Nevertheless, even at slow physiologic heart rates these channels would be constitutively active.

How these mutations confer constitutive activity in a KCNE1 obligate manner remains unclear. Restier *et al* hypothesize that these mutations may disrupt salt bridges that form in the open or closed state of the channel.[17] In the open state model of the channel, S140 and V141 are in close proximity to E160 in S2 and R237 in S4 of the same subunit. Because E160 and R237 are predicted to form a salt bridge, disruption of this interaction could slow deactivation. An engineered mutation R237A, resulted in a channel with markedly slowed deactivation.[18] However, this slowed deactivation was not KCNE1 dependent. Alternatively, in the closed state E160 is predicted to interact with R231 while S140 and V141 remain in close proximity (Figure 10).[19] Either mutation might disrupt the E160-R231 interaction resulting in slowed deactivation. Further, R231 and R237 are conserved charges in the S4 voltage sensor domain of KCNQ1.

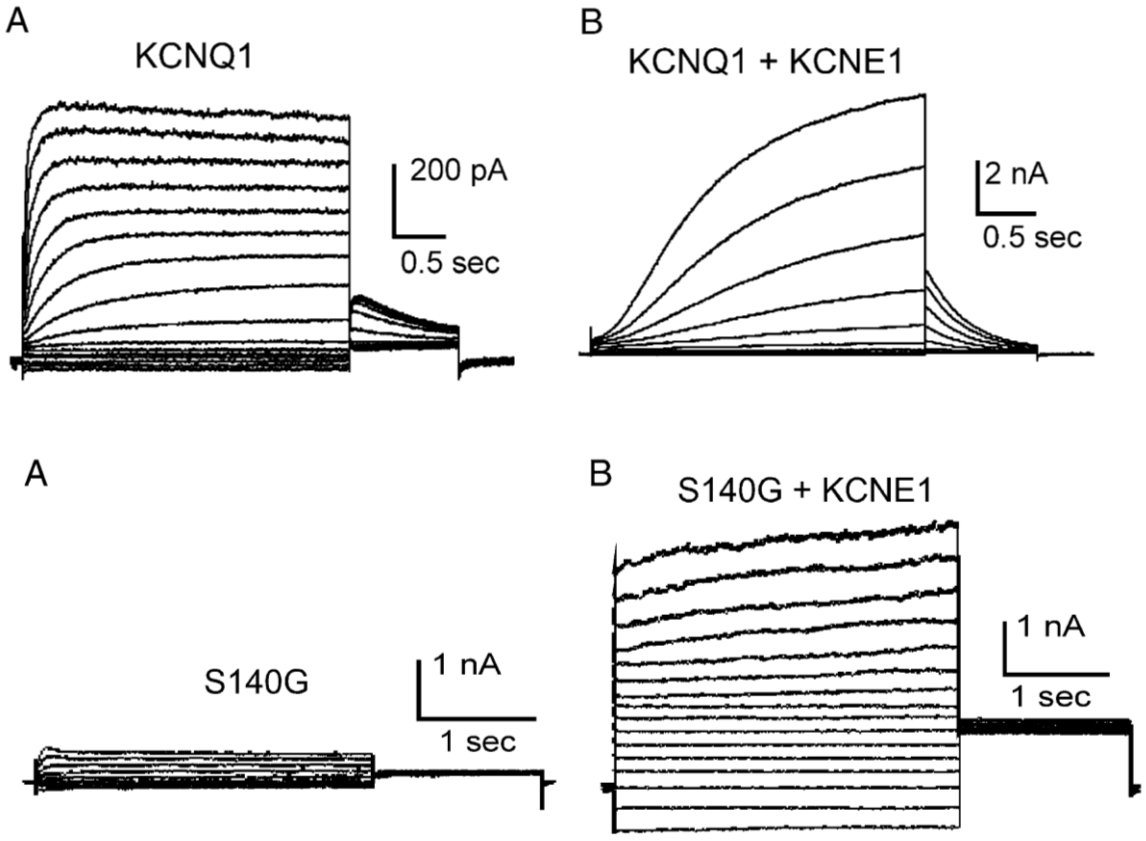

Figure 9. KCNE1 modulates KCNQ1 and KCNQ1-S140G. Whole-cell patch clamp recording from COS-7 cells transfected with DNA encoding KCNQ1 (top row) or KCNQ1-S140G (bottom row) alone (A) or with KCNE1 (B). Adapted from Bendahou, *et al.* 2005.[16]

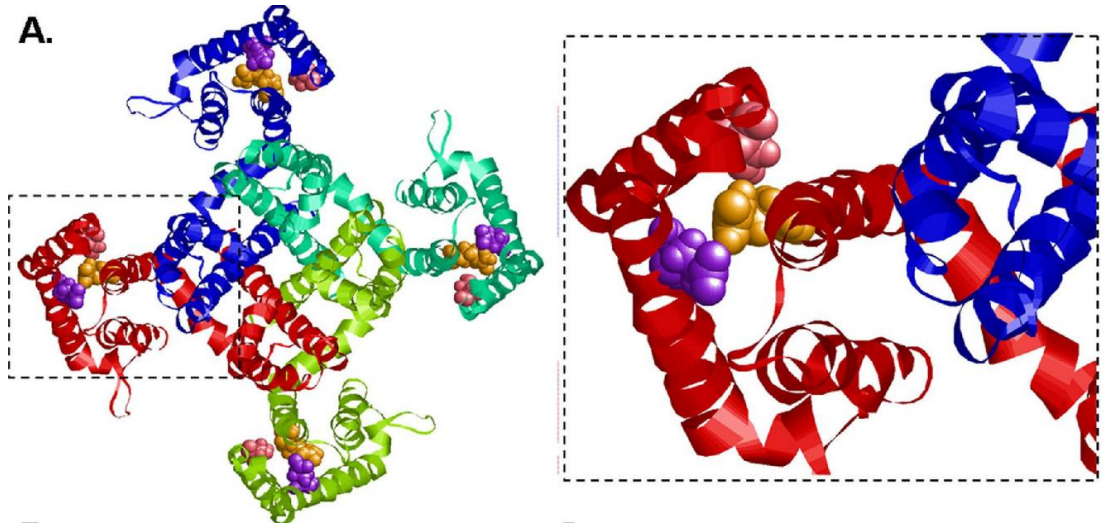

Figure 10. Structural model of KCNQ1 in the closed state from the "extracellular" side looking into the pore. *Left*: Full view; The backbone of each individual Q1 α-subunit is shown as a different colored ribbon. The space filled atoms for the S140 (pink), E160 (purple), and R231 (orange) residues are shown in each α-subunit. *Right*: Red α subunit magnified. The side chains of S140 and E160 are predicted to be close enough to form van der Waals contacts with R231 in the closed state. Adapted from Bartos *et al* 2011.[19]

Supporting the disruption of this interaction as a broader AF mechanism are the recently described familial AF (FAF) associated mutations R231H and R231C.[19,20] R231H was identified in 5 unrelated families causing high penetrance for early onset AF.[20] Electrophysiological studies demonstrate an increase in I_{Ks} is predicted to shorten the action potential duration in atrial cells. Similarly, R231C has been linked to FAF.[19] While R231C-I_{Ks} was constitutively active, overall there was not an increase in current density as seen with S140G-I_{Ks} or V141M-I_{KS}. This constitutive activity was still predicted with computational modeling to shorten the atrial action potential. Complicating the association of these KCNQ1 mutations with FAF is the noted pleiotropy with QT prolongation. While not highlighted in the original publication, many family members with S140G mutation also demonstrated a prolonged QT interval. In addition, the R231 site was associated first with LQTS. Although R231C has constitutive activity, the overall decrease in current density also classifies it as a loss-of-function mutation. Indeed, R231C is linked to LQT1 in other families. R231H-I_{Ks} did not increase with PKA activation consistent with the borderline and adrenergic-induced QT prolongation seen in some patients. Nevertheless these mutations together suggest a FAF 'hotspot' dependent on KCNE1.

Although these identified FAF mutations possibly have a similar mechanism, an unrelated KCNQ1 mutation and mutations in auxiliary subunits or interacting partners that augment potassium current also are associated with early onset FAF. KCNQ1-IAP54-56 is a duplication and insertion of the amino acids IAP in the N-terminus of KCNQ1.[21] This FAF mutation resulted in larger and faster activation, but not constitutively activity, of I_{Ks}. A mutation S64R in natriutetic peptide precursor A (NPPA) increased the current density and activation rate of I_{Ks} as well.[21] Although we have focused on I_{Ks}, mutations in other KCNEs have also been linked to FAF and increased KCNQ1 current density: KCNE2-R27C,[22] KCNE2-X124N,[23] KCNE3-V17M.[24] The identification of these mutations suggest a general increase in KCNQ1 current can result in increased AF susceptibility.

These *in vitro* data are consistent with the theory that increased K^+ current from these mutation would cause shortening of atrial action potentials in myocytes. Nevertheless, these studies are limited by the mutation characterization in a heterologous expression system, which does not completely recapitulate the native myocyte condition. Moreover, predicted effects on action potentials were demonstrated through computational modeling, which again may not completely recapitulate the native myocytes. One attempt to evaluate an FAF mutation in a native myocyte was the use of a mouse model with myocardial specific (α-cardiac MHC promoter) transgenic overexpression of KCNQ1-S140G.[25] While the mutation caused frequent episodes of atrioventricular block that could be terminated by the KCNQ1-specific inhibitor HMR-1556, episodes of AF were not

observed.[25] These data suggest that mouse cardiac myocytes are not an appropriate cellular model of the human phenotype in this genetic disorder. Also missing from this discussion is the fact that familial AF does not present during childhood suggesting that genetic predisposition alone is not sufficient to cause the disease. A brief discussion of AF provides a framework for how FAF mutations relate to disease manifestation and provide possible therapeutic opportunities.

Atrial fibrillation

Atrial fibrillation (AF) is the most common sustained cardiac arrhythmia in adults. The prevalence for AF increases exponentially with age, affecting <1% under 50 years old, 6% over 65 years old, and 11% over 75 years old.[26] Because of our aging population, AF's incidence in the US is projected, by one estimate, to increase from 2.3 million in 2000 to nearly 16 million in 2050.[26] AF is characterized by a rapid, irregular electrical activation of the atria that leads to quivering or fibrillation of the chamber musculature resulting in impaired propulsive force. Short periods of AF result in palpitations, light-headedness, and shortness of breath. Long durations of AF can lead to heart failure, and thromboembolic complications such as stroke, due to stasis of blood within the atria. AF confers a 6x increased risk for ischemic stroke and is associated with premature death.[27] The cost of AF is estimated to exceed $6 billion annually.[28]

The majority of AF, known as secondary AF, occurs within the context of structural heart disease, such as congestive heart failure or coronary artery disease, with onset past the age of 65. An estimated 10-30% of AF, designated as lone AF or LAF, does not occur in the context of overt heart disease and has an age of onset less than 65 years.[29-32] Genetic predisposition to AF has been demonstrated in populations[33, 34] and in families segregating specific mutations.[35] These mutations include potassium channels[2, 15, 22, 24, 36-40] and sodium channels.[41-43] LAF that runs in families is also termed familial AF. While identified FAF mutations shed light on the underlying basis of FAF susceptibility, the molecular etiology of AF is still not well understood. Current theories about the pathogenesis of AF involve triggers acting on a susceptible substrate that induces AF. In a substrate with increased I_{Ks}, the action potential duration (APD) is predicted to be shortened. One manner in which AF would be more likely to develop in this circumstance is that the tissue effective refractory period (ERP) would be abbreviated. If triggered, this abbreviated ERP could give rise to the development of reentrant circuits. Because FAF does not present during childhood, other factors acquired during life are presumed to interact with the genetically determined cellular substrate for the full clinical presentation (Figure 11). The additive or synergistic effects of combined genetic and acquired factors in determining AF susceptibility has not been explored at the mechanistic level. The anticipated contribution of these factors to substrate susceptibility varies depending on type of AF and age of onset (Figure 12).

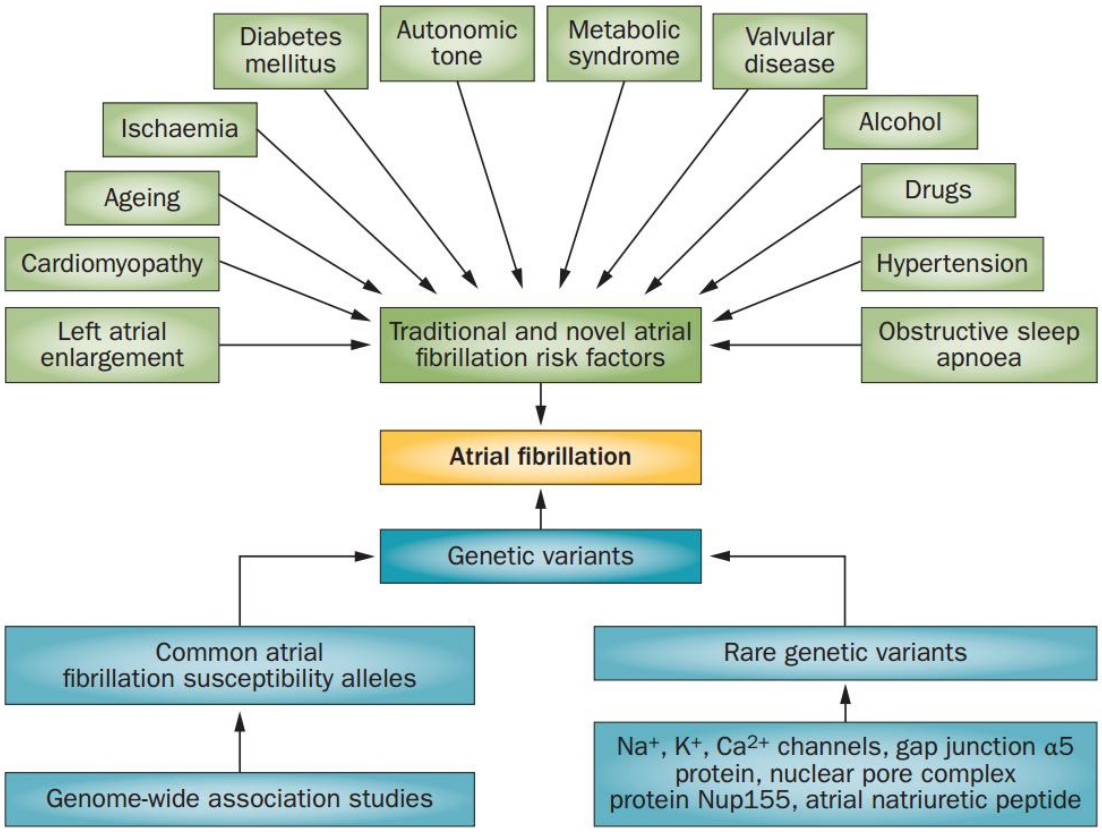

Figure 11. A 'two-hit' hypothesis states that a combination of genetic (blue) and an acquired (green) risk factor is required for the development of atrial fibrillation. Darbar and Roden, 2013.[10]

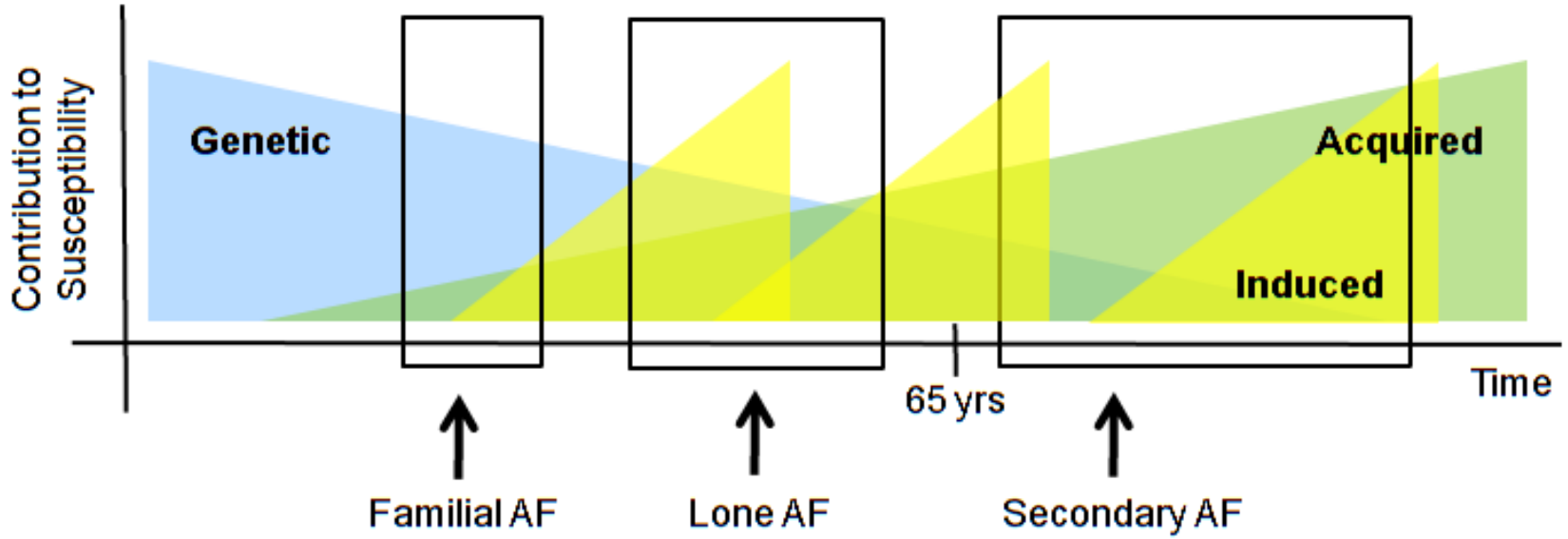

Figure 12. Contribution of genetic (blue), acquired (green), and induced (yellow) factors to atrial fibrillation (AF) substrate susceptibility over time. Approximate onset of familial, lone, and secondary AF indicated by the boxes.

Although interactions between genetic and acquired factors can lead to AF substrate susceptibility and AF development, the currently available therapeutics are not mechanistically targeted and coarsely applied to all AF arrhythmias regardless of genesis. While AF can be categorized by presumed etiology, for therapeutic purposes AF is categorized into three types based on episode duration: paroxysmal (lasts less than 7 days, terminates spontaneously), persistent (does not terminate spontaneously but can be converted to sinus rhythm), or permanent. Repeated episodes of AF lead to electrical remodeling of the atria and progression of AF to an increasingly persistent or permanent state. To treat the AF arrhythmia itself, the basic strategies fall to either rate or rhythm control. A number of clinical trials have explored whether pharmacological rate or rhythm control confer different outcomes and have found no difference in patient survival between rate and rhythm control strategies.[44-46] Current guidelines from the American College of Cardiology (ACC), American Heart Association (AHA), and European Society of Cardiology (ESC) recommend a rate control strategy for all asymptomatic patients.[47] For rate control, the primary categories of therapeutics are β-blockers such as atenolol or propranolol, calcium channel blockers such as verapamil, and digoxin. Rate control alone can often diminish AF symptoms. However, many patients find AF symptoms intolerable and rhythm control is pursued. Pharmacologically sinus rhythm can be with restored sodium channel blockers such as flecainide or propafenone, or multi-channel blockers such as amiodarone or quinidine. Many of these blockers are broad and block a number of specific ion channels. Further these ion channel blockers can put

patients at risk of ventricular arrhythmias such as QT prolongation and torsade de pointes, hypotension, and other side effects. Because long-term use of antiarrhythmics is often undesirable or not efficacious, rhythm control sometimes can be achieved through electrical cardioversion or radiofrequency ablation of the AV node, the AF circuit, or ectopic foci near the pulmonary veins. Despite expansion in our understanding of the genetic basis of AF, genotype or mechanism focused therapies for AF are lacking and there remains an opportunity for personalized genotype-directed therapy.

Objective

As summarized above, KCNQ1 is a widely expressed pore forming voltage gated potassium subunit. Together with the auxiliary subunit KCNE1, KCNQ1 forms the slow component of the delayed rectifier potassium current, I_{Ks}. In the heart, I_{Ks} is critical for the repolarization and for action potential shortening in response to β adrenergic stimulation. Loss-of-function mutations in I_{Ks} lead to LQT1 while gain-of-function mutations have been linked to familial AF susceptibility. A group of FAF associated mutations, S140G, V141M, R231H, and R231C, have constitutive activity in part because of impaired deactivation. These residues are hypothesized to interact in the closed state model of the channel suggesting a common mechanism. Nevertheless, how these observed properties in heterologous systems translate to a native myocyte is not known. Furthermore, because AF does not present in childhood, what acquired factors are needed for clinical manifestation of the disease is unknown.

In our approach, we focused on KCNQ1-S140G, the first identified and best studied causative mutation associated with familial AF. Because transgenic mouse models of KCNQ1-S140G did not produce AF, we first focused on developing a native rabbit atrial myocyte model system as a model organism to better elucidate the mechanism of AF associated with KCNQ1-S140G. In this dissertation, we test the hypotheses that KCNQ1-S140G causes increased atrial potassium current density with resulting shortening of action potential duration by investigating the cellular consequences of KCNQ1-S140G in rabbit atrial myocytes. Lastly, we explored targeted genotype-specific therapy of this mutation based on the hypothesis that KCNQ1-S140G has distinct pharmacological properties that render it susceptible to targeted inhibition.

CHAPTER II

HIGH YIELD MULTI-CHAMBER ISOLATION, CULTURE, AND TRANSFECTION OF ADULT CARDIOMYOCYTES

Introduction

While the electrophysiological effects of many FAF mutations have been described in heterologous sytems, how these mutations alter an adult atrial action potential is not known and only hypothesized through the use of mathematical modeling. FAF-linked mutations expressed in transgenic mice illustrate how different the mouse atria is than human atria and some cases rather inadequate for evaluating the AF phenotype.[25] The difficulty in isolating robust yields adult atrial myocytes is a key methodological issue for connecting the observed heterologous electrophysiological defects with the increased AF susceptibility observed in families.

Rabbits are a well-studied model and are commonly used for whole-heart and tissue studies. Rabbit cardiomyocytes are more human-like than cardiomyocytes isolated from mouse, rat or guinea pig due to expression of important potassium currents such as the slow delayed rectifier current, I_{Ks} (not expressed in mouse or rat myocytes), and the transient outward current, I_{to} (not present in guinea pig myocytes). In addition, rabbits are significantly more economical and useable in a laboratory with standard equipment than larger animals such as pig, dog or

sheep. Acutely isolated primary cells are more physiologically native than immortalized cardiac cell lines. Another alternative cell platform, human iPSC-derived cardiomyocytes, offers immature myocytes that exhibit electrophysiological properties more similar to neonatal than adult cells.[48]

We developed methods for high yield isolation of adult atrial myocytes concomitantly with ventricular myocytes from both guinea pig for preliminary methods development and rabbits for experiments. We describe novel modifications to the classic Langendorff enzymatic isolation method to produce reliable yields of adult rabbit atrial myocytes. We developed cultured conditions to extend the viability of these myocytes, and identified adenovirus as a reliable transfection method for exogenous protein expression in these cells. Further, we demonstrate the utility of cultured adult atrial myocytes for electrophysiological experiments.

Methods

Cardiac myocyte isolation from adult guinea pigs

Myocytes were isolated from adult Hartley guinea pigs 250-300g of either sex (Charles River USA), as previously described with modifications.[49]

Preparation

Three solutions were prepared for isolation: physiologic saline solution (PSS) with and without Ca^{2+} (Table 1) and Kraft-Brühe solution (KB) (Table 2). For a single isolation, solutions were divided into tubes as indicated in Table 3. All solutions were bubbled with 100% O_2 for duration of use, except digestion solution for which bubbling was stopped after enzyme was added to avoid frothing. Before each isolation, the peristaltic pump was adjusted to 5 ml per min flow rate with water filled tubing (1.42 mm internal diameter). Due to tubing stretch over the course of each isolation, the rate needed to be increased with each subsequent isolation. The tubing was changed approximately every 10 isolations when the top pump speed was unable to achieve required flow rate. The water bath temperatures were adjusted so the solution was 35°C at the cannula.

Anesthesia and surgery

The guinea pig was weighed and then anticoagulated with 500 units heparin injected intraperitoneally (i.p.) in the lower abdominal quadrant using a 25 gauge needle. After 5 mins, the guinea pig was anesthetized with 100 mg/kg of pentobarbital (i.p.) When the guinea pig no longer responded to a firm ear pinch, it was placed on the dissecting area, ventral side up, and limbs were secured with tape. The chest was shaved and wiped down with 70% ethanol. Withdrawal reflexes, tested with a firm toe pinch, were monitored frequently. Areflexia onset typically occurred 5 min after pentobarbital administration.

Table 1. Physiologic saline solution components

	mM
NaCl	140
KCl	5.4
$MgCl_2$	2.5
Glucose	11
HEPES	5.5
± $CaCl_2$	1.5

pH 7.4 at 37°C

Table 2. Kraft-Brühe solution components

	mM
K-glutamate	110
KH_2PO_4	10
KCl	25
$MgSO_4$	2
Taurine	20
Creatine	5
EGTA	0.5
Glucose	20
HEPES	5

pH 7.4 at 37°C

Table 3. Solution division for guinea myocyte isolation

Solution	**ml**	**Use**
dH_2O	40	Rinsing bubbler between solutions
PSS + Ca^{2+}	50	Dissecting dish
PSS + Ca^{2+}	30	1st 5 min perfusion
PSS	30	2nd 5 min perfusion
PSS	50	20 min digestion
KB	50	Trituration, filtering and plating

Heart excision

After a deep plane of anesthesia was achieved, a small incision was made below the xiphoid process and the ribcage was cut away from the diaphragm. Using large scissors, the ribcage was removed by cutting along either side. The great vessels were secured with curved tweezers. Scissors cut above the tweezers to remove the heart and ensure enough residual aorta length for cannulation.

Aortic cannulation

The heart was immediately placed in a dissecting dish with warmed PSS + Ca^{2+} solution. The heart was gently massaged between fingers to expel excess blood from the ventricles. Extra tissue, such as the lung and aortic arch, were removed. The aorta was cannulated on a 1/16" female Luer lock connector with 200 series barb and secured with surgical thread.

Perfusion and enzymatic digestion

The heart was mounted on a Langendorff perfusion apparatus and perfusion was begun with PSS + Ca^{2+} for 5 min. The coronary vessels were monitored for blood clearance, and the aorta was re-cannulated if necessary to achieve full perfusion. Then perfusate was switched to PSS and the heart was monitored for lack of contraction as calcium stores were depleted. After 5 mins, perfusate was switched to PSS with 0.4 mg/ml collagenase II (Worthington, Lot #49H11299). The enzymatic perfusion was continued for 18 min if the guinea pig was <300 g or 20 min for larger animals. Perfusate was recycled as needed.

Tissue dispersion

After digestion termination, the heart was placed in a 60 mm dish with KB solution. The desired portions of the heart (any chamber) were separated and placed in a new dish. The tissue was coarsely minced with scissors, and gently triturated with a wide-tipped plastic transfer pipette. The supernatant was filtered through 100 μM nylon mesh into either an Eppendorf tube (atria) or 15 ml conical tube (ventricle).

Washes and plating

The myocytes were centrifuged slowly to form a loose pellet (500 rpm, 3 min). The supernatant was removed and the cells resuspended in fresh KB solution. This wash step was repeated. For acute experiments, myocytes were stored at 4°C in KB solution. For culture experiments, myocytes were plated in tissue culture dishes, incubated at 37°C, and after 3 h, solution was changed to warmed culture media.

The experimental procedure for isolating guinea pig cardiac myocytes was approved by Vanderbilt University Institutional Animal Care and Use Committee.

Cardiac myocyte isolation from adult rabbits

Myocytes were isolated from hearts of male New Zealand White rabbits (6-7 lbs from Charles River Canada), using the method of Bassani, *et al*.[50] with significant modifications.

Preparation

Prior to isolation, initial wash, enzyme wash, and bovine serum albumin (BSA) solutions (Table 4) were prepared from a 1L of 10x MEM solution (Table 5). Solutions were filtered into sterile containers and stored at 4°C . On the day of isolation, each solution was heated to 37°C and the pH was brought to 7.35. For each isolation, 400 ml initial wash, 200 ml enzyme solution, and 400 ml BSA solution were prepared. The peristaltic pump flow and recycling lines were checked for integrity. The flow rate was calibrated to 25 ml/min. Because the elasticity of the pump tubing decreased with each use, pump speed was increased as needed to ensure the proper flow rate. Pump tubing typically can be used for 10 isolations. The temperature at the cannula was confirmed to be 37°C. After the heart was mounted, the temperature of the solution exiting the heart at this flow rate was 35°C. The initial wash and enzyme solutions were bubbled with 95% O_2 - 5% CO_2 gas. Note that the concentration of sodium bicarbonate used was specific for this gas composition. When bubbling with 100% oxygen, 4.76 mM $NaHCO_3$ was used.

Table 4. Rabbit isolation solutions components

Initial wash solution		**Enzyme wash solution**		**BSA solution**	
$NaHCO_3$	23.8 mM	$NaHCO_3$	23.8 mM	$NaHCO_3$	23.8 mM
		Taurine	8 mM	BSA	1%
		$CaCl_2$	0.02 mM	$CaCl_2$	0.5 mM

Table 5. 10x Rabbit isolation MEM solution

MEM powder (Joklik modification without $NaHCO_3$)	119 g
Insulin	400 units
Penicillin-Streptomycin	50,000 units
Pyruvic acid	24.9 mM
Na-HEPES	100 mM
HEPES	100 mM

Sedation and anesthesia

After transfer from the animal facility to lab, rabbits were kept in a covered carrier with ambient nature sounds playing to reduce anxiety for at least 20 min. If the rabbit was agitated in the animal facility, the time was increased to 1 h. Rabbits that vocalized or thumped in the animal facility were not transferred, and the isolation was delayed for at least one day. After anxiety subsided, rabbits were sedated with 2.4 mg/kg acepromazine, injected intramuscularly in the caudal thigh muscle. The rabbit was returned to the carrier with eyes covered by gauze to further reduce anxiety. After 5-15 min, the rabbit typically was non-responsive to a strong ear pinch. The rabbit was placed on the dissection platform, and the ear was cleaned with 70% ethanol. Using a thumb to occlude and distend the dorsal ear vein, the vein was cannulated with a 23 gauge butterfly infusion needle and intravenous 40 mg/kg pentobarbital sodium and 1000 units heparin were administered. The anesthesia level was monitored frequently by checking corneal and withdrawal reflexes and assessing heart rate. If arreflexia was not achieved in 20 min, additional i.v. bolus of 20 mg/kg pentobarbital sodium was administered. The dissection plane was prepared by spraying with 70% ethanol, shaving fur and applying betadine soap to the skin.

Heart excision

After achieving a deep plane of anesthesia, a midline incision was made and the fascial plane was cut to expose the chest muscle. The abdominal wall was incised below the xiphoid process. The xiphoid process was grasped with tweezers and poultry shears were used to cut along the sternum for a thoracotomy. The chest cavity was opened with retractors and the rapidly contracting heart was visualized. The pericardium was torn and removed. The great vessels were secured between fingers and cut with fine scissors as distally from the heart as possible to ensure that enough ascending aorta was preserved for Langendorff cannulation. The heart was lifted vertically and remaining pulmonary vessels were cut to release the heart.

Langendorff perfusion

After rapid excision of the heart, it was arrested on ice. Over the course of 5 min, the heart was transferred between three cold beakers of initial wash solution and the heart was inverted between washes to flush blood from the ventricles. At the end of 5 min, the aorta was grasped with tweezers and cannulated on a barbed Luer coupler. Initially the aorta was secured with an alligator clip and then more securely tied with surgical thread. Then through the aorta, the coronary vessels were flushed with 30 ml of cold initial wash solution applied by a syringe. If blood was not cleared from the coronary vessels (Figure 13), the cannula was repositioned more distal to the heart because the coronaries occasionally branch from proximal ascending aorta.

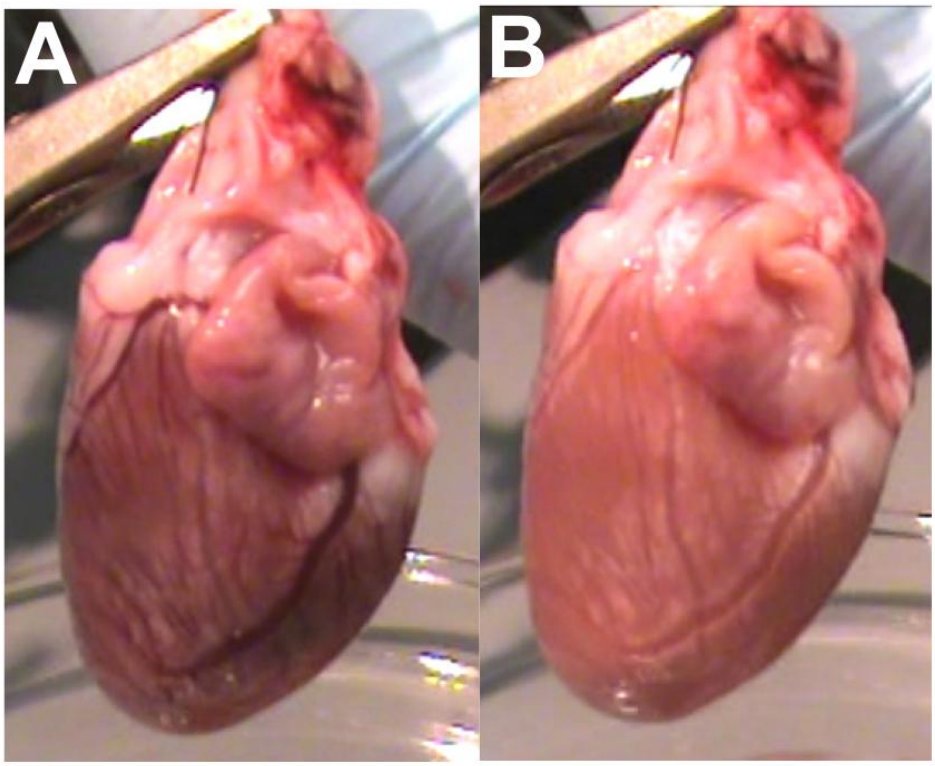

Figure 13. Representative example of coronary vessels clearing in an adult rabbit heart. **A**, Adult rabbit heart with coronary vasculature filled with blood after excision from rabbit. **B**, Same adult rabbit heart with cleared coronary vasculature after retrograde aortic perfusion with 30 ml initial wash (see methods).

The heart was then mounted on a Langendorf perfusion apparatus and perfusion was begun at 37°C for 10-15 min with initial wash solution gassed with 95% O_2 and 5% CO_2. As the heart warmed to 37°C, it typically began contracting for a few minutes. Because the initial wash solution was nominally calcium free, the heart should stop contracting once the calcium stores are depleted.

Atrial perfusion

During this initial perfusion and once the heart stopped contracting, the pulmonary vessels were closed with microvessel clips to perfuse both atrial chambers at high pressure (Figure 14). The atrial chambers were punctured twice at their apex with a 22 gauge needle. These punctures should not deflate the atria but rather facilitate flow of solution.

Initial enzymatic digestion

After sufficient atrial perfusion rate was achieved, Liberase TH (Roche Applied Sciences, Indianapolis, IN) was thawed and added to the enzyme wash solution at 0.05 mg/ml. Due to its hydroscopic properties, Liberase TH upon arrival was suspended in sterile H_2O and stored in 1 ml aliquots (5 mg/ml) at -20°C. The enzyme was used within 3 months. The perfusion solution was carefully switched to avoid perfusion of air bubbles in the enzyme wash solution. After 1 min, the recycling line was switched to the enzyme wash solution. After 5 min, a small incision was made in the left ventricle in an area between major coronary vessels (Figure 15).

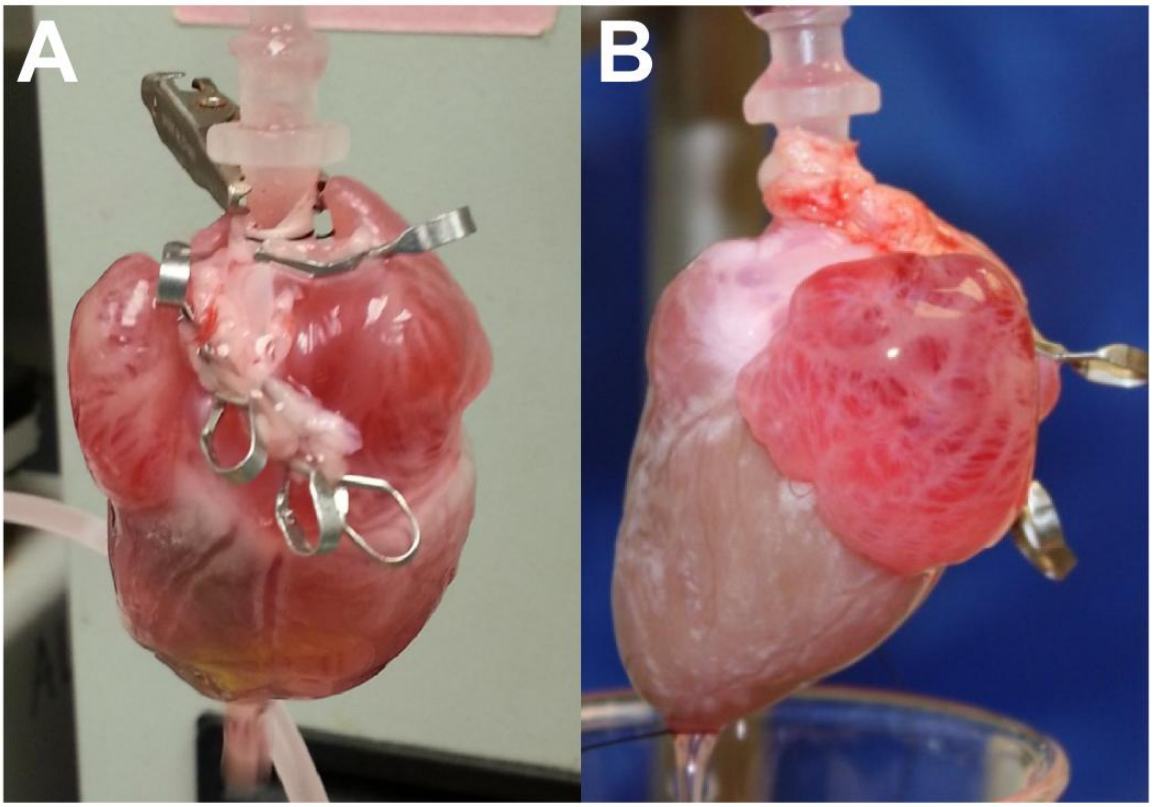

Figure 14. Atrial perfusion on the Langendorff apparatus. **A,** microvessel clamps occlude pulmonary veins to perfuse the atria. **B,** high pressure perfusion inflates the left atrial chamber.

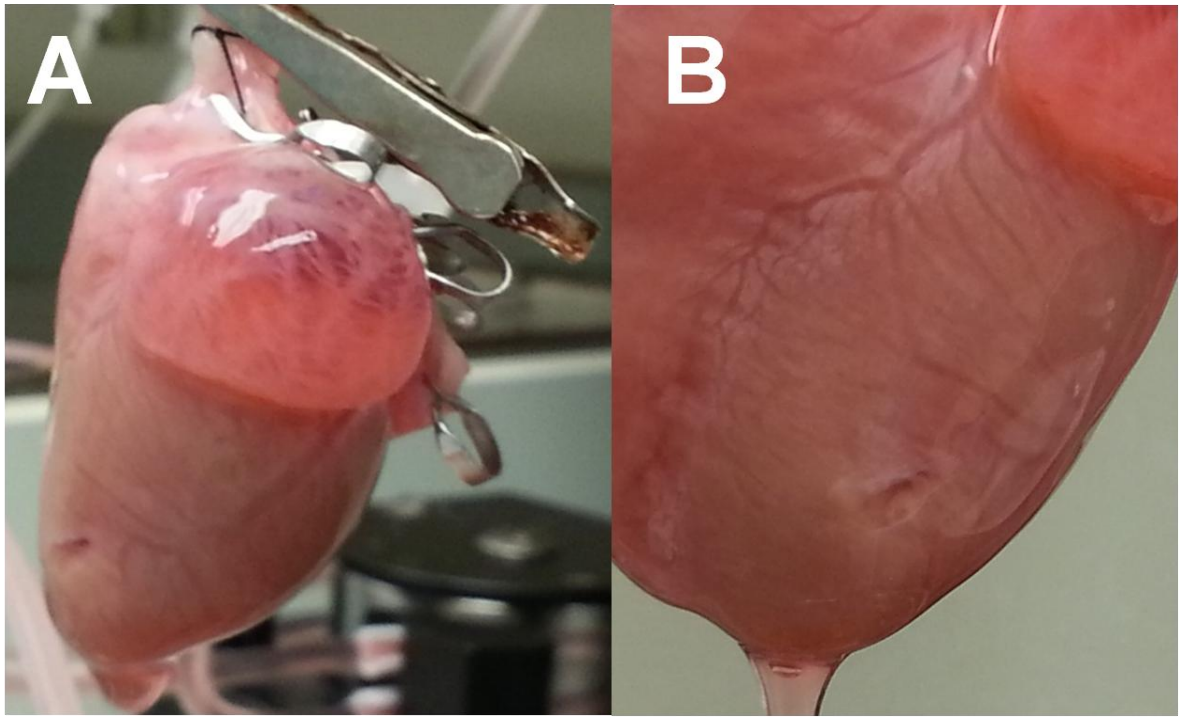

Figure 15. Representative sampling site for enzymatic digestion monitoring. **A**, Whole heart orientation to sampling location and **B,** enlarged view of sampling site on left ventricle between major coronary vasculature.

Serial tissue samples (30 s - 1 min) were taken from this incision with fine tweezers and inspected immediately by light microscopy. When the majority of ventricular myocytes released were quiescent rods (7-20 min) (Figure 16), the atria were removed from the heart and placed in enzyme solution. The remaining heart was placed in BSA solution on ice.

Atrial enzymatic digestion

Either atrium was recannulated on the Langendorff apparatus (Figure 17). Serial samples were taken from the perfused atrium until the sample edges contained packets of rod-shaped atrial myocytes and the majority of released atrial myocytes were quiescent rods (5-20 minutes) (Figure 18). Typically, atria digestion was not complete until the tissue lost integrity and samples were difficult to grasp with tweezers. The atrium was removed and placed in BSA solution. The other atrium was recannulated on the apparatus and the digestion process repeated.

Tissue dispersion

The desired tissue was finely minced, gently triturated with a wide-bore pipette, and the supernatant filtered through a 100 µm cell strainer (BD Biosciences, San Jose, CA). These steps were repeated until all tissue had been filtered. The myocytes were allowed to settle into a soft pellet by gravity for 30 – 60 min at room temperature. Then the supernatant was aspirated, and myocytes were resuspended in fresh BSA solution.

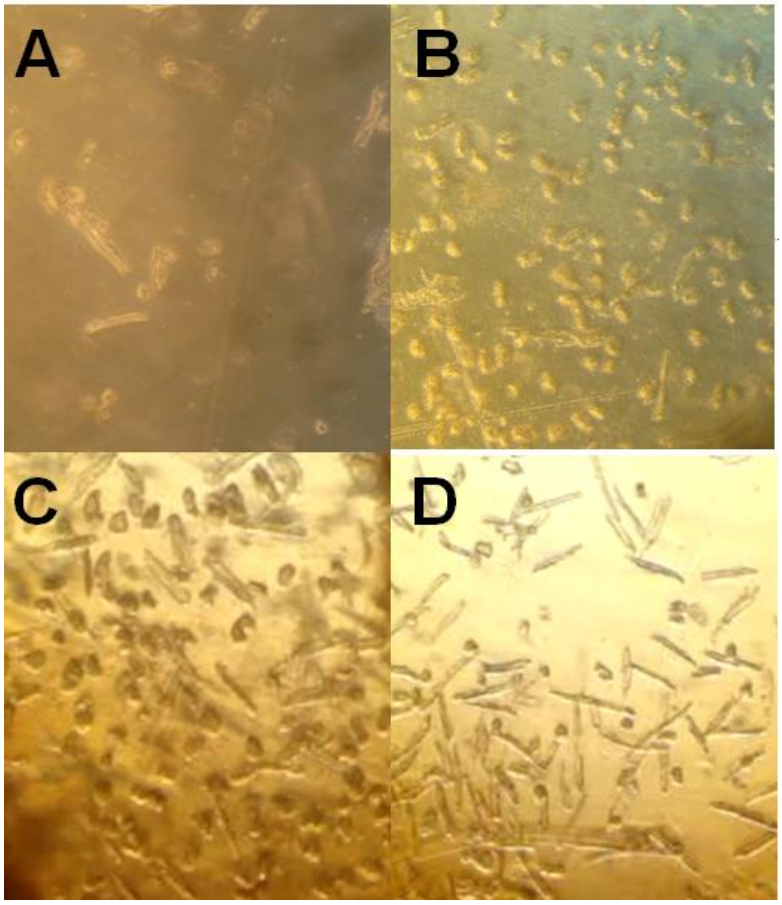

Figure 16. Serial sampling of rabbit adult left ventricular myocyte during enzymatic digestion. **A** through **D** show serially collected samples examples. **A**, early sample with few mostly hypercontracted cells; **B,** majority of myocytes released are hypercontracted; **C**, mix of hypercontracted and rod-shaped ventricular myocytes; **D**, majority of cells released are rod-shaped, an ideal time to stop ventricular enzymatic digestion.

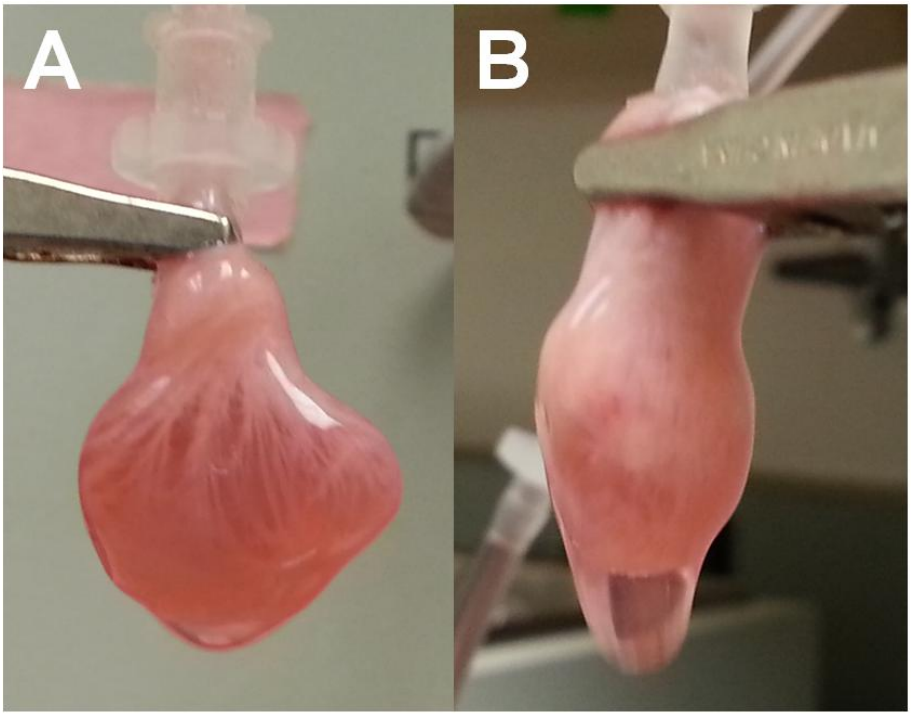

Figure 17 Representative examples of secondary atrial cannulation on Langendorff apparatus; **A,** Left atrial cannulation and **B,** right atrial cannulation.

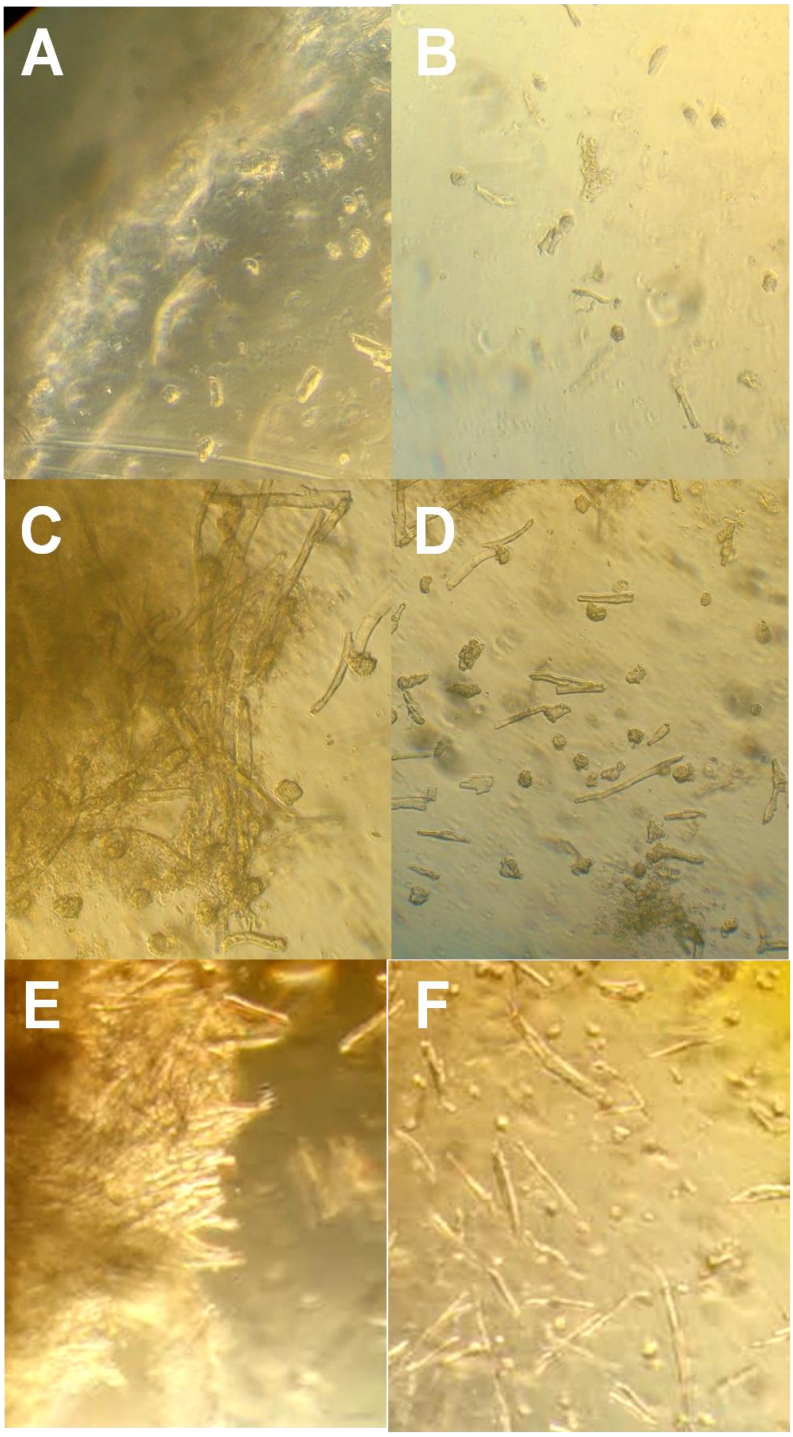

Figure 18. Serial sampling of rabbit adult left atrial myocytes during enzymatic digestion. Rows represent sampling progression. Left column is the margin of sample and right column illustrates released myocytes morphology. **A and B,** early sample with few rod shaped myocytes visible at sample margin and few released myocytes. **C and D,** intermediate sample with mix of rod-shaped and hypercontracted myocytes both at sample margin and released. **E and F**, ideal sample for digestion termination with rod-shaped myocytes in loose packets at tissue margin and majority of released myocytes are rod-shaped.

The experimental procedure for isolating rabbit cardiac myocytes was approved by Vanderbilt University Institutional Animal Care and Use Committee.

Staining of acutely isolated cardiac myocytes

Rabbit cardiac myocytes membranes and t-tubules were stained as previously described.[51] Briefly, acutely isolated cells from all four cardiac chambers were stained with wheat germ agglutinin conjugated to Alexa-flour 594 and fixed with 4% paraformaldehyde. Importantly, membranes were not permeabilized prior to staining. Samples were stored in PBS suspension at 4°C.

Culture of adult cardiac myocytes

Myocyte culture media

Three myocyte culture media bases were used for guinea pig myocyte culture optimization: MEM with Hank's salt (Table 6), Media 199 (Table 7), and Ham's F-10 (Table 8). Excitation-contraction couplers used were 2,3 butane-dione monoximine (BDM) at 10-30 mM and blebbistatin (BLB) 5-200 μM. pH buffer augmentation was achieved with addition of 4 mM $NaHCO_3$ and 10 mM HEPES and pH to 7.4 at 37°C with NaOH. Media was added 15 min - 5 h post isolation.

Table 6. MEM-based myocyte culture media components

MEM with Hank's salt	500 ml
Penicillin	50 units/ml
Streptomycin	50 µg/ml
BSA	1%
Insulin-transferrin-selenium-X	1x

Table 7. Media 199-based myocyte culture media components

Media 199	500 ml
Penicillin	50 units/ml
Streptomycin	50 µg/ml
L-carnitine	2 mM
Creatine	5 mM
Taurine	5 mM

Table 8. Ham's F-10-based myocyte culture media components

Ham's F-10	250 ml
DMEM	250 ml
Penicillin	50 units/ml
Streptomycin	50 µg/ml
Insulin	1 mg/ml
Transferrin	5 mg/ml
LiCl/$NaSeO_4$	0.01 mM
Thyroxine	0.1 mM
Ascorbic acid	2.5 mM

For adult rabbit myocytes, cells were placed into culture 3 h post isolation with media consisting of MEM supplemented with Hank's salts, 2 mM L-glutamine (Gibco-Invitrogen, Life Technologies, Grand Island, NY), insulin-transferrin-selenium-X supplement, penicillin (50 units/ml), streptomycin (50 µg/ml), 1% bovine serum albumin, 10 µM blebbistatin at pH 7.4 at 37°C (modified from Kabaeva, *et al*. 2008 [52]).

Coating cover slips with extracellular matrices

Laminin from Engelbreth-Holm-Swarm murine sarcoma basement membrane (Sigma-Aldrich St. Louis, MO), fibronectin (Roche Applied Sciences, Indianapolis, IN), or poly-L-lysine (VWR, Radnor, PA) were used to coat glass coverslips to promote myocyte adherence. Laminin was diluted 1mg to 50 ml MEM solution and stored in 1 ml aliquots at -20°C. Laminin was used at 100 µl to each 15 mm round cover slip. Fibronectin was prepared by adding 1 ml water to 1 mg fibronectin and incubating for 10 mins at 37°C with 5% CO_2. Then 20 ml MEM plus 1% penicillin/streptomycin was added. Fibronectin was stored at -20°C. Fibronectin was used with 100 µl per 15mm round cover slip. 0.01% poly-L-lysine solution (Trevigen, Gaithersburg, MD) was stored at 4°C. 1 ml was used to coat a 35 mm dish. After addition of any matrix, the dish was incubated at 37°C with 5% CO_2 for at least 1 h. The excess matrix was removed. Culture media was added for storage or the dish was used immediately for myocyte culture.

Transfection of adult cardiac myocytes

Human KCNQ1 and KCNE1 cDNAs were generated as described previously.[3] The S140G mutation was engineered in KCNQ1 using QuikChange mutagenesis (Stratagene Corp, La Jolla, CA). For most test transfections, empty vector controls were used, either pIRES2-eGFP or pIRES2-dsRedMST. All constructs were verified by sequencing of the entire open reading frames.

Electroporation

Acutely isolated guinea pig myocytes were electroporated using the ECM 830 (BTX, Harvard Apparatus, Inc., Holliston, MA) with pIRES2-eGFP plasmids using permutations of the following parameters: time post isolation (5 min - 3 h), temperature (4°C , 20-23°C, or 37°C), suspension media (PBS, KB, DMEM, culture media), DNA amount (1-20 µg), field strength (250-1000V), and pulse duration (3-7 ms). Poly(ethylenimine) (PEI) (Sigma-Aldrich St. Louis, MO) was also used to enhance transfection, but was found to be immediately toxic to myocytes even at low concentration when combined electroporation.

Lipid transfection

Transient lipid transfection of adult cardiac myocytes was attempted with pIRES2-eGFP plasmid in multiple ratios with different lipid transfection reagents: FuGENE6 (Promega, Madison, WI), FuGENEHD (Promega, Madison, WI), SuperFect (Qiagen Inc, Valencia, CA), Lipofectamine 2000 (Invitrogen, Life Technologies, Grand Island, NY), Lipofectamine LTX (Invitrogen, Life Technologies, Grand Island, NY), and Lipofectamine Plus (Invitrogen, Life Technologies, Grand Island, NY). PEI was added to promote transfection. For lipofectamine trials, conditions were tested with and without a 3 h incubation at 1% CO_2.

Biolistic transfection

Preparation of DNA bullets

Gold beads (12.5, 25, or 50 mg of 0.6, 1.0, or 1.6 micron) were added to an Eppendorf tube. Then, 100 µl of 0.05M Spermidine was added. The tube was sonicated for 20 s., 12.5-100 µg DNA diluted in dH_2O for 50 µl total volume was then added, and sonicated. While vortexing the eppendorf (at level 5), 100 µl of 1M CaCl2 was added dropwise to the tube. The tube was briefly sonicated. The solution was allowed to precipated at room temperature for 10 min. The tube was briefly centrifuged, the supernatanted aspirated, and resuspended in 3.2 ml fresh 100% ethanol or 100% ethanol- polyvinylpyrollidone (PVP) mixture (0.007, 0.015, or 1.0 mg/ml ethanol). Well-shaken mixture was loaded into bullet tubing,

previously dried for at least 20 min with 0.4 lpm N_2, and fed into the prep station. After 4 min, the supernatant was carefully removed. The tubing was slowly turned to evenly distribute gold, and then spun continuously for 20 sec on the prep station. The tubing was dried for 5 min with N_2 gas. The tubing was cut into 0.5" shells with a tube cutter. The bullets were stored in scintillation vials with DriRite and stored at 4°C. Bullets were used within 3 months of preparation.

Biolistic transfection of myocytes

The bullet vial was allowed to reach room temperature and loaded into the Helios Gene Gun (Bio-Rad Laboratories, Hercules, CA) cartridge holder. The gun was assembled and attached to helium tank. The media was aspirated from target cell culture dishes. The gun was aimed parallel to tissue culture dish, either point black or using the barrel length as a spacer. The gun was fired at 50-350 PSI. Fresh culture media was immediately added to cells. An example set-up is illustrated (Figure 19).

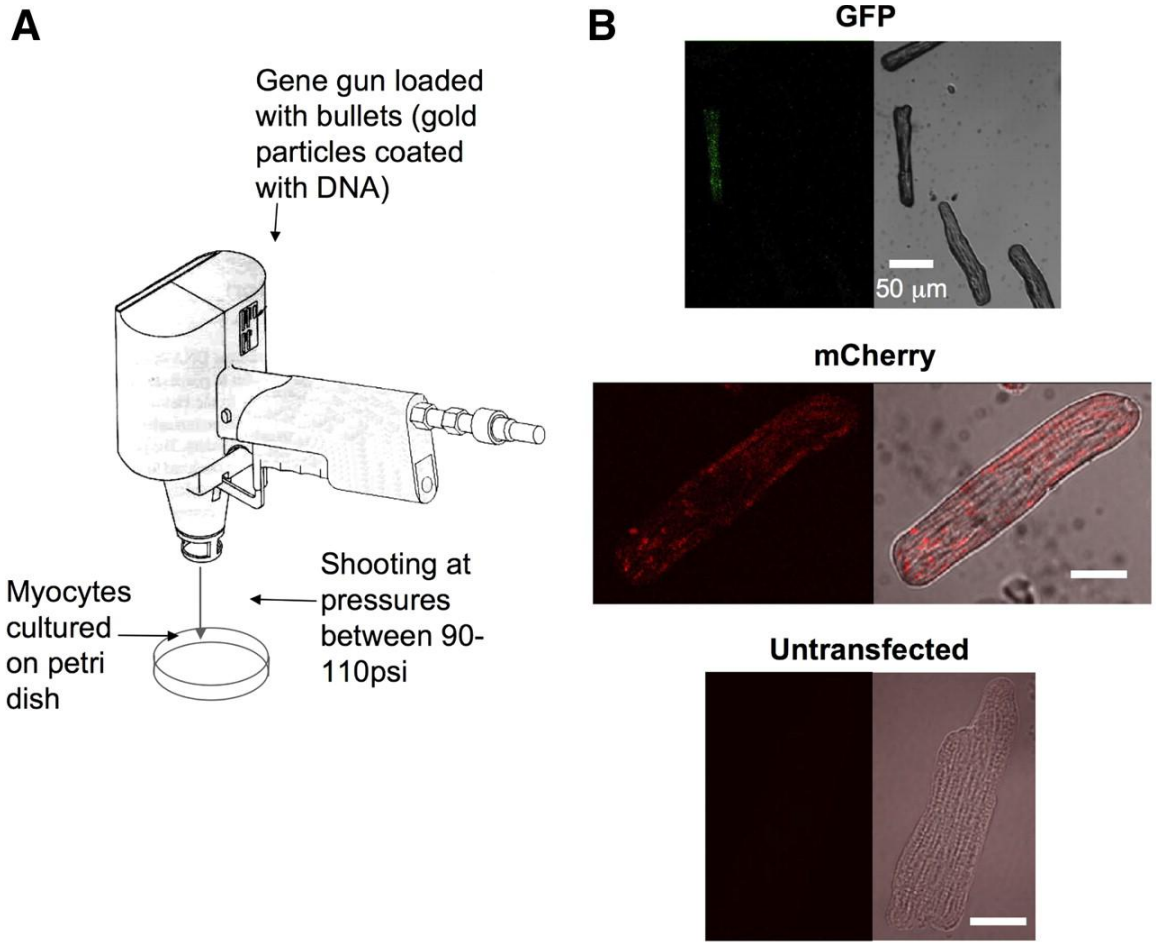

Figure 19. Biolistics method for transfection of adult cardiac myocytes. **A,** schematic of the protocol employed for transfection of freshly isolated adult rat ventricular myocytes using the Helios Gene Gun; **B**, *top*: wide field fluorescence and bright field overlay image of adult rat ventricular myocytes transfected with eGFP acquired with a 10x objective. The transfected myocyte glows green. *Middle*: a rate vetnricular myocyte transfected with mCherry acquired with 60x objective. *Bottom*: an untransfected myocyte imaged as for mCherry. Adapted from Dou, *et al.* 2010.[53]

Lentiviral transduction

Lentiviral plasmids

Lentivirus was generated using plasmids (pLL-eGFP, PAX2, and pMD2.G) that were a generous gift of Nick Markham in Al Reynold's laboratory at Vanderbilt University. A payload plasmid was created from pLL-eGFP to express pLL-CMV-mcs-IRES2-dsRedMST.

Lentivirus generation

Lentivirus was generated using the following protocol. On day 0, HEK 293FT cells were plated at $1x10^6$ in 60 mm dishes to acheive 50-70% confluency the following day. On day 1, a calcium phosphate transfection was prepared. First 12 µl of 25 mM chloroquine (stored at -20C) was added to 293FT cells. Then transfection cocktail was prepared in the following order: 6.6 µg of payload plasmid (pLenti-CMV-mcs-IRES2-dsRedMST), 5 µg of packaging plasmid (PAX2), 2 µg envelope plasmid (pMD2.G), 21 µl 2M $CaCl_2$, up to 170 µl sterile dH_2O and 170 µl BES-1 buffer (500 ml stock): 5.33 g BES powder (Calbiochem), 8.18 g NaCl, 0.75 ml of 1.5 mM Na_2PO_4 and pH 6.95 with NaOH. The cocktail was mixed for 15s with a P1000 pipette. The mixture was added to 293FT cells dropwise and slowly swirled to mix. Cells were incubated 5-7 h and then fresh

media was added. On day 2, the culture media was changed. On day 3, the virus was harvested with a 10 ml syringe and passed through a 0.45 micron filter. The harvested virus was stored at 4°C for up to a week or stored at -80°C for up to a year in small single use aliquots.

Lentiviral transduction

For transduction, a small amount of media was added to plated myocytes. Polybrene (8 µg/ml) was added to the media. Virus was added to the cells and incubated for 3-12 h. Then, the media was replaced. Cells were monitored daily for fluorescent expression of viral marker (dsRedMST).

Adenoviral transduction

Adenoviral vectors

Adenoviral vectors, pAd5-CMVK-NpA and pAd5-(9.2-100)delta1.6KbE3, were obtained from the University of Iowa Gene Transfer Vector Core (supported in part by the NIH and the Roy J. Carver Foundation). Using the pAd5-CMVK-NpA vector, we created a shuttle vector for IRES2-dsRedMST.

Adenovirus generation

Adenovirus was generated using the RAPAd^{TM} system as previously described (Figure 20).[54] In brief, each shuttle vector and the backbone vector pAd5-(9.2-100)delta1.6KbE3 were co-precipitated with calcium-phosphate into human embryonic kidney (HEK) 293 cells in 60 mm Petri dishes. When 60% of cells had detached (12-14 days), the cells and media were harvested, lysed through repeated freezing/thawing cycles, and amplified in HEK cells (typically using 5-10 150 mm Petri dishes). After 60% of cells detached from the large dishes (1-3 days), cells were pelleted by centrifugation and resuspended 5 ml of viral storage solution (10 mM Tris, 2 mM $MgCl_2$, 4% sucrose, pH 8.0). The supernatant was stored at −80°C and the virus was used within 3 months for test transductions. Myocytes were incubated with virus for 24 h, and transduction rate was evaluated at 48 h.

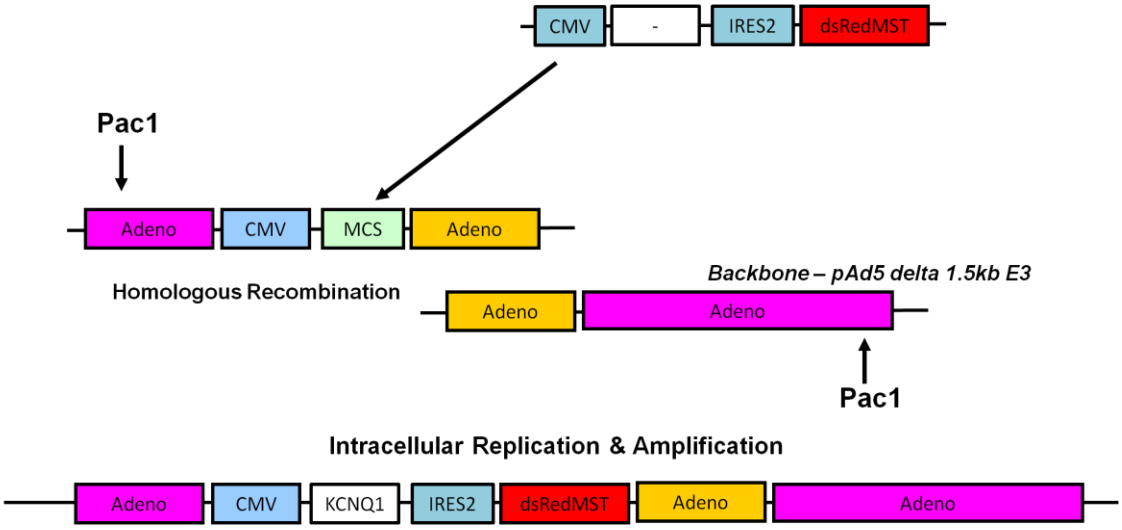

Figure 20. Adenovirus generation vectors. Shuttle vector was created by cloning dsRedMST vector into adenoviral multi-cloning site. Both shuttle and backbone vector were digested with Pac1 restriction enzyme to linearize. Linear shuttle and backbone vectors were transfected with calcium-phosphate into HEK293 cells where they underwent homologous recombination to create full adenoviral vector. Intracellular replication and amplification in cells yielded adenovirus capable of transducing the dsRedMST gene into target cells. Adapted from University of Iowa Gene Transfer Core.

Voltage clamp electrophysiology

Potassium currents were recorded from myocytes cells using the whole-cell configuration of the patch clamp technique.[55] The extracellular solution contained in mM: 137 NaCl, 5.4 KCl, 2 $CaCl_2$, 1 $MgCl_2$, 10 Glucose, 10 HEPES, 0.05 $CdCl_2$, pH 7.4. The standard intracellular solution contained in mM: 110 K Glutamate, 10 KCl, 10 NaCl, 14 EGTA, 5 HEPES, 2 $CaCl_2$, 5 Mg-ATP, pH 7.2. Pipette solution was diluted 5-10% to prevent activation of swelling-activated currents. Patch pipettes were pulled from thick wall borosilicate glass (World Precision Instruments, Inc.) with a multistage P-97 Flaming-Brown micropipette puller (Sutter Instrument Co., Novato, CA) and heat-polished with a Micro Forge MF 830 (Narashige International USA, Inc., East Meadow, NY). After heat polishing, the resistance of the patch pipettes was 2-4 megaohms in the standard solutions. A 2% agar bridge with composition similar to the control bath solution was used as a reference electrode. Unless otherwise stated, all chemicals were obtained from Sigma-Aldrich (St. Louis, MO).

Whole-cell currents were recorded at room temperature (20–23°C) using an Axopatch 200B amplifier (MDS Analytical Technologies, Sunnyvale, CA). Test pulses were generated using Clampex 8.1 (MDS Analytical Technologies), and whole-cell currents were acquired at 5 kHz and filtered at 1 kHz. The access resistance and apparent membrane capacitance were estimated as described previously.[56] Whole-cell currents were not leak subtracted. Junction potentials

were zeroed with the filled pipette in the bath solution. All recordings were started 4 min after achieving a whole cell patch.

For guinea pig atrial myocyte potassium currents, whole-cell currents were measured during a series of 2 s voltage steps from a holding potential of −40 mV to test potentials ranging from −40 to +60 mV (in 10 mV increments) followed by a 1 s step to −30 mV to record tail currents with a 10 s interpulse duration. Due to presence of an endogenous inward background potassium current in guinea pig atrial myocytes,[57] the cells needed to be held at a higher holding potential than -80 mV to prevent activation of this current.

For rabbit atrial myocyte potassium currents, whole-cell currents were measured during a series of 2 s voltage steps from a holding potential of −80 mV to test potentials ranging from −80 to +60 mV (in 10 mV increments) followed by a 1 s step to −30 mV to record tail currents with a 20 s interpulse duration. The extended interpulse duration was used to allow for recovery of the transient outward potassium current, I_{to}.

Current clamp electrophysiology

Action potentials were elicited from atrial myocytes using the whole-cell configuration of the patch clamp technique[55] and previously described solutions.[58] The extracellular solution contained in mM: 140 NaCl, 5.4 KCl, 1 $MgCl_2$, 1 $CaCl_2$, 7.5 glucose, 0.33 NaH_2PO_4, and 5 HEPES, pH 7.4. The intracellular solution contained in mM: 120 KCl, 10.25 NaCl, 5 $MgCl_2$, 0.36 $CaCl_2$, 5 HEPES, 5 EGTA, 5 creatine phosphate (Tris), 5 glucose, and 5 K_2ATP, pH 7.2. Patch pipettes were pulled from thick wall borosilicate glass (World Precision Instruments, Inc., Sarasota, FL) with a multistage P-97 Flaming-Brown micropipette puller (Sutter Instrument Co., Novato, CA) and heat-polished with a Micro Forge MF 830 (Narashige International USA, Inc., East Meadow, NY). After heat polishing, the resistance of the patch pipettes was 1.5-2.5 megaohms in the above solutions. A 2% agar bridge with composition similar to the control bath solution was used as a reference electrode.

Action potentials were elicited at room temperature (20–23°C) using an Axopatch 700B amplifier (MDS Analytical Technologies, Sunnyvale, CA). Pulses were generated using Clampex 9.1 (MDS Analytical Technologies), and action potentials were acquired at 10 kHz. No current was injected to maintain resting membrane potentials. To elicit action potentials, a stimulus threshold was determined for each myocyte, using a protocol of 0.1 nA steps of 3-4 ms duration (Figure 21).

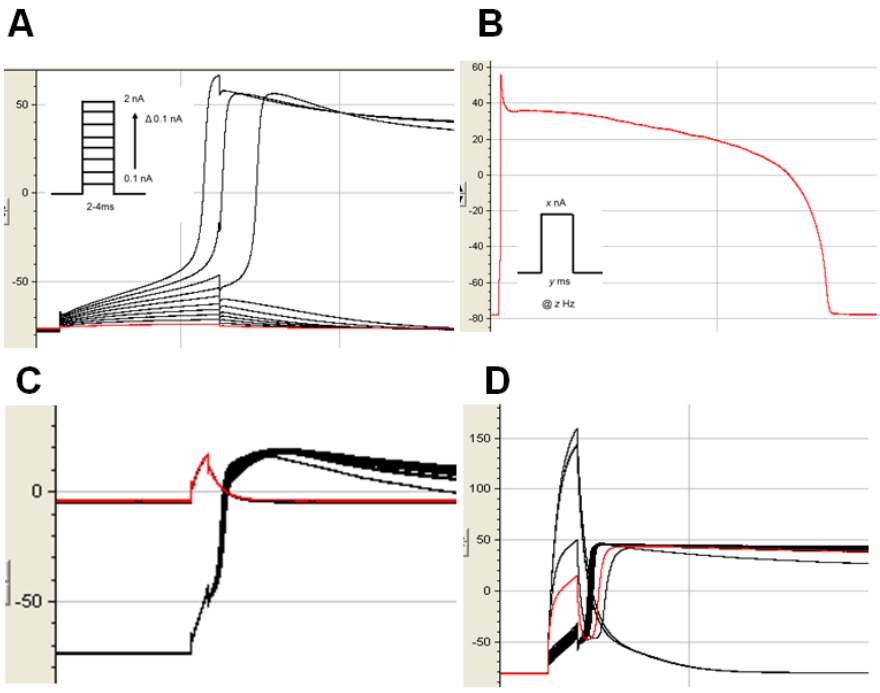

Figure 21. Eliciting action potentials from adult cardiac myocytes. **A,** Example of threshold protocol with square wave current injection to determine optimal stimulus to elicit action potential with overstimulus exceeding the action potential amplitude (top trace), smooth activation of the action potential (middle trace), and understimulus with delayed activation of the AP, the threshold of AP activation (lowest AP). **B,** Example of AP elicited at optimal stimulus with no activation artifact, typically 1.25x threshold stimulus; **C**, Example of action potential before and after small leak (<50 mV) leak developed in the seal; **D**, Example of action potential as whole-cell seal closes, increasing the mV during the stimulus pulse.

Results

Calcium-tolerant cardiac myocytes

High yields of calcium-tolerant cardiac myocytes from all chambers were obtained for both adult guinea pig and adult rabbit hearts. Once the optimal lot of collagenase II was identified and digestion time was determined empirically, guinea pig ventricular and atrial myocytes could be isolated simultaneously. The key step for high yield of guinea pig atrial myocyte isolation was waiting 3 h before adding culture media or bath solution for patch clamp experiments when cells get exposed to physiologic levels of calcium. Slow calcium titration or shorter recovery period resulted in hypercontraction of myocytes. Ventricular myocytes could tolerate exposure to higher calcium concentrations earlier than atrial myocytes. Acutely isolated myocytes had crisp cellular borders and clearly visible striations (Figure 22).

While guinea pig atrial and ventricular myocytes could be isolated simultaneously with high yields, rabbit atrial myocyte isolation proved more challenging. Modifications to the traditional Langendorff method were critical to achieve high yields of rabbit atrial myocytes. First, the pulmonary vessels were clamped with microvessel clips to inflate both atrial chambers at high pressure in order to achieve atrial perfusion. The atria were then punctured at their apex to facilitate the drainage of the perfusate without loss of pressure. Further, we found

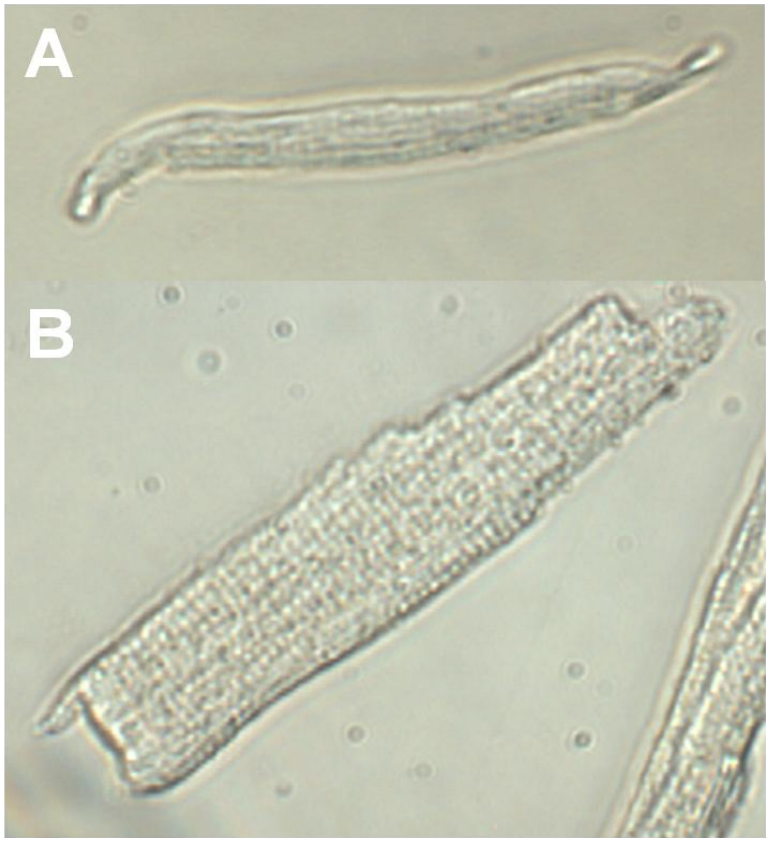

Figure 22. Acutely isolated guinea pig adult cardiac myocytes. **A**, left atrial myocytes and **B**, left ventricular myocyte captured at 40x with light microscopy.

enzymatic digestion using Liberase TH was more reliable with less lot-to-lot variability than commonly used collagenases. To monitor the progression of the enzymatic digestion, we employed a novel serial sampling technique that enabled a reproducible high yield of isolated cardiomyocytes. For ventricular digestion, a small superficial incision was made in the ventricular wall within the area between the major coronary vessels. Serial tissue samples were excised every 0.5-1.0 minutes from the incised myocardium and the extent of myocyte release was assessed immediately by light microscopy. When the majority of released myocytes appeared as quiescent (non-contracting) and rod-shaped, the left and right atria were removed from the heart and placed in enzyme solution while the remaining cardiac chambers (right and left ventricles) were placed in cold BSA-solution to stop enzymatic activity.

Critical to rabbit atrial myocyte isolation and exclusive to our protocol, each atrium was recannulated one at a time on the Langendorff apparatus (modified Langendorff prep) and enzymatic perfusion was resumed. Serial tissue samples were taken from the atrial wall and examined by light microscopy until the majority of cells released were quiescent and rod-shaped. Then, the atrium was removed from the perfusion apparatus. The desired segments of atrial and ventricular tissue were minced in BSA solution, gently triturated, and filtered.

Three key steps further enriched the percentage of rod-shaped myocytes by separating them from hypercontracted, dying cells and preventing cellular damage. First, the healthy myocytes were allowed to settle into a loose pellet by gravity for 30 minutes at room temperature, leaving unhealthy myocytes in suspension. Second, after myocyte resuspension in fresh BSA solution, the cells were plated on laminin-coated coverslips. Healthy myocytes express laminin receptors and adhere to laminin within 1 h. Non-adherent dying myocytes lacking intact laminin receptors get removed with subsequent washes. Third, myocytes anchored to laminin were then left to recover for 2-3 h after the completion of enzymatic digestion before being exposed to physiologic calcium levels in either bath solution for electrophysiology experiments or media for extended culture. Healthy myocytes had crisp borders with clearly visible striations (Figure 23). The time elapsed between the enzymatic digestion and the exposure to high calcium concentration solutions permits the healing of the cell membranes. Again, atrial myocytes were found to be more sensitive than ventricular myocytes. Ventricular myocytes could better tolerate centrifugation or early calcium exposure than atrial myocytes. Both yields improved with the gentler methods of gravity filtration and longer recovery times before calcium exposure.

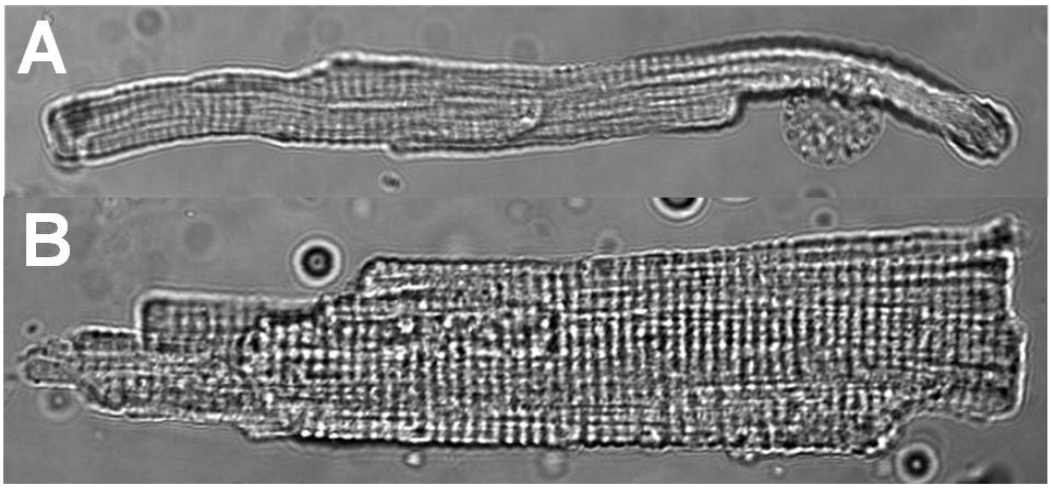

Figure 23. Acutely isolated rabbit adult cardiac myocytes. **A**, left atrial myocyte and **B**, left ventricular myocyte, captured at 63x with light microscopy.

Optimizing culture conditions for adult cardiac myocytes

Because we wanted to express mutant potassium channels in adult cardiac myocytes and most transfection methods typically need 48 h for protein maturation, we sought to optimize culture conditions to extend myocyte viability. Most published experiments with adult cardiac myocytes have been conducted acutely.

First, because cardiac myocytes do not adhere to glass coverslips and lack of adherence results in significant decrease in viability and differentiation,[59] we explored three extracellular matrices for cell culture plating: laminin, fibronectin, and poly-L-lysine. Cardiac myocytes adhered to all three matrices. However, poly-L-lysine allowed the adherence of all cells, regardless of cell viability. With fibronectin and laminin, dead or dying myocytes, known to express fewer of the required receptors, did not adhere and were aspirated with the subsequent exchange of culture media. There was no significant difference in myocyte viability or morphology noted between cardiac myocytes plated on laminin or fibronectin. Laminin is significantly less expensive, so all experiments were conducted with this more economical option.

During our initial myocyte isolations from guinea pig heart, we tested three different bases for myocyte culture media: MEM + Hank's salt, Media 199, Ham's F-10. Initial cultures showed highest number of striated myocytes after 48 h in MEM + Hank's salt base (Figure 24). However, after 72 h, a significant number of myocytes had blebs and difficult to see striations. Based on the insights in Kabaeva *et al* (2008)[52] on culture of adult mouse cardiac myocytes, we explored two critical facets to optimize our myocyte cell culture: addition of buffer and excitation-contraction (EC) uncoupler.

Although MEM + Hank's salt media contains buffer chemicals to maintain pH, the addition of sodium bicarbonate and HEPES plus bringing the pH to 7.4 at 35°C significantly improved the health of myocytes based on cell morphology (Figure 25). Further, the myocyte media retained pH sensitive phenol red color after 24 h incubation with the added buffer compared to the yellow color indicating <7.0 pH in the non-augmented media.

Because isolated adult cardiac myocytes tended to dedifferentiate in culture, the addition of EC uncouplers in culture have been employed to help maintain cell morphology and cell differentiation. For example, 2,3 butane-dione monoximine (BDM), developed in 1955 initially as a chemical phosphatase,[60, 61] is a well-characterized non-competitive inhibitor of skeletal muscle myosin-II.[62] However, milimolar concentrations of BDM are required to uncouple EC in myocytes.

Figure 24. Representative guinea pig adult atrial myocytes cultured with different media bases for 48 h. **A,** MEM-base cultured myocyte with crisp membrane borders, some visible striations and minor membrane blebs evident; **B**, F-10 base cultured myocyte with significant blebs and rounded ends, **C,** Media 199 base media with no visible striations, some blebs, and indistinct membrane borders.

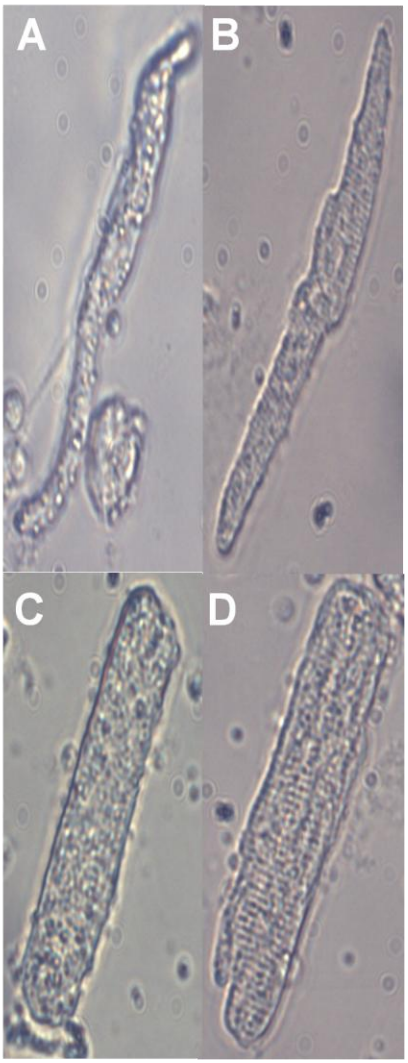

Figure 25. Buffer augmentation in media increases myocyte health in culture. Representative 48 h cultured adult guinea pig myocytes with and without buffer augmentation. **A, B,** guinea pig left atrial myocytes and **C, D** guinea pig left ventricular myocytes cultured without pH buffer augmentation in left column (**A, C**) and with pH buffer augmentation in right column (**B,D**). Buffer augmentation significantly decreases membrane bleb formation and membrane striations are more distinct.

At these concentrations, BDM has been shown to inhibit voltaged-gated calcium currents,[63] transient outward potassium currents,[64] sodium-calcium exchanger[65] and gap junction communication.[66] We explored using a different EC uncoupler, blebbistatin (BLB). Identified in 2003, BLB binds to the ADP-Pi complex of myosin II with high affinity in the micromolar range,[67] and was first used as an EC uncoupler in cardiac myocytes in 2008.[52] BLB is now commonly used in rabbit whole-heart optical mapping to limit movement artifacts.[68] BLB has also been shown not to inhibit critical ionic currents in myocytes at these concentrations.[69] We tested both BDM and BLB as EC uncouplers in guinea pig myocyte culture. Cardiac myocytes treated with BLB had increased viability, membrane integrity, and maintained morphology of adult cardiac myocytes (Figure 26).

However, high concentrations of BLB made myocyte membranes stiff and difficult to achieve a seal in whole cell patch clamp experiments. We tested concentrations of 1-200 μM BLB to achieve optimal balance in maintaining cell viability and achieving whole cell patch clamp. Lower concentrations slightly decreased the yield of viability myocytes over time and cell membrane edges were less crisp but did facilitate the ability to achieve whole cell patches for electrophysiology experiments. We used 5 μM as the minimal concentration of BLB concentration required to maintain myocyte viability and differentiation. All rabbit myocytes were cultured using this concentration of BLB with optimized media and added buffer on laminin (Figure 27).

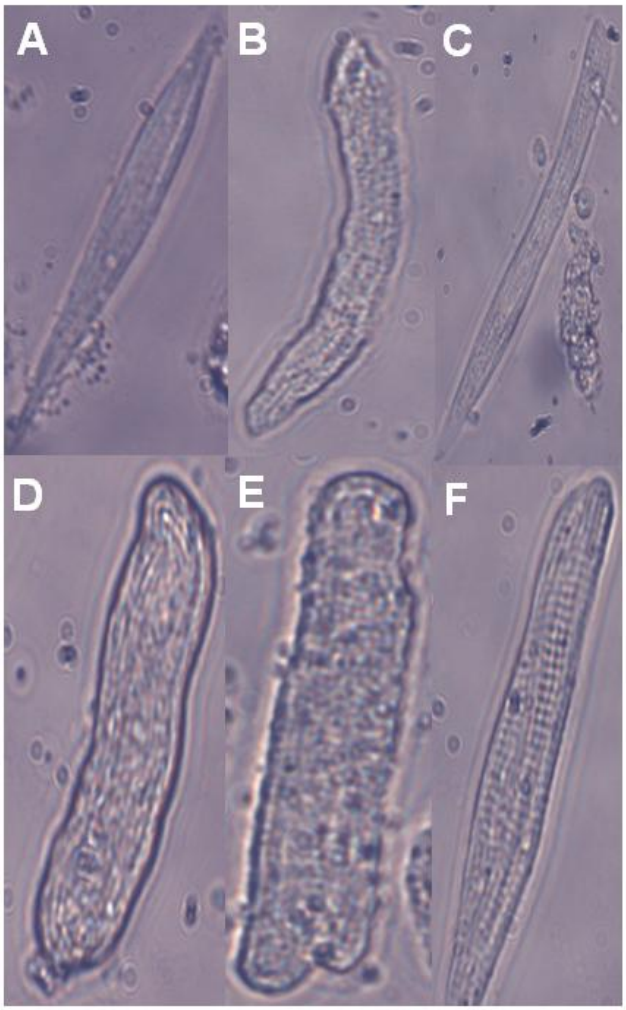

Figure 26. Blebbistatin extends culture viability of guinea pig adult myocytes. **A, B,C** are representative adult guinea pig left atrial myocytes and **D,E,F** are representative adult guinea pig left ventricular myocytes after 120 h in cultured with either no EC uncoupler (left column, **A,D**), 30 mM BDM (middle **column B, E**), or 100 μM BLB (right column **C,F**).

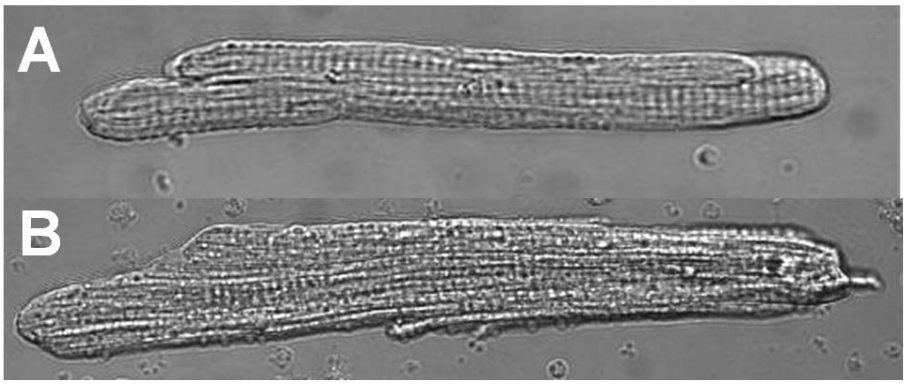

Figure 27. Representative adult rabbit myocytes cultured for 72 h in optimized culture conditions; **A,** left atrial myocyte and **B,** left ventricular myocyte.

Transfection of adult cardiac myocytes

Having established optimal culture conditions for adult cardiac myocytes, we used several methods to attempt to transfect these myocytes with plasmids expressing dRedMST: electroporation, lipid transfection, biolistics, lentivirus and adenovirus. Extensive experiments and many permutations of variables were unsuccessful in transfecting with electroporation or lipid based methodology. Variable success was achieved with biolistics, lentivirus and adenovirus.

Biological ballistics, or biolistics using the "gene gun", is a method that has recently been successfully employed to transfect acutely isolated adult rat ventricular myocytes.[53] In biolistics, DNA is precipitated on to small gold beads with calcium phosphate. These 'bullets' are loaded into small tubes or 'cartridges,' which are then shot with an air gun, specifically designed 'gene gun,' using helium gas at adjustable pressure. We optimized this method for transfection of adult guinea pig atrial myocytes. We observed the highest transfection rates using larger gold beads (1.6 μm diameter), 100 PSI, a PVP concentration of 0.015 mg/ml, 0.5 mg of gold delivered per shot (microcarrier loading ratio), 2 μg DNA to 1 mg gold (for a 2:1 DNA loading ratio), and shooting from a distance equal to the barrel length. Further, highest myocyte survival was achieved if cells were shot 24 h post-isolation. Expression of dsRedMST could be visualized 24 h after transfection, 48 h after isolation (Figure 28).

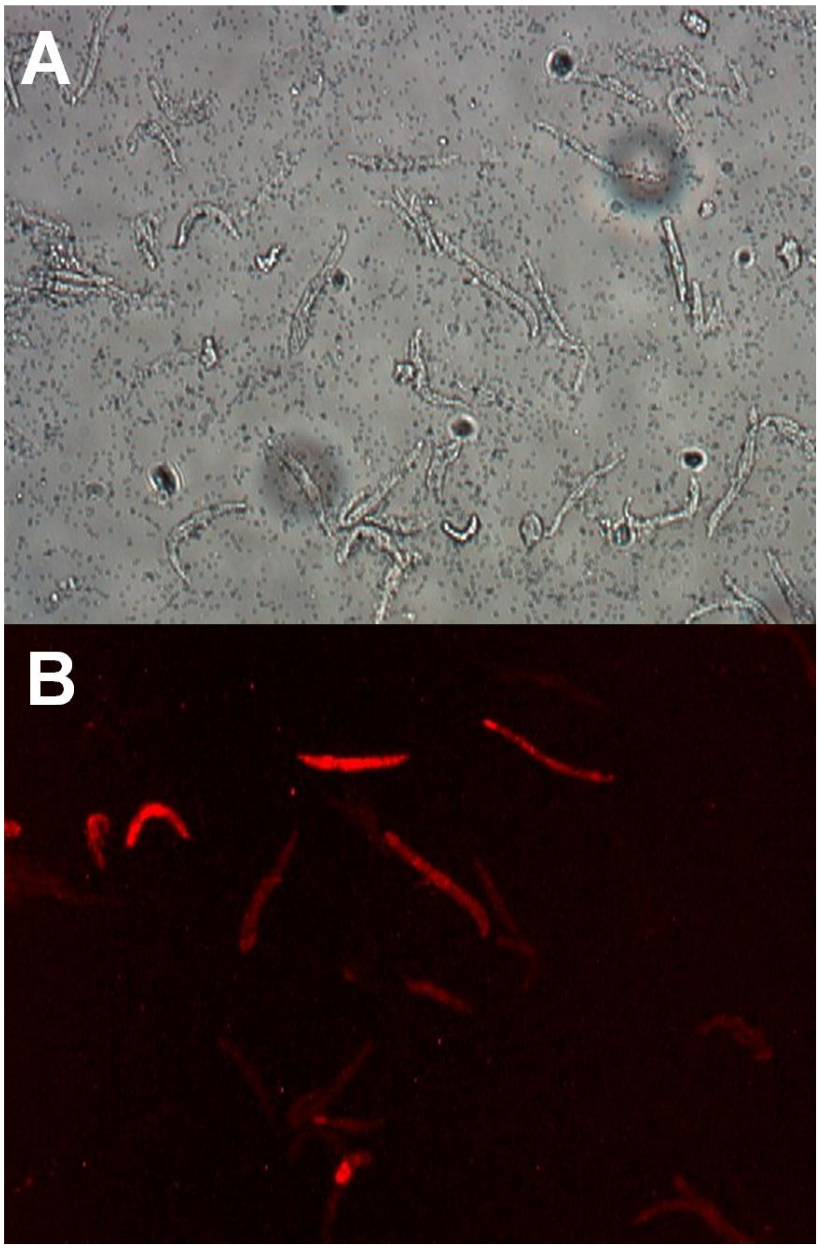

Figure 28. Biolistic transfection of adult guinea pig atrial myocytes with dsRedMST. **A,** bright field image at 10x with bullets visible **B,** same field under fluorescence illustrating expression of dsRedMST in myocytes.

Unfortunately, biolistics did not succeed with the more fragile adult rabbit atrial myocytes. In particular, the pressure used to shoot the atrial myocytes could not be refined to transfect the atrial myocytes without killing the cells whereas lower pressures resulted in the bullets 'rolling' off the atrial myocytes.

Two different viral delivery systems, lentivirus and adenovirus, were employed to optimally transduce rabbit atrial myocytes. Lentivirus transduction of guinea pig myocytes was successful. Lentivirus had the advantage of fast virus generation time (3-5 d), but the resulting titers are inconsistent. In addition, the time to transgene expression was over 5 days and the transduction rate had a very low efficiency. Lentivirus integrates into the target cell genome, which could have deleterious effects. This property is more optimal for creating stable cell lines. Due to these limitations, we opted for the longer to generate (6 weeks) but more reliable transduction with adenovirus. Using dsRedMST expression maker, both adult guinea pig and rabbit atrial myocytes were transduced with adenovirus at high efficiency in a shorter time frame (2 days) (Figure 29) .

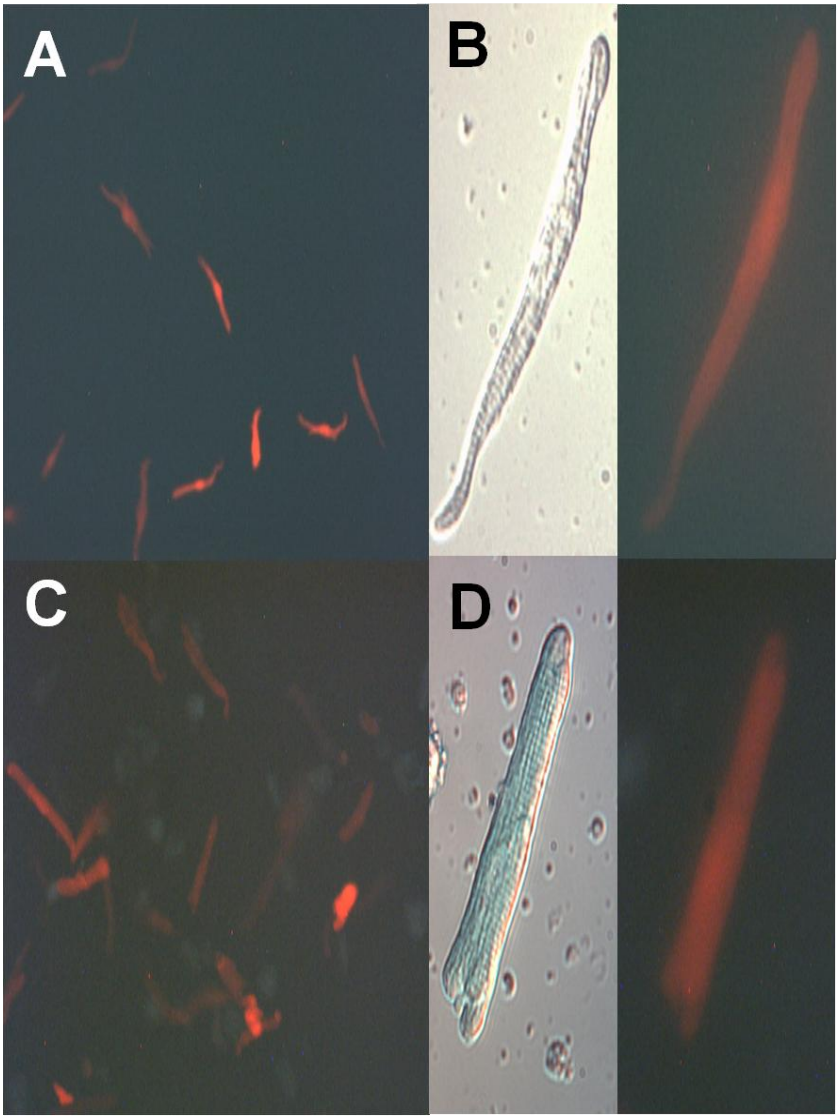

FIgure 29. Adenoviral transduction of guinea pig and rabbit adult atrial cardiac myocytes with dsRed-MST. **A,** 10x fluorescent image of guinea pig atrial myocytes expressing dsRedMST and **B,** 40x bright-field (R) and fluorescent image (L) of a single guinea pig atrial myocyte. C, 10x fluorescent image of rabbit atrial myocytes expressing dsRedMST; D, 40x bright-field (R) and fluorescent image (L) of a single rabbit atrial myocyte.

Electrophysiology of adult cardiac myocytes

To ascertain whether cardiac myocytes cultured under the conditions we developed maintained hallmark electrophysiological properties, we conducted whole-cell patch clamp experiments to ascertain potassium currents (Figure 30). Previously described differences were observed between guinea pig and rabbit atrial cardiac myocytes. Guinea pig atrial myocytes had a distinct background inward potassium current. To best measure outward potassium current, we held the resting membrane potential at -40 mV. Slowly activating outward currents consistent with predominantly I_{Ks} and I_{Kr} were observed. In rabbit atrial myocytes, a significant fast activating current was noted and attributed to Ito. Because of significant run-down of I_{to} with short interpulse duration (5s), the interpulse duration was extended to 20s to better record the outward current properties. Further, action potentials elicited from cultured guinea pig and atrial myocytes were consistent with anticipated results (Figure 31).

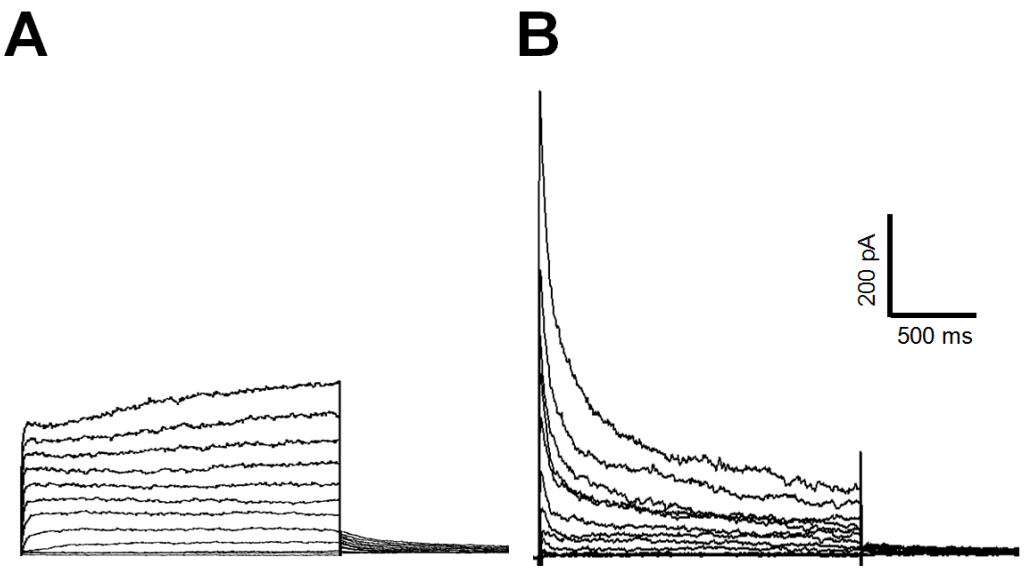

Figure 30. Representative potassium current recording from cultured adult atrial cardiac myocytes. Potassium currents from 48 h cultured **A**, guinea pig left atrial cardiac myocyte and **B**, rabbit left atrial cardiac myocyte/

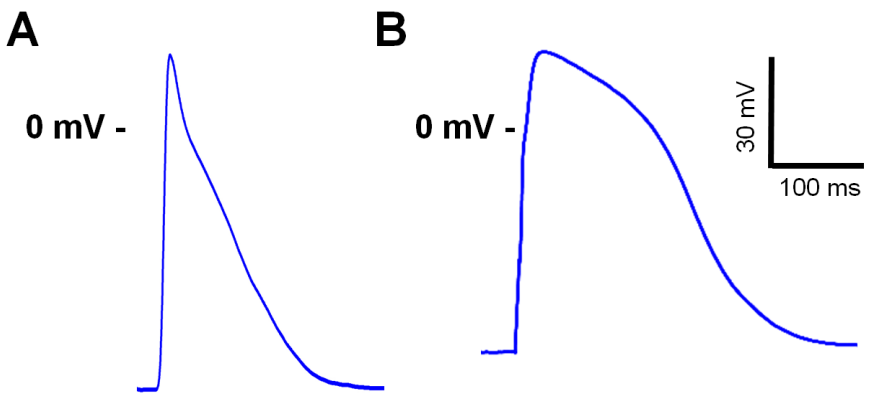

Figure 31. Representative action potential recording from cultured adult atrial cardiac myocytes. Action potentials from 72 h cultured **A**, guinea pig left atrial cardiac myocyte action potential and **B**, rabbit left atrial cardiac myocyte action potential.

Discussion

We developed methods for high yield isolation, extended culture, and transfection of adult cardiac myocytes suitable for electrophysiological experiments. While guinea pig atrial and ventricular myocytes could be isolated simultaneous once an optimal lot of collagenese II was identified and digestion time was empirical determined, multi-chamber isolation of adult rabbit myocytes required more extensive modifications to the traditional Langendorf methods. Using a novel serial sampling technique, we were able to achieve reproducible high yields of both ventricular and atrial myocytes. Importantly, the optimal digestion time varied widely between rabbit heart preparations. After achieving optimal ventricular digestion, left and right atria are removed and sequentially recannulated for further perfusion (modified Langendorff preparation). Yields of calcium tolerant cardiomyocytes were further enriched by gravity pelleting rather than centrifugation between wash steps, plating on laminin-coated coverslips, and at least a 2 h recovery time before exposure to physiological levels of calcium in culture media.

The culture of adult cardiac myocytes with preserved morphology for 5 days was optimized though the use of laminin as an extracellular matrix to promote cell adherence, the identification of MEM as a base for culture media, the augmentation of pH buffering capacity, and the use of a low concentration of the E/C-uncoupler, blebbistatin. Although the transfection of adult cardiac myocytes was not achieved through multiple parameter optimization of electroporation and

lipid-based methods, biolistics and viral methods were successful. Using biolistics, guinea pig atrial myocytes were reliabley transfected with rapid fluorescent marker gene expression time (<24 h); whereas rabbit atrial myocytes proved too fragile to withstand biolistic impalement. Lentiviral and adenoviral methods both were successful to transduce adult cardiac myocytes; adenovirus-mediated transduction was most efficient with high titers and robust expression of in myocytes. Electrophysiology confirmed the utility of these isolated cultured myocytes for future experiments.

The key advantage to these methods is the ability to isolate robust quantities of high quality adult mammalian cardiomyocytes from both atria and ventricles at the same time and from the same animal with a *reliable method* to monitor enzymatic digestion progression for both chambers to determine their best termination time. The availability of large quantities of healthy isolated adult atrial myocytes adds considerable value to studying adult arrhythmias such as atrial fibrillation, the most common sustained cardiac arrhythmia encountered in the clinical practice.

There are limitations to using isolated cardiomyocytes from any source. Because these are isolated primary cells, studies are limited to answering specific questions related to single cells such as the duration of the action potential and the characteristics of component ionic currents. Determining the effective refractory period, measuring conduction velocity, and analyzing the development of arrhythmogenic foci are better answered at the tissue or whole heart level.

Isolated atrial and ventricular adult guinea pig and rabbit myocytes can be used for the acute study of their structural (microanatomy), functional and pharmacological properties (electrophysiology and calcium dynamics). Robust yields of high quality cells are fundamental to obtain reproducible results and expand the opportunities to subacute studies such as viral transduction for gene overexpression or suppression with RNA interference that require short term tissue culture. Cultured myocytes also provide a platform for longer term studies of drug toxicity. Using these developed methods, we explore the effects of familial atrial fibrillation mutation, KCNQ1-S140G, expression on adult rabbit cardiac myocytes.

CHAPTER III

FAMILIAL ATRIAL FIBRILLATION ASSOCIATED KCNQ1 MUTATION SHORTENS ADULT RABBIT ATRIAL ACTION POTENTIAL DURATION AND INCREASES TRIGGERED ACTIVITY

Introduction

Atrial fibrillation is the most common sustained cardiac arrhythmia and its incidence is exponentially increasing in our society with an anticipated affected population exceeding 16 million by 2050.[1] Recent identification of monogenic causes of atrial fibrillation have provided insight into the substrate susceptibility required for the generation of the AF phenotype. Intriguingly, although the electrophysiological consequences of these mutant FAF-associated genes are present at birth, the clinical manifestation of FAF does not occur until later in life suggested the necessity of acquired factors for the full clinical phenotype. Electrophysiological characterization of KCNQ1 mutations associated with FAF suggest a gain-of-function phenotype with many mutations resulting in constitutive activity in physiologic conditions.[2, 15, 19, 20] Mathematical modeling has been used to extrapolate the results of these gain-of-function mutation to atrial myocytes, but no studies have investigated the consequences of expression in native atrial myocytes.

Having established cell isolation conditions and exogenous gene expression methods for rabbit atrial myocytes in the previous chapter, our approach here is to investigate the consequences of S140G-I_{Ks} expression in rabbit atrial myocytes. We hypothesized that expression would shortened action potential duration. At a tissue level, this abbreviated APD would contribute to a shortened tissue effective refractory period, leaving the atria vulnerable to triggered re-entrant circuits. We tested this hypothesis by first electrophysiologically characterizing the endogenous expression of I_{Ks} in rabbit atrial myocytes and then by using a modified adenovirus to exogenously express S140G-I_{Ks} in adult rabbit atrial myocytes.

Here we present evidence that under our recording conditions I_{Ks} is not endogenously expressed in rabbit atrial myocytes. Further, to express I_{Ks} in rabbit atrial myocytes, a modified adenoviral promoter must be used to generate the potassium channel expressing virus and that a very high MOI is necessary to generate expression. In S140G-I_{Ks} expressing myocytes, we demonstrated evidence of triggered activity at low frequency stimulation and a shorter action potential duration at higher frequency with hyperpolarized resting membrane potential compared to WT-I_{Ks} expressing myocytes. Overall, we illustrate effects of the FAF-associated mutation S140G-I_{Ks} in a native adult atrial myocyte supporting the notion that a shortened APD likely underlies substrate susceptibility.

Methods

Adenoviral vectors

Human KCNQ1 and KCNE1 cDNAs were generated as described previously.[3] The S140G was engineered in KCNQ1 using QuikChange mutagenesis (Stratagene Corp, La Jolla, CA). Adenovirus vectors, pAd5-CMVK-NpA and pAd5-(9.2-100)delta1.6KbE3, were obtained from the University of Iowa Gene Transfer Vector Core (supported in part by the NIH and the Roy J. Carver Foundation). Using the pAd5-CMVK-NpA vector, we created shuttle vectors for KCNQ1-IRES2-DsRedMST, S140G-IRES2-DsRedMST, KCNE1-IRES2-eGFP, and IRES2-DsRedMST. Shuttle vectors were initially made using the CMV promoter. However, using this promoter, the KCNQ1 and S140G shuttle vectors failed to generate a virus. Thus a modified CMV promoter was used for all shuttle vectors. This modified promoter consisted of the CMV immediate early promoter sequence immediately followed by the last 358 nucleotides of IRES2. This modification was hypothesized to attenuate promoter efficiency and enabled more efficient generation of KCNQ1 encoding adenovirus.

Adenoviral generation

Adenovirus was generated using the RAPAd^{TM} system as previously described.[54] In brief, each shuttle vector and the backbone vector pAd5-(9.2-100)delta1.6KbE3 were co-precipitated with calcium-chloride into human embryonic kidney (HEK) 293 cells in 60 mm Petri dishes. When 60% of cells had

detached (12-14 days for KCNE1 and vector-only viruses; 17-25 days for KCNQ1 and S140G), the cells and media were harvested, lysed through repeated freezing/thawing cycles, and amplified in HEK cells (typically using 5-10 150 mm Petri dishes). After 60% of cells detached from the large dishes (1-3 days), cells were pelleted by centrifugation and resuspended in 5 ml of viral storage solution (10 mM Tris, 2 mM $MgCl_2$, 4% sucrose, pH 8.0). Cells were then lysed and centrifuged. The supernatant was stored at −80°C in single use aliquots and the virus was used within 5 months.

Adenoviral confirmation

Activity of each virus prep was confirmed for fluorescent marker (Figure 32) and potassium channel expression by transduction and subsequent whole cell patch clamp of CHO cells (Figure 33) stably expressing the coxsackie adenovirus receptor (CHO-CAR cells), generously provided by Dr. Jeffrey Bergelson at the University of Pennsylvania.[70] CHO-CAR cells were grown at 37°C with 5% CO_2 in F-12 nutrient mixture medium supplemented with 10% fetal bovine serum (FBS, Atlanta Biologicals, Atlanta, GA), penicillin (50 units/ml), streptomycin (50 µg/ml), and L-glutamine (2 mM). 0.1 or 0.01 µl of each viral prep was added to a 35 mm dish of 60% confluent CHO-CAR in 0.5 ml media and incubated for 4 h. Virus was aspirated and fresh culture media was added. Retrospectively, adenovirus was added at an approximate multiplicity of infection (MOI) of 0.5-1.

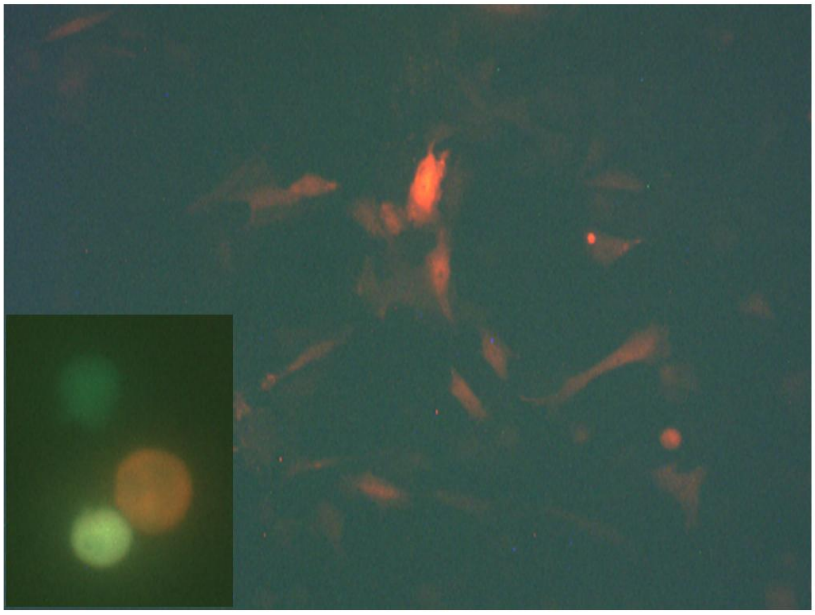

Figure 32. Representative fluorescence expression in CHO-CAR cells after adenoviral transduction; *Image*: CHO-CAR cells 36 h after KCNQ1-IRES2-DsRedMST transduction, captured at 10x, illustrating the variable degree of fluorescence expression. *Inset*: Co-transduction of CHO-CAR cells with KCNQ1-WT-IRES2-DsRedMST and KCNE1-IRES2-eGFP captured at 40x, illustrated the fluorescence expression of red (Q1-DsRedMST), green (E1-eGFP), and yellow (Q1-DsRedMST and E1-eGFP co-expression).

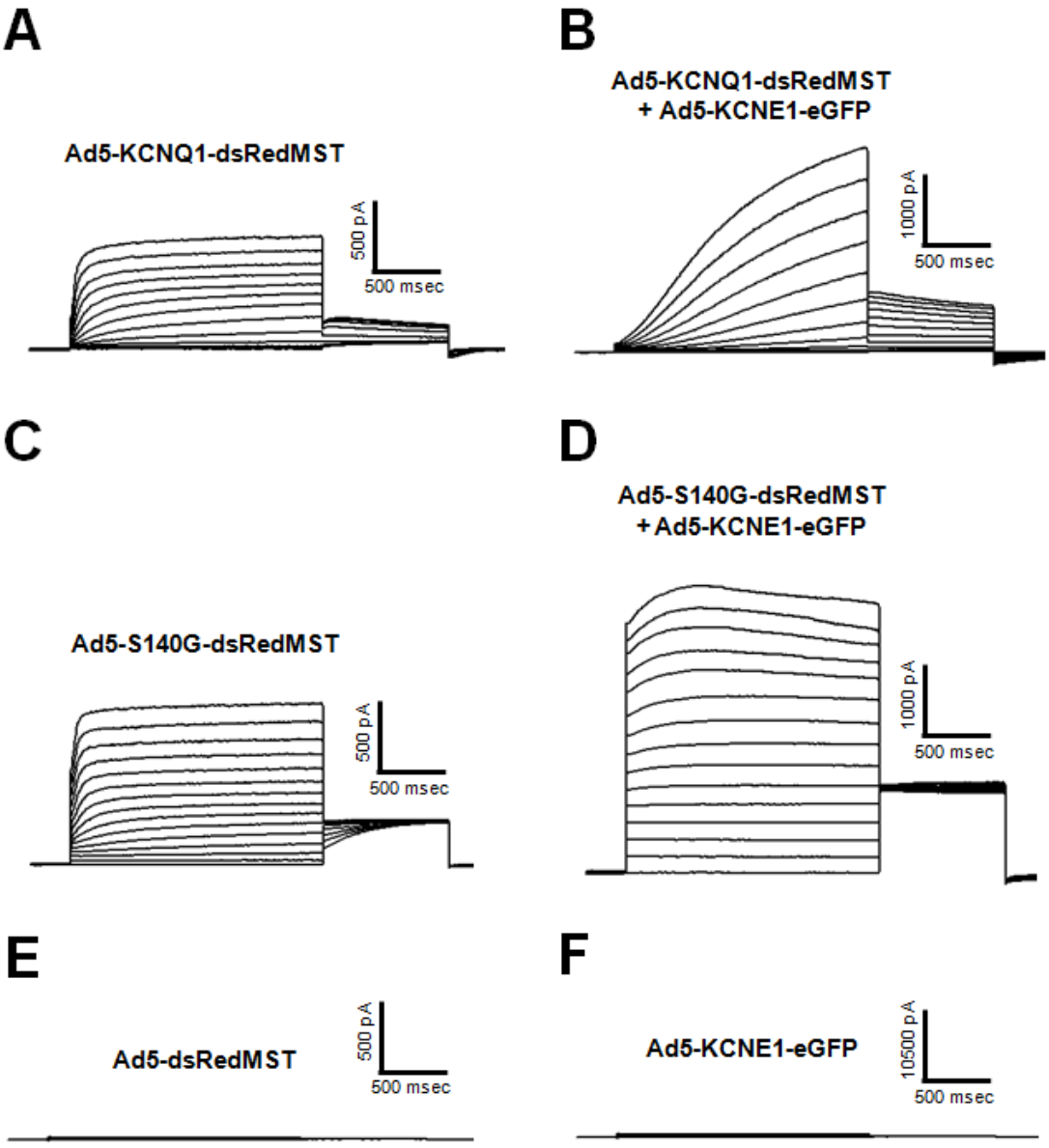

Figure 33. Representative potassium currents recorded from CHO-CAR cells after adenoviral transduction; **A**, KCNQ1 tranduction alone; **B**, KCNQ1 + KCNE1 co-transduction; **C**, S140G transduction alone; **D,** S140G and KCNE1 co-transduction; **E**, dsRedMST alone transduction; **F**, KCNE1 transduction alone.

After 36 h, potassium currents were recorded from fluorescent CHO-CAR cells using standard solutions. The extracellular solution contained in mM: 132 NaCl, 4.8 KCl, 1.2 $MgCl_2$, 1 $CaCl_2$, 5 glucose, and 10 HEPES, pH 7.4. The intracellular solution contained in mM: 110 potassium-aspartate, 1 $CaCl_2$, 10 HEPES, 11 EGTA, 1 $MgCl_2$, and 5 K_2ATP, pH 7.35. Pipette solution was diluted 5-10% to prevent activation of swelling-activated currents. Patch pipettes were pulled from thick wall borosilicate glass (World Precision Instruments, Inc.) with a multistage P-97 Flaming-Brown micropipette puller (Sutter Instrument Co., Novato, CA) and heat-polished with a Micro Forge MF 830 (Narashige International USA, Inc., East Meadow, NY). After heat polishing, the resistance of the patch pipettes was 2-4 megaohms in the standard solutions. A 2% agar bridge with composition similar to the control bath solution was used as a reference electrode. Unless otherwise stated, all chemicals were obtained from Sigma-Aldrich (St. Louis, MO).

Whole-cell currents were recorded at room temperature (20–23°C) using an Axopatch 200B amplifier (MDS Analytical Technologies, Sunnyvale, CA). Test pulses were generated using Clampex 9.1 (MDS Analytical Technologies), and whole-cell currents were acquired at 5 kHz and filtered at 1 kHz. The access resistance and apparent membrane capacitance were estimated as described previously.[8] Whole-cell currents were not leak subtracted. Junction potentials were zeroed with the filled pipette in the bath solution. All recordings were started 4 min after achieving a whole cell patch. Whole-cell currents were measured

during a series of 2 s voltage steps from a holding potential of −80 mV to test potentials ranging from −80 to +60 mV (in 10 mV increments) followed by a 1 s step to −30 mV to record tail currents with a 20 s interpulse duration. Representative images of fluorescent CHO-CAR cells (Figure 32) and potassium channel currents (Figure 33) were obtained for all viral preps to confirm subunit and marker expression.

Adenoviral titer

After confirmation of virus expression, viral titer was determined using the tissue culture infective dose 50 ($TCID_{50}$) method as described for the AdenoVator™ Vector System (QBioGene, Carlsband, CA) (Figure 34). For multiplicity of infection (MOI) calculations, titers were converted to plaque forming units (PFU) by the following equation: $PFU = 0.69*TCID_{50}$. The titers achieved ranged from 10^9 to 10^{10} PFU/ml.

Rabbit left atrial myocyte isolation

Left atrial myocytes were isolated from hearts of male New Zealand White rabbits (6-7 lbs from Charles River Canada), using the method of Bassani, *et al*.[50] with modifications. Briefly, rabbits were sedated with intramuscular acepromazine and then anesthetized with intravenous pentobarbital sodium. Hearts were excised quickly and arrested on ice for 5 minutes in nominally calcium-free minimum essential medium solution (MEM, Joklik modification). Hearts were Langendorf perfused at 37°C for 10-15 min in the same MEM solution gassed with 95% O_2

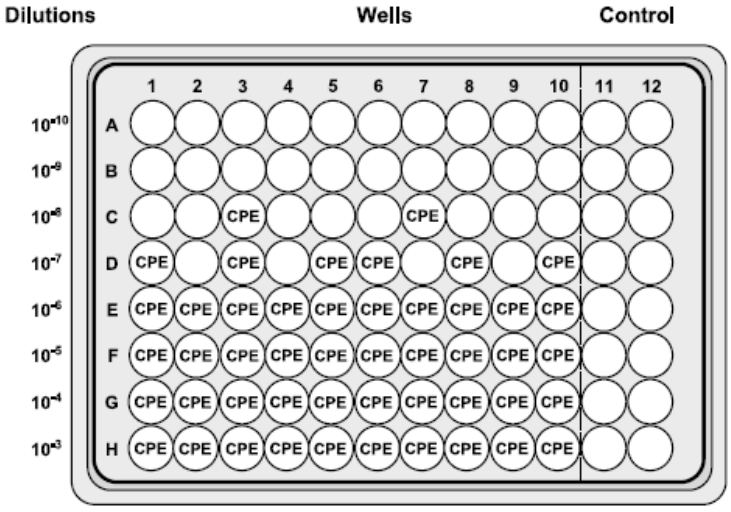

Results

Determine the ratio of positive wells per row.

Dilution	Ratio
10^{-10}	0/10 = 0
10^{-9}	0/10 = 0
10^{-8}	2/10 = 0,2
10^{-7}	6/10 = 0,6
10^{-6}	10/10 = 1
10^{-5}	10/10 = 1
10^{-4}	10/10 = 1
10^{-3}	10/10 = 1

In this example, 100 % of the wells at dilution 10^{-6} are positive, and 0 % of the wells at dilution 10^{-9} are positive, therefore the titer can be precisely determined using the KÄRBER statistical method: For 100 μL of dilution, the titer is $T = 10^{1 + d\,(S - 0.5)}$

d = Log 10 of the dilution (= 1 for a ten-fold dilution).
S = the sum of ratios (always starting from the first 10^{-1} dilution) = 1+1+1+1+1+1+0.6+0.2+0+0 = 6.8

If some of the lowest dilutions are omitted, like 10^{-1} and 10^{-2} above, they still have to be included in the calculation as ratios of 1.

Titer: $T = 10^{1+1\,(6.8\,-\,0.5)} = 10^{7.3}$ (for 100 μL aliquot of virus)
$T = 10^{8.3}$ (equivalent to 2×10^{8}) $TCID_{50}$ / mL

Between duplicates, the difference in titers should be ≤ 0.7 Log.

Figure 34. Typical results of tissue culture infective dose 50 (TCID50) adenoviral titering method with calculation explanation. CPE indicates cytopathic effect, in which any portion of the well demonstrates cell death as compared to the control wells. Adapted from AdenoVator.

and 5% CO_2. During initial perfusion, the pulmonary vessels were closed with microvessel clips to perfuse both atrial chambers at high pressure, and the atrial chambers were punctured twice at their apex to facilitate flow-through. Then the perfusion was switched to MEM solution containing 0.05 mg/ml Liberase TH (Roche Applied Sciences, Indianapolis, IN). After 5 min of enzymatic digestion, a small incision was made in the left ventricle in the area between major coronary vessels. Serial tissue samples (30 s - 1 min) were taken from this incision with fine tweezers and inspected immediately by light microscopy. When the majority of ventricular myocytes released were quiescent rods (7-20 min), the left atrium was removed from the heart, the remaining heart was removed from the Langendorf apparatus, and left atrium was recannulated on the Langendorff apparatus. Serial samples were taken from the perfused atrium until the sample edges contained packets of rod-shaped atrial myocytes and the majority of released atrial myocytes were quiescent rods (5-20 minutes). The left atrium was removed and placed in MEM solution containing 1% bovine serum albumin (BSA). The tissue was minced, gently triturated with a wide-bore pipette, and filtered through a 100 μm cell strainer (BD Biosciences, San Jose, CA) into a 50 ml conical tube. The myocytes were allowed to settle into a soft pellet by gravity for 30 – 60 min at room temperature. Then the supernatant was aspirated, and atrial myocytes were resuspended in fresh BSA solution. Myocytes were plated on laminin-coated glass coverslips, and incubated at 37°C with 5% CO_2. The experimental procedure for isolating rabbit cardiac myocytes was approved by Vanderbilt University Institutional Animal Care and Use Committee.

Rabbit myocyte division for electrophysiology & storage

For three rabbit myocyte isolations, left and right atria were divided into 9 regions (Figure 35). These regions plus the septum were divided. One-quarter was minced, triturated, and plated for electrophysiological experiments and culture. The remaining three-quarters was placed in a screw-capped cryovial, labeled with region, and flash frozen in liquid nitrogen. The labels indicated atrial septum or right or left atria (R or L), anterior, middle, or posterior orientation (A, M, P), and upper, middle, lower area (U, M, L) for a total of 19 regions per rabbit heart atria. In addition, samples of the apical and basal regions of the left and right ventricle and interventricular septum were stored in labeled cryovials and flash frozen in liquid nitrogen. All vials were stored at -80°C .

Atrial myocyte culture and adenoviral transduction

Three hours after termination of enzymatic digestion, myocytes were placed into culture media consisting of MEM supplemented with Hank's salts, 2 mM L-glutamine (Gibco-Invitrogen, Life Technologies, Grand Island, NY), insulin-transferrin-selenium-X supplement (Gibco-Invitrogen, Life Technologies, Grand Island, NY), penicillin (50 units/ml), streptomycin (50 µg/ml), 1% bovine serum albumin, 5 µM blebbistatin at pH 7.4 (modified from Kabaeva, *et al*. 2008)[52]. In some experiments, 6 h post isolation atrial myocytes cultures were paced at 1, or 3 Hz pacing frequency using C-Dish culture dish 4-well electrode and C-Pace EP Culture Pacer (IonOptix LLC, Milton, MA). Pacing decreased the number of viable at 48 h by approximately 50% compared to non-paced cultures.

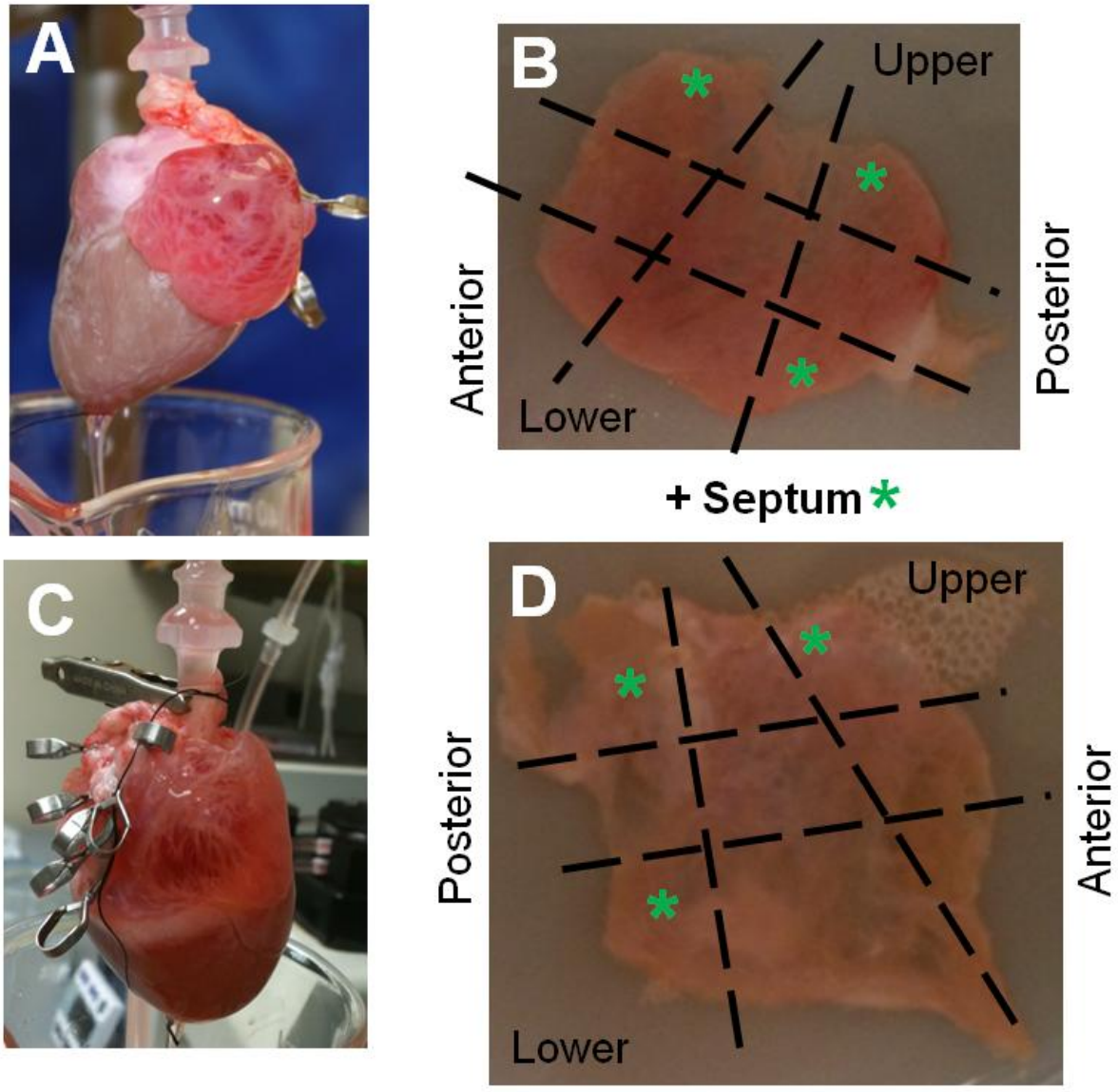

Figure 35. Atrial regional divsions for electrophysiology and -80°C tissue library. **A,** whole heart orientation of the left atria and **C** of the right atria. Example left (**B**) and right (**D**) atria prior to divisions in the same orientation as whole heart images. Dotted lines indicate division lines to be cut with scissors. Labels indicate regional nomenclature. Green * indicate regions from which potassium currents were recorded.

To optimize viral transduction of atrial myocytes, virus was added to the myocytes at a MOI of 1-2,000 immediately after plating in culture media to 6 h post-isolation. Virus was incubated with myocytes for various durations (3 h, 6 h, 12h, 24 h, 36 h, and 48 h). Best expression was achieved after 40 h incubation with an MOI of 2000 added immediately after plating (Figure 3.5). To express WT-I_{Ks}, adenoviruses Ad5-KCNQ1-DsRedMST and Ad5-KCNE1-eGFP were used to co-infect myocytes, whereas S140G-I_{Ks} was generated by co-infecting myocytes with adenoviruses Ad5-S140G-DsRedMST and Ad5-KCNE1-eGFP. Ad5-dsRedMST infection was used for vector only controls. Infected myocytes were cultured at 37°C in 5% CO_2 and used for electrophysiology experiments starting at 40 hours post-isolation. The efficiency of dual transduction of healthy-appearing (striated, rod-shaped) myocytes was approximately 15-20%.

Voltage clamp electrophysiology

Potassium currents were recorded from adult rabbit atrial myocytes cells using the whole-cell configuration of the patch clamp technique.[55] The extracellular solution contained in mM: 137 NaCl, 5.4 KCl, 2 $CaCl_2$, 1 $MgCl_2$, 10 glucose, 10 HEPES, 0.05 $CdCl_2$, pH 7.4. In experiments with drug application, bath solution containing vehicle (<0.01% dimethyl sulfoxide) or HMR-1556 (1 nM - 2 μM) was applied by pencil perfusion using the Automate Valve-link perfusion system. HMR-1556 ((3R,4S)-(+)-N-[-3-hydroxy-2,2-dimethyl-6-(4,4,4-trifluorobutoxy) chroman-4-yl]-N-methyl-ethanesulfon-amide), was synthesized by the

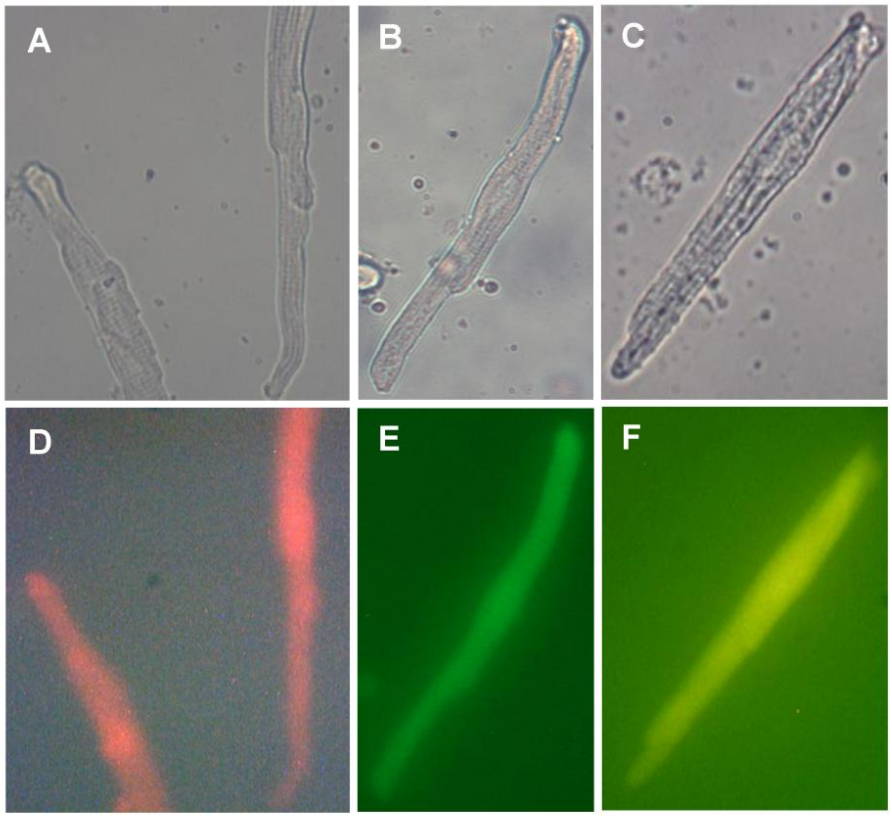

Figure 36. Adenoviral transduction of adult rabbit left atrial myocytes after 52 hours in culture. Representative bright field (**A-C**) and fluorescent (**D-F**) images of the same atrial myocytes. Myocytes were transduced with Ad-S140G-dsRedMST (**A,D**), Ad-KCNE1-eGFP (**B,E**), or both Ad-S140G-dsRedMST and Ad-KCNE1-eGFP (**C,F**).

Vanderbilt Institute of Chemical Biology Synthesis Core using a published method.[71] In experiments with β-adrenergic stimulation, 1 μM or 10 μM isoproterenol and 250 or 1 mM 8-bromo-cAMP were applied by pencil perfusion for 1-10 minutes. Isoproterenol was freshly prepared prior to each use. 8-bromo-cAMP was used from -20°C frozen stocks at 100 mg/ml in dH_2O, prepared in low light conditions. All solutions with 8-bromo-cAMP were covered with aluminum and experiments were conducted in low light conditions. The standard intracellular solution contained in mM: 110 K-glutamate, 10 KCl, 10 NaCl, 14 EGTA, 5 HEPES, 2 $CaCl_2$, 5 Mg-ATP, pH 7.2. Pipette solution was diluted 5-10% to prevent activation of swelling-activated currents. In experiments with pipette applied factors, 250 μM 8-bromo-cAMP or 10 μM phosphatidylinositol 4,5-bisphosphate (PIP2) were added to the pipette solution. PIP2 was prepared from 1 mg/ml stock chloroform/methanol/water solution, stored at -20C, as provided by manufacturer (Avanti Polar Lipids, Inc Alabaster, AL). PIP2 solution (10 μl) was added to a glass test tube and the solution was allowed to evaporate (<5 mins). Then, 1 ml pipette solution was added to PIP2 and the tube was sonicated for 30 mins prior to use for patch clamp.

Patch pipettes were pulled from thick wall borosilicate glass (World Precision Instruments, Inc.) with a multistage P-97 Flaming-Brown micropipette puller (Sutter Instrument Co., Novato, CA) and heat-polished with a Micro Forge MF 830 (Narashige International USA, Inc., East Meadow, NY). After heat polishing, the resistance of the patch pipettes was 2-4 megaohms in the standard solutions.

A 2% agar bridge with composition similar to the control bath solution was used as a reference electrode. Unless otherwise stated, all chemicals were obtained from Sigma-Aldrich (St. Louis, MO).

Whole-cell currents were recorded at room temperature (20–23°C) using an Axopatch 200B amplifier (MDS Analytical Technologies, Sunnyvale, CA). Test pulses were generated using Clampex 9.1 (MDS Analytical Technologies), and whole-cell currents were acquired at 5 kHz and filtered at 1 kHz. The access resistance and apparent membrane capacitance were estimated as described previously.[56] Whole-cell currents were not leak subtracted. Junction potentials were zeroed with the filled pipette in the bath solution. All recordings were started 4 min after achieving a whole cell patch.

Whole-cell potassium currents were measured during a series of 2 s voltage steps from a holding potential of −80 mV to test potentials ranging from −80 to +60 mV (in 10 mV increments) followed by a 1 s step to −30 mV to record tail currents with a 20 s interpulse duration.

Current clamp recording

Action potentials were elicited from atrial myocytes using the whole-cell configuration of the patch clamp technique[55] and previously described solutions.[58] The extracellular solution contained in mM: 140 NaCl, 5.4 KCl, 1 $MgCl_2$, 1 $CaCl_2$, 7.5 glucose, 0.33 NaH_2PO_4, and 5 HEPES, pH 7.4. The

intracellular solution contained in mM: 120 KCl, 10.25 NaCl, 5 $MgCl_2$, 0.36 $CaCl_2$, 5 HEPES, 5 EGTA, 5 creatine phosphate (Tris), 5 glucose, and 5 K_2ATP, pH 7.2. Patch pipettes were pulled from thick wall borosilicate glass (World Precision Instruments, Inc., Sarasota, FL) with a multistage P-97 Flaming-Brown micropipette puller (Sutter Instrument Co., Novato, CA) and heat-polished with a Micro Forge MF 830 (Narashige International USA, Inc., East Meadow, NY). After heat polishing, the resistance of the patch pipettes was 1.5-2.5 megaohms in the above solutions. A 2% agar bridge with composition similar to the control bath solution was used as a reference electrode.

Action potentials were elicited at room temperature (20–23°C) using an Axopatch 700B amplifier (MDS Analytical Technologies, Sunnyvale, CA). Pulses were generated using Clampex 9.1 (MDS Analytical Technologies), and action potentials were acquired at 10 kHz. No current was injected to maintain resting membrane potentials. To elicit action potentials, a stimulus threshold was determined for each myocyte, using a protocol of 0.1 nA steps of 3-4 ms duration. The stimulus used for experiments was approximately The stimulus was used to elicited action potentials at 0.1 Hz for 5 mins for an equilibration period. Then, action potentials were elicited for 3 min each at 0.25 Hz, 0.5 Hz, and 1 Hz.

Current clamp data analysis

Data were collected for each experimental condition from at least three separate myocyte isolations and analyzed using a combination of Clampfit 9.1 (MDS Analytical Technologies) and Excel 2007 (Microsoft). Data were transferred from Clampfit to Excel with each recording frequency for each myocyte contained in a separate file. The first column of the file contained the time in msec in 0.1 msec increments. The subsequent columns contained the value, in mV, recorded during each stimulus and elicited action potential. Each column represented a stimulated action potential recording. Each file contained all action potentials recorded over the 3 min recording period. With assistance from Jonathan Campbell (MSOR candidate at SMU), a Visual Basic for Applications (VBA) program in Excel was written to read each file and to determine for each recorded action potential the following parameters: resting membrane potential, amplitude, overshoot, and action potential duration at 20% (APD_{20}), 50% (APD_{50}), and 90% (APD_{90}) (Figure 37). Depending on the number of files, this analysis program could take well over 2 hours to run.

Key mathematical functions in Excel allowed for the rapid determination of each of these parameters for high-throughput analysis (simplified examples in Figure 38). The *average* function was used to determine the resting membrane potential (RMP) in mV, defined as the average value observed 10 ms prior to the stimulus. The overshoot was defined as the highest value after the current stimulus. The *max* function was used to determine the overshoot. The amplitude

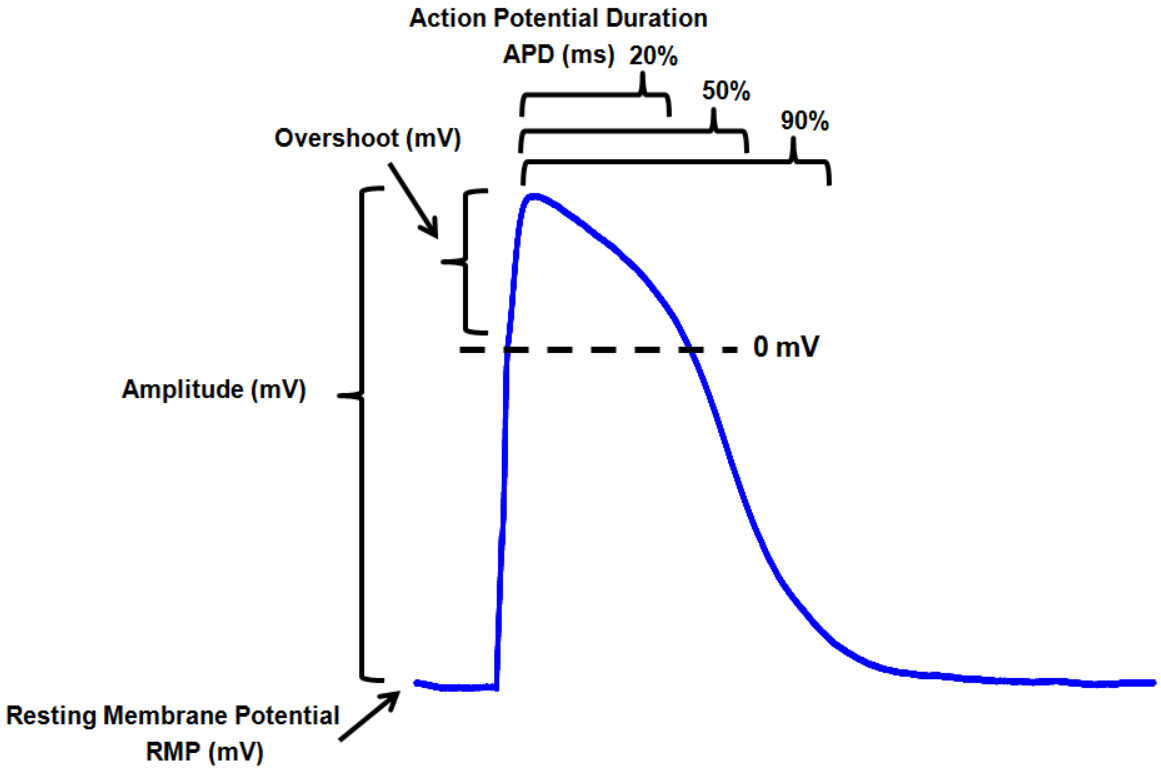

Figure 37. Illustration of action potential analysis parameters on an example atrial action potential recording.

of the action potential, defined as the total height of the AP, was determined as the overshoot minus the resting membrane potential. The *index* function was critical to determining the action potential duration (APD). The APD was defined as time from the action potential overshoot to the return to RMP. Using the *index* and *match* functions, we first determined the time to overshoot. The *index* function provides the value from an *index* when the range value *matches* your defined parameter, using the *match* function. Here, the index is the time column in msec, the range is the action potential trace, and the value to match is the overshoot. The index function will return the time value from the same row as the overshoot value in the trace designated. The $ symbols are used to maintain same index row and column as the function is copied over the worksheet. Then, the duration for 90% repolarization is determined. Ninety percent repolarization is equal to the overshoot value minus 90% amplitude. Because there will be two points on the trace equal to this value (during AP upstroke and during AP repolarization), the range is limited to after the overshoot value. The index function will return the time at which 90% repolarization is reached. Then the overshoot time is subtracted to get the APD_{90} value. A simplified example of this function is illustrated in Figure 38.

All parameters determined were placed in a new Excel file organized by recording file name and trace number (Figure 39). To assess accuracy, parameters for randomly selected action potentials in each recording were verified manually using Clampfit. This master data list was copied into another

B5 {=INDEX($A$1999:$A$20007,MATCH(TRUE,B1999:B20007<(B3-(0.9*B1)),0))}

	A	B	C	D	E	F	G	H	I	J
1	Amplitude	75.19531	76.96533	77.75878	78.97949	79.71191	81.05468	81.54296	81.11572	82.4584
2	Resting Membrane	-57.9957	-57.389	-58.9211	-59.7794	-59.8888	-60.2554	-61.8706	-61.5381	-62.361
3	Overshoot	16.8457	19.16504	18.61572	18.95141	19.59228	20.23315	19.40918	19.31763	19.7448
4	Overshoot Time	80.5	82.1	83.6	84.4	84.8	84.6	85.5	86	86.4
5	Duraiton(90%)	280.6	325.1	352.1	386.5	384.2	392.9	379.8	382.4	407
6	Peak to 90%	200.1	243	268.5	302.1	299.4	308.3	294.3	296.4	320.6
7	Time (msec)	Trace #1	Trace #2	Trace #3	Trace #4	Trace #5	Trace #6	Trace #7	Trace #8	Trace #9
8	0	-57.7698	-57.8003	-58.8074	-59.906	-59.8144	-60.2722	-61.7981	-61.676	-62.1948
9	0.1	-57.7087	-57.7393	-58.7463	-59.906	-59.7839	-60.1807	-61.8591	-61.7065	-62.2253
10	0.2	-57.8003	-57.7087	-58.8074	-59.906	-59.7534	-60.1807	-61.8286	-61.7371	-62.1643
11	0.3	-57.7087	-57.6782	-58.8074	-59.8755	-59.7839	-60.2112	-61.8896	-61.7065	-62.1338
12	0.4	-57.7698	-57.6782	-58.8379	-59.906	-59.8144	-60.2112	-61.9202	-61.676	-62.1948
13	0.5	-57.7087	-57.6782	-58.7769	-59.9365	-59.7534	-60.2112	-61.8591	-61.615	-62.2253
14	0.6	-57.7087	-57.6782	-58.7463	-59.9365	-59.7229	-60.1501	-61.8896	-61.6455	-62.2253

Amplitude = Overshoot – RMP

Resting Membrane Potential (RMP) = Average (10ms)

Overshoot (OS)= Max( )

To determine APD_{90}:

1) Determine time to OS

Give Index "A" Value (time in msec)

```
=INDEX($A$8:$A$20007,
    MATCH(TRUE,B8:B20007=B3,0))
          when range "B" matches B3 (OS)
```

2) Determine time to 90% Action Potential

Give Index "A" Value (time in msec)

```
=INDEX($A$1999:$A$2007,
  MATCH(TRUE,B1999:B20007<(B3-(0.9*B1)),0))
       when range "B" matches OS
                minus 90% Amplitude
```

3) APD_{90} = time to 90% AP Time – time to OS

Figure 38. Example calculation of action potential parameters using Excel functions. Specifically, APD_{90} is calculated using the *Index* and *Match* formula functions.

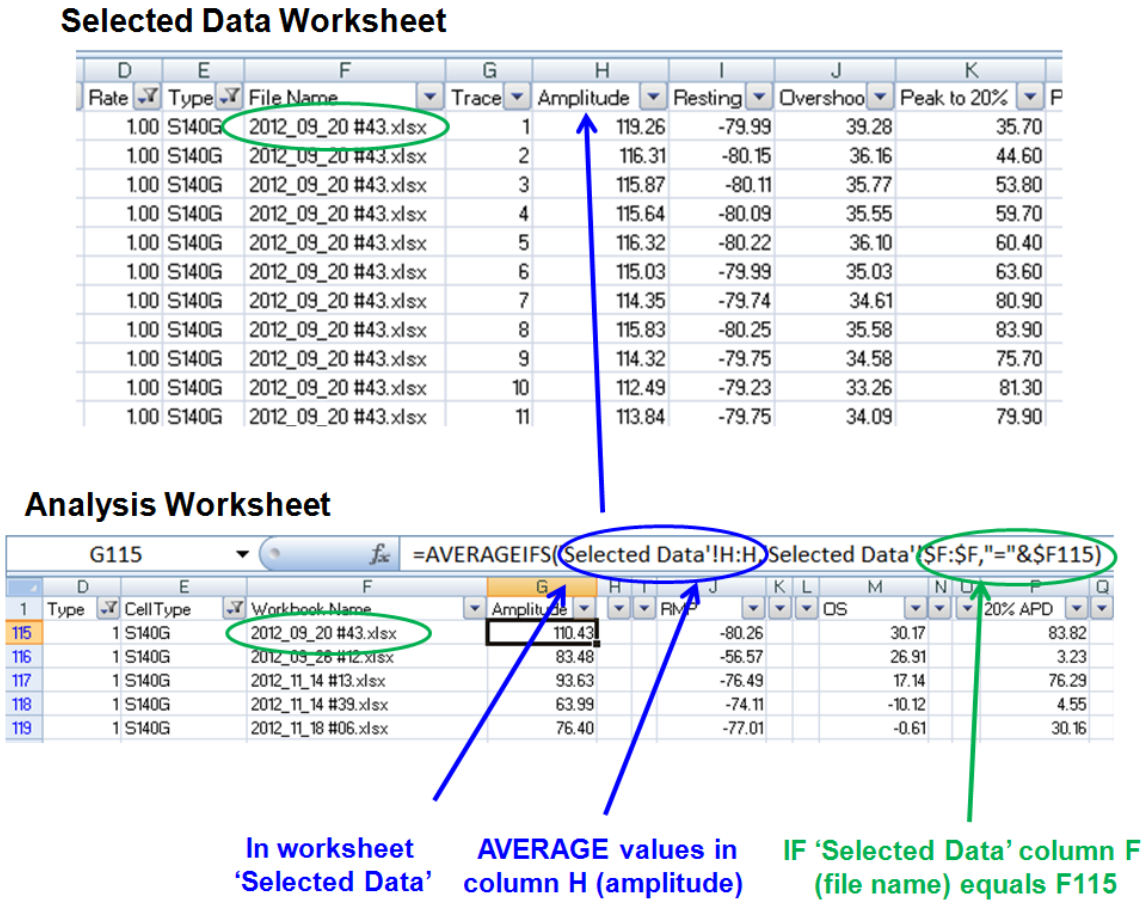

Figure 39. Data analysis of VBA analysis program parameters using the Excel *AverageIfs* function. In this example, the amplitude values in the Selected Data Worksheet are averaged if the file name in the Selected Data worksheet matches the file name in the Analysis Worksheet.

worksheet. This new worksheet was then filtered to include or exclude certain parameters, such as RMP below -40 mV or amplitude >10 mV to exclude traces where the cell is too depolarized or an AP fails to be stimulated. Alternatively, the file could be culled to only included, for example, the first trace or the last 10 traces from each recording. To analyze this selected dataset, a new worksheet was created and utilized the *AverageIfs* function (note that this functions requires Excel2007 or later versions). For example, to average all of the amplitudes for a certain file in your analysis worksheet, the amplitude column is designated in the selected data worksheet but the values are only averaged if the file name column equals file name in your analysis worksheet (Figure 39). Once created, this A*verageIfs*-based analysis worksheet can remain the same and be used with different selected datasets. Together, this program and analysis method allow for powerful, thorough analysis of action potential data.

This action potential trace-by-trace parameter determination gives one the opportunity to analyze trends in the action potential over time. To visualize these trends, we added the automated creation of graphs to the VBA program (Figure 40). These graphs also served as another measure of quality control. The first graph plotted the last recorded action potential trace. The second graph generated plotted the amplitude, overshoot, resting membrane potential, and a value called 'seal'. Seal was a value in the middle of the stimulus pulse; a rise in this value over the course of a recording indicated a closing of the whole cell seal

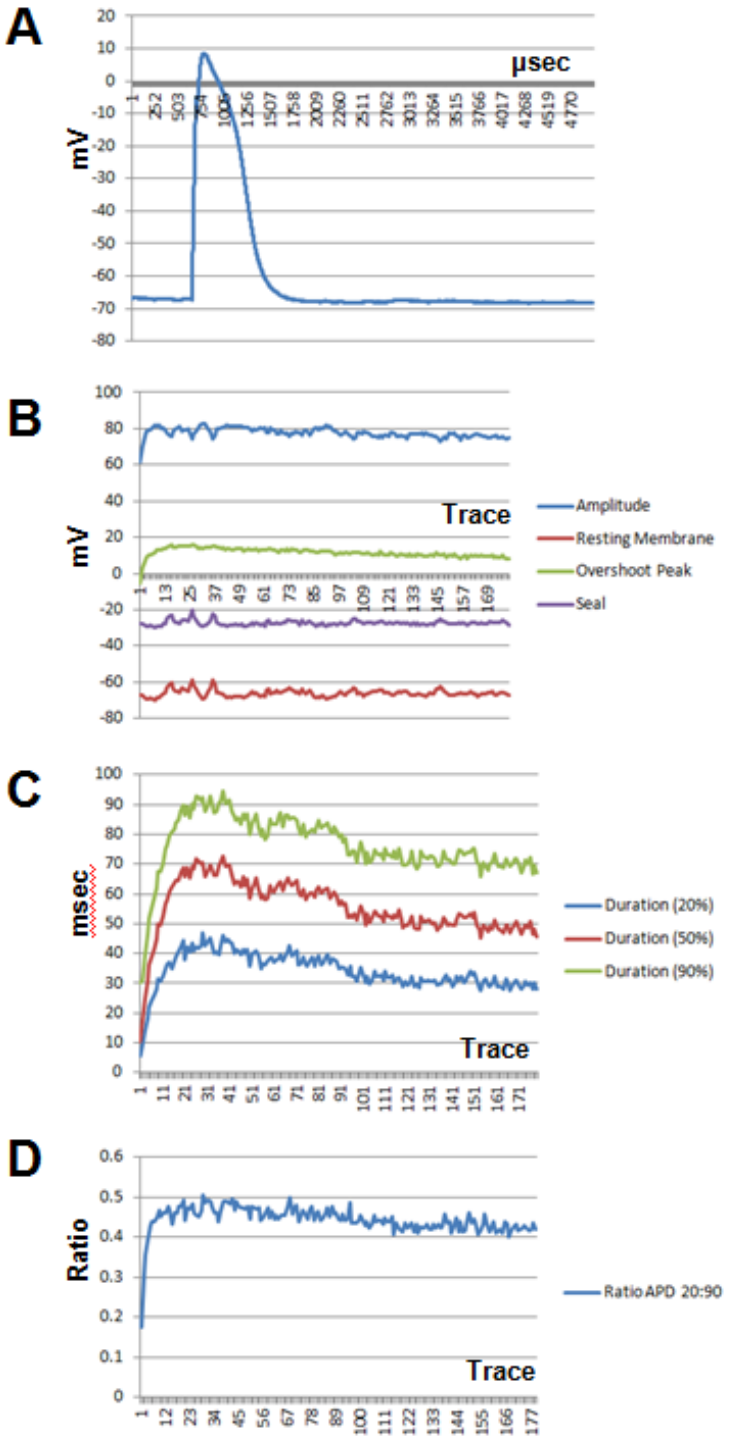

Figure 40. VBA analysis program generated graphs. Example graph illustrates VBA program determined parameters for action potentials elicited at 1 Hz for 3 min recorded from adenovirally transduced, S140G-I_{Ks} expressing adult rabbit atrial myocyte. **A**, Last action potential recorded; **B**, Amplitude, resting membrane potential, overshoot peak, and seal values by trace number; **C**, APD_{20}, APD_{50}, and APD_{90} by trace number; **D**, Ratio of APD_{20} to APD_{90} by trace number.

(see Figure 21). Aberrations in any of these measurements could indicate a number of disruptions or issues in the current clamp recording: loss of recording seal integrity, hypercontraction of the myocyte, stimulus failing to elicit an AP, or triggered activity. One example of triggered activity is an EAD that extends over one trace into the next (Figure 41). The Clampfit recording in a trace view would give a view of what looks like recording disruption. However, continuous view allows the visualization of an EAD that extends over multiple traces. In the graph, the resting membrane would register as elevated, the trace amplitude would be much shorter, and the seal value would be much higher. The third graph illustrates the APD_{20}, APD_{50}, APD_{90} over time. This visualization of the APDs allows determination of when the steady-state APD is achieved as well as the variations from AP to AP. In the fourth graph, the APD_{20} to APD_{90} ratio is illustrated. This ratio of often used to quantify the AP morphology. In addition to visualization of trends over time, any abnormal values are highlighted in these graphs. This awareness triggers investigation of the original Clampfit recording and inquiry into the inclusion those traces in the data analysis.

For the analysis in this chapter, the parameters were averaged for the last 10 recorded action potentials in each experimental condition. Differences between two groups were assessed using unpaired Student's *t* test. Statistical tests were performed using SigmaStat 2.03 (Systat Software, Inc.).

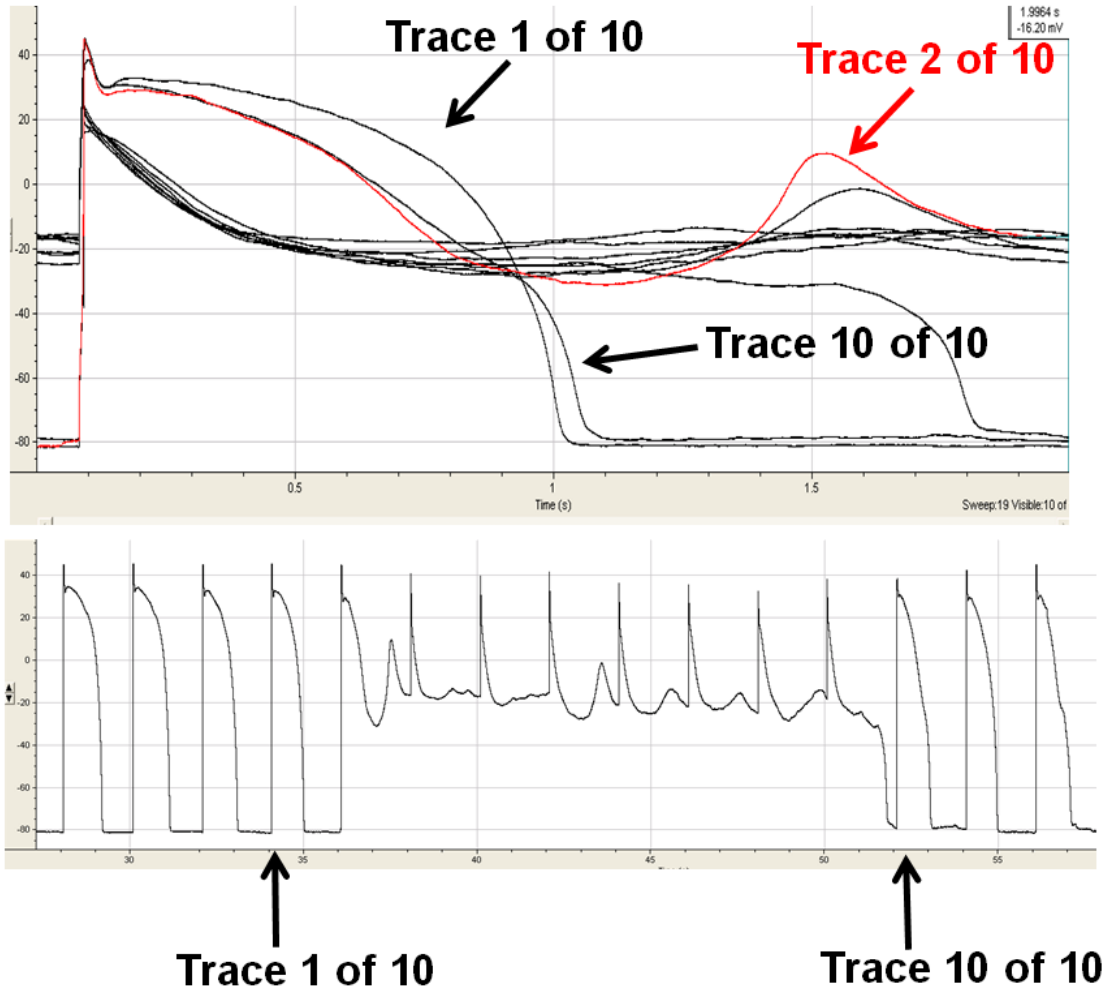

Figure 41. Single trace view versus continuous view of an early-after-depolarization (EAD). *Upper panel*: Trace view can mask an EAD that extends over multiple traces. The start of the EAD is shown in red. *Lower panel*: Continuous view clearly illustrates the full extent of the EAD.

Results

Absence of endogenous HMR-1556 sensitive K^+ current in adult rabbit atrial cardiac myocytes

To determine the baseline I_{Ks} levels in rabbit atrial myocytes, whole-cell voltage clamp experiments were conducted. We recorded total potassium current levels and then applied the I_{Ks}-specific blocker, HMR-1556. With digital subtraction, we determined the levels of HMR-1556 sensitive current. Initially, we recorded potassium currents 3 days post-isolation to mimic a post-viral transduction time point. However, no HMR-1556 sensitive current was recorded. Because some ionic currents are down-regulated over time in tissue culture, and electrical stimulation during culture has been shown to mitigate this effect, we electrically paced our atrial cultures at 3Hz; no HMR-1556 sensitive current was recorded. Notably, assessing myocyte pacing capture was difficult due to the presence of excitation-contraction upcoupler, blebbistatin, in the media. Further, many myocytes did not survive pacing. To assess whether difficulties measuring current were due to culture conditions, we measured potassium currents from atrial myocytes 3 h, 24 h, and 48 h post-isolation and were unsuccessful in recording HMR-1556 sensitive current (Figure 42). These data suggest that under baseline voltage clamp conditions, 1 μM HMR-1556-sensitive potassium current is not activated in rabbit atrial myocytes.

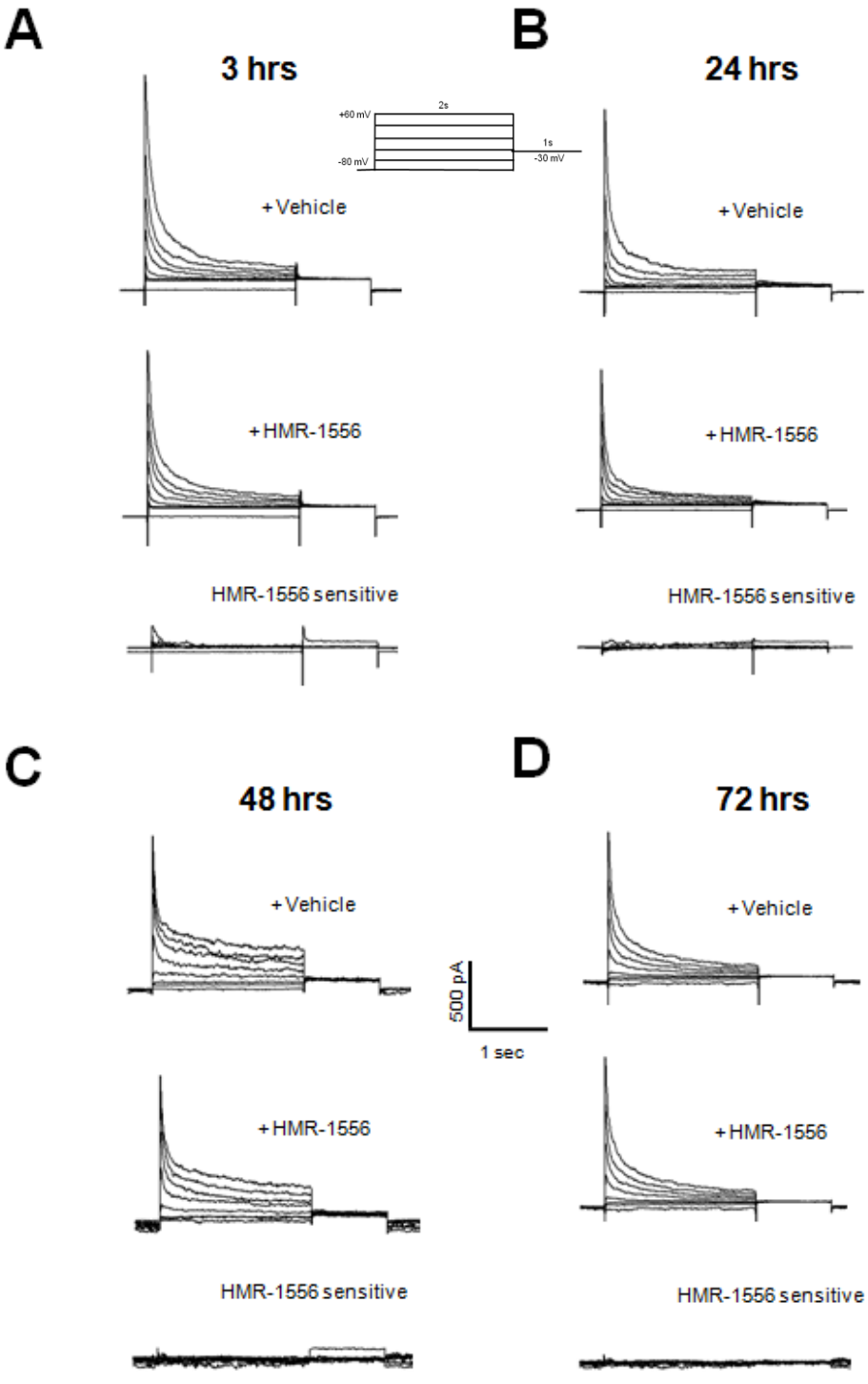

Figure 42. Absence of HMR-1556 sensitive potassium current in adult rabbit atrial myocytes over time. Representative HMR-1556 sensitive potassium current recorded from adult rabbit atrial myocytes from 3 hsr to 72 h post-isolation. Standard activation protocols were used to record potassium currents from vehicle treated myocytes and myocytes after 1 min application of 1 μM HMR-1556.HMR-1556 sensitive current was determined by digital subtraction of HMR-1556 treated from vehicle treated recordings. **A,** 3 h; **B**, 24 h; **C**, 48 h, and **D**, 72 h after atrial myocyte isolation.

We sought to activate endogenous I_{Ks} in rabbit atrial myocytes through β-adrenergic stimulation and phosphatidyl-inositol 4,5-bisphosphate PIP2 enhancement. Studies in heterologous systems have demonstrated that cAMP-mediated PKA-phosphorylation of Ser^{27} on KCNQ1 N-terminus enhances I_{Ks} current density.[6] First, we applied 1 μM or 10 μM of freshly prepared isoproterenol, a β-adenoreceptor agonist, to the bath. We also added 1 μM isoproterenol to the myocyte culture media and incubated the cells overnight. This overnight isoproterenol exposure induced rapid contraction in a subset of atrial myocytes. However, no HMR-1556 sensitive current was recorded with any form of isoproterenol stimulation. As an alternative to isoproterenol stimulation, we used 8-bromo-cAMP, a cell permeable analog of cAMP and activator of protein kinase A, a downstream effector of β-adrenergic stimulation. Neither 250 μM or 1 μM 8-bromo-cAMP induced HMR-1556 sensitive current or increases in potassium current density. Although 8-bromo-cAMP is membrane permeable, we also added it to the intracellular solution; no HMR-1556 sensitive current was induced. Phosphatidyl-inositol 4,5-bisphosphate (PIP2) is a phospholipid and known activator of I_{Ks}.[7, 8] We added PIP2 to the pipette solution to stimulate I_{Ks}; yet again no HMR-1556 sensitive current was induced. Together, these data suggest that endogenous HMR-1556 sensitive current is not present in rabbit atrial myocytes under these recording conditions.

Given the documented heterogeneity in recorded I_{Ks} current in adult rabbit ventricular myocytes,[72] we hypothesized that a similar regional heterogeneity may exist in rabbit atrial myocytes. The rabbit atria were divided into 19 regions and potassium currents from at least 3 atrial myocytes in 7 non-adjacent regions were recorded during superfusion of 10 μM isoproterenol (Figure 35). While morphological differences were noted with regards to cell size, none of these regions had enhanced HMR-1556 sensitive current.

Variable HMR-1556-sensitive current with viral transduction of KCNQ1, S140G, or KCNE1 subunits

Although endogenous HMR-1556 sensitive current was not detected, KCNQ1 and/or KCNE1 may be expressed in rabbit atrial myocytes, yet not together to result in HMR-1556 sensitive I_{Ks}. To determine whether KCNQ1 subunit was expressed, we transduced rabbit atrial myocytes with adenovirus encoding KCNE1. With viral-KCNE1 expression, 50-100 pA of HMR-1556 sensitive current was detected in all atrial myocytes examined. In addition, compared to non-transduced myocytes a decrease in the initial peak current density was noted. These data suggest that KCNE1 expression augments a low level of endogenous KCNQ1 and likely alters other potassium channels in rabbit atrial myocytes. The decrease in peak current density suggests alterations to I_{TO}, but without using I_{TO}-specific blockers this possibility is speculative.

Conversely, to establish whether the KCNE1 subunit was expressed in rabbit atrial myocytes, we transduced rabbit atrial myocytes with either adenovirus encoding KCNQ1 or S140G. Compared to dsRedMST vector-only transduced myocytes, a significantly greater late K^+ current density was observed with either KCNQ1 or S140G expression. However, in approximately half of the myocytes did this increase result in measureable 1 μM HMR-1556 sensitive current (Figure 43). The non-HMR-1556 sensitive increase likely is due to KCNQ1 current alone. The variable recording of HMR-1556 sensitive current suggests heterogeneous expression of endogenous KCNE1.

Together, these electrophysiological data with viral KCNQ1 or KCNE1 subunit expression suggests a low level of endogenous KCNQ1 expression in most atrial myocytes and non-uniform expression of KCNE1. Verification using other modalities such as mRNA or protein expression levels would be vital to supporting this observation. Importantly, these data do not rule out a subpopulation of atrial myocytes with HMR-1556 sensitive current. However, to assess the effects of S140G-I_{Ks} or KCNQ1-I_{Ks} on an atrial action potential, both subunits will need to be expressed. Indeed, dual transduction with S140G and KCNE1 adenovirus results in consistent HMR-1556-sensitive potassium current.

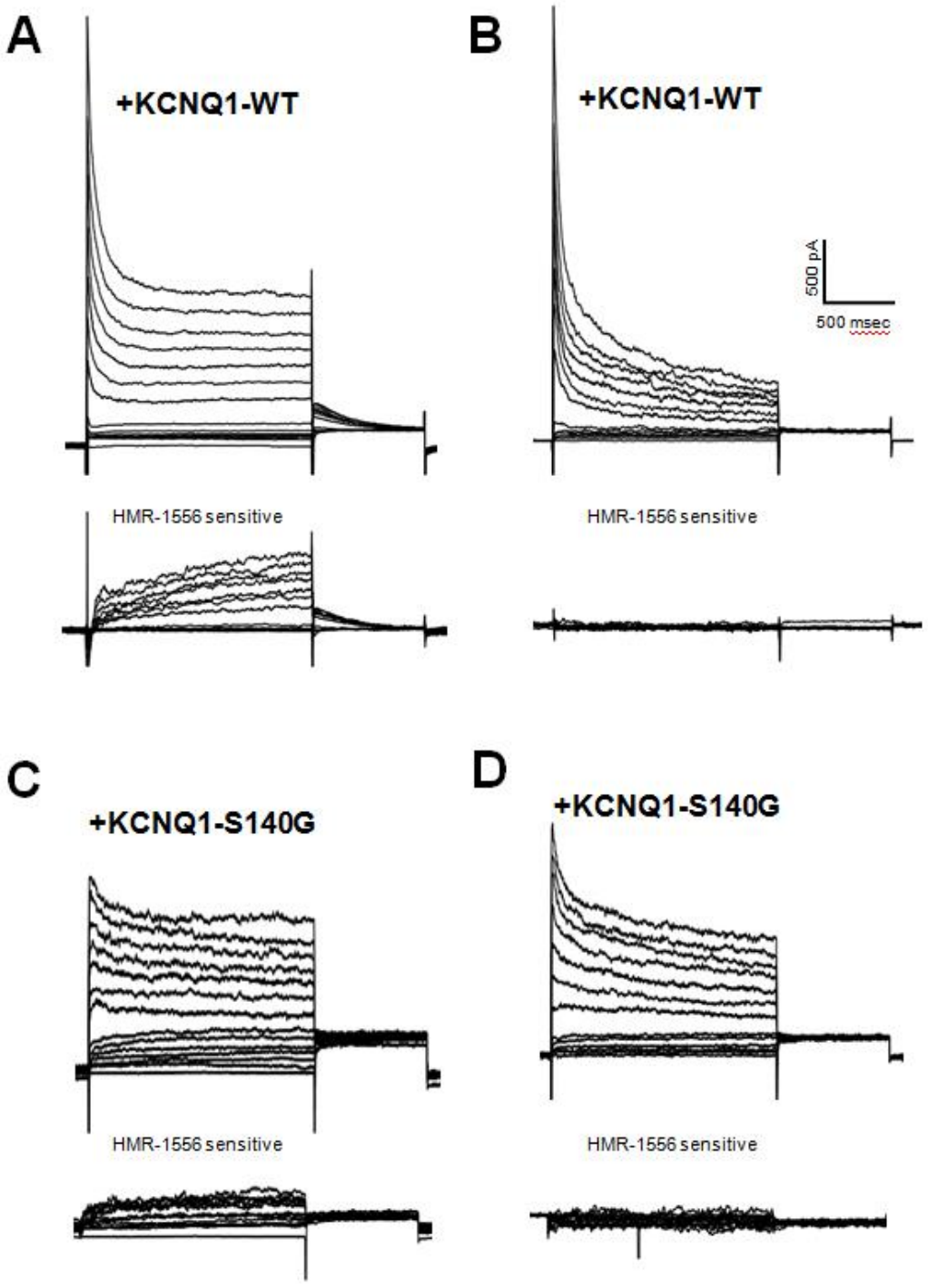

Figure 43. HMR-1556 sensitive potassium current is not consistently measured in KCNQ1-WT and KCNQ1+S140G expressing rabbit atrial myocytes. Representative traces of rabbit atrial myocyte potassium currents (above) and HMR-1556 sensitive potassium currents (below) with KCNQ1-WT expressed in **A** and **B**; S140G-WT expressed in **C** and **D.**

S140G-I_{Ks} induces triggered activity at low frequency and shortens action potential duration at high frequency stimulation

Having established that dual adenoviral transduction of KCNQ1 or S140G and KCNE1 is needed to produce reliable HMR-1556 sensitive current, we explored the effects of exogenous I_{Ks} on adult rabbit atrial action potentials. First, atrial myocytes were transduced with vector-only controls (adenoviruses expressing only dsRedMST). However, recording from these myocytes in the current clamp configuration was very difficult. A gigaohm seal and subsequent whole cell were obtained in <5% of myocytes. The resting membrane potentials often were significantly depolarized (-30 mV to -20 mV). In cells in which a good whole cell seal was achieved, the action potentials were initially generated spontaneously and later the myocytes failed to fire even with stimulus (Figure 44). No action potentials could be obtained past the 5 min equilibration period. With adenovirus expressed WT-I_{Ks} and S140G-I_{Ks}, the whole cell seal could be achieved reliably with 40-60% efficiency. At low frequency action potential stimulation (0.1 or 0.25 Hz), 46% of atrial myocytes transfected with S140G-I_{Ks} displayed abnormal action potential morphology in at least one stimulated action potential (Figure 45). Unexpectedly, this morphology typically had a prolonged action potential duration (APD) with hallmarks of a precursor early after depolarization (EAD) (a bump), yet rarely was a full EAD with second upstroke triggered. Further, during these low frequency recordings, 27% of myocytes expressing S140G-I_{Ks} fired at least one spontaneous action potential. In the WT-I_{Ks} controls, no abnormal

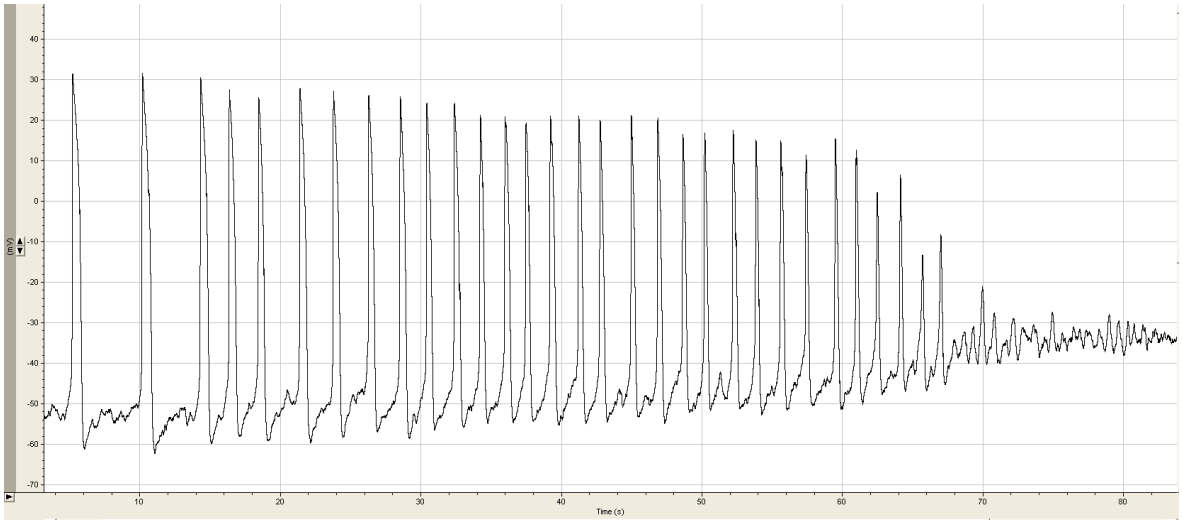

Figure 44. Representative trace of spontaneous activity and subsequent membrane depolarization over 90 s in dsRedMST-expressing adult rabbit left atrial myocytes at 40 h post-isolation. This depolarization likely results from changes in ion channel expression resulting from prolonged tissue culture.

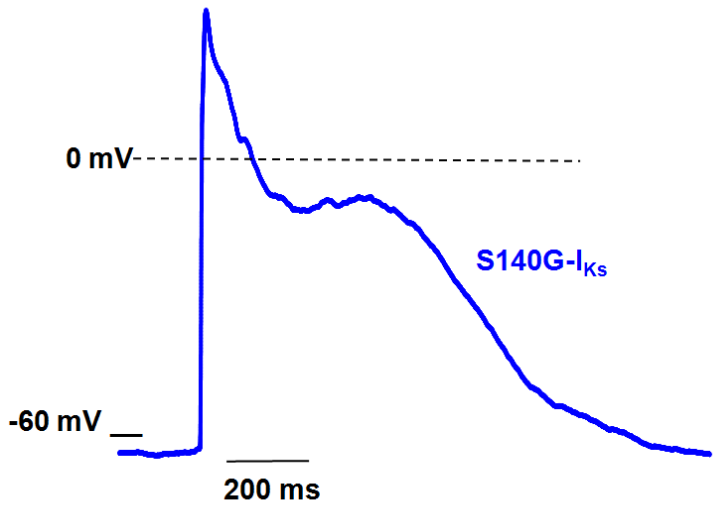

Figure 45. Representative abnormal action potential morphology in a myocyte expressing S140G-I_{Ks}. From action potentials elicited at low frequencies of either 0.1 Hz or 0.25 Hz, 46% of myocytes expressing S140G-I_{Ks} demonstrated abnormal morphology with a bump during repolarization, but not second upstroke of a full EAD compared to 0% WT-I_{Ks}.

morphology or triggered activity was seen in any frequency recordings. When paced at faster frequencies (0.5 or 1 Hz), cells expressing S140G-I_{Ks} had a significantly shorter action potential duration compared to WT-I_{Ks} expressing atrial myocytes (Figure 46). Further, S140G-I_{Ks} induced rate dependent APD shortening at 1 Hz compared to 0.25 Hz (see Table 9). WT-I_{Ks} expressing myocytes had no significant difference in rate dependent APD. Overall, expression of S140G-I_{Ks} significantly hyperpolarized the resting membrane potential of the atrial myocytes compared to WT-I_{Ks} expression (S140G-I_{Ks}: -70.5 ±2.2 mV; WT-I_{Ks} -60.5 ± 3.5 mV). Together, S140G-I_{Ks} expression in rabbit atrial myocytes results in increased triggered activity at low frequency and both rate-dependent and subunit-specific shortening of APD at high frequency stimulation.

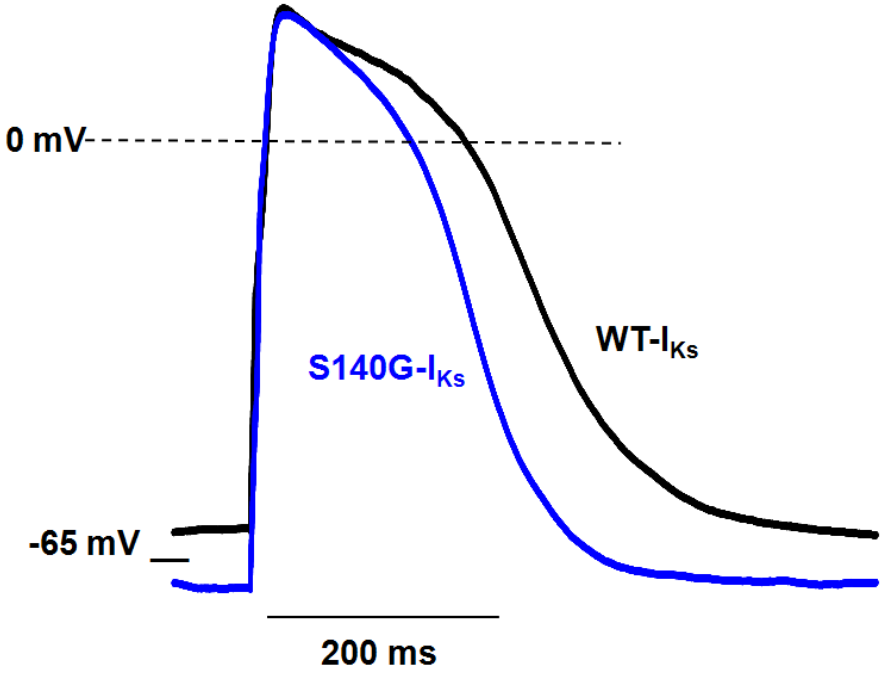

Figure 46 S140G-I_{Ks} expression shortens the action potential duration in adult rabbit atrial myocytes at 40 h post-isolation. Representative action potentials expresses WT-I_{Ks} (black) or S140G-I_{Ks} (blue).

Table 9. Action potential duration in rabbit atrial myocytes expressing WT-I_{Ks} and S140G-I_{Ks}

	Hz	n	APD_{20}	APD_{50}	APD_{90}
WT-I_{Ks}	0.25	11	206.3 ±52.4	289.8 ± 67.8	532.4 ± 88.6
S140G-I_{Ks}	0.25	13	137.2 ± 41.3	234.8 ± 66.4	374.8 ± 80.7$^{\#}$
WT-I_{Ks}	0.50	10	216.3 ± 42.5	307.9 ± 51.0	542.3 ± 66.5
S140G-I_{Ks}	0.50	12	70.3 ± 18.0*	130.8 ± 25.6*	236.9 ±40.2*
WT-I_{Ks}	1.00	10	235.9 ± 30.3	328.4 ± 33.2	538.6 ± 48.8
S140G-I_{Ks}	1.00	12	62.43 ± 14.1*	106.8 ± 21.8*	212.9 ± 33.4*

* $p<0.01$ compared to WT-I_{Ks} of same frequency
$^{\#}$ $p<0.05$ compared to 1 Hz S140G-I_{Ks}

Discussion

The discovery of monogenic causes of familial atrial fibrillation has provided an opportunity to investigate AF substrate susceptibility outside of the many contributory factors involved in the generation of secondary atrial fibrillation. Here, we advance the insights garnered from monogenic characterization of AF mutations in heterologous systems and mathematical model by investigating S140G-I_{Ks} expression in a native atrial myocyte model system. We developed methods for adenoviral expression of S140G-I_{Ks} and computer analysis of action potential parameters in a high throughput fashion. There are limitations to this computational analysis and opportunities to improve its utility. Specifically, triggered activity is not well recognized. The program is written to only recognize one action potential per trace. Delayed-after-depolarizations (DADs) are missed by this automated analysis. Further, early-after-depolarizations (EADs) are not - seen as a single event when they extend over multiple traces. Nevertheless, it allows trace-by trace analysis in a high throughput manner not possible in a short time scale with manual analysis. Using these methods, we demonstrated that S140G-I_{Ks} shortened APD and increased triggered activity in rabbit adult atrial myocytes.

Overcoming critical issues in methods was key for our studies. Exogenous expression of potassium channels in adult rabbit atrial myocytes was enabled by using a modified CMV promoter, using a very high titer, and an extended infection period to elicit expression. In addition, we developed a VBA-based computer program for the high-throughput analysis of action potential recordings. This program allowed for analysis of all action potential recorded and rapid analysis of multiple stimulation frequencies rather than only a small subset of APs typically described. Collectively, these methods greatly facilitated these investigations.

Our results demonstrate that under our recording conditions, rabbit atrial myocytes do not have endogenous HMR-1556 sensitive current expressed acutely or over time in culture. Further, attempts to stimulate endogenous I_{Ks} adrenergically or with the addition of PIP2 failed to produced HMR-1556 sensitive current. Electrophysiological recordings with either KCNE1 or KCNQ1 subunit adenoviral expression suggest that most rabbit atrial myocytes likely have a low level of KCNQ1 expression and variable expression of KCNE1. Thus to reliably generate WT-I_{Ks} or S140G-I_{Ks}, we co-transduced rabbit atrial myocytes with KCNQ1 and KCNE1 subunits. The lack of HMR-1556 sensitive current in an electrophysiological survey is not unexpected but does not rule out I_{Ks} expression in rabbit atrial myocytes. In the literature, rabbit atrial myocytes are not well characterized. Potassium currents underlying I_{Ks} are similarly under studied in these cells. Given the heterogeneity of I_{Ks} expression in ventricular myocytes, a

more precise and thorough regional analysis may yield a more complete expression picture. Determining regional mRNA or protein levels of I_{Ks} may elucidate any regional enhancement and give a more complete picture to better target electrophysiological studies. Despite the lack of endogenous I_{Ks}, rabbit atrial myocytes still provide a more human-like native atrial myocyte milleau in which to investigate the effects of S140G-I_{Ks} expression.

Action potential recordings revealed that S140G-I_{Ks} expression compared to WT-I_{Ks} expression hyperpolarized the resting membrane potential, and shortened action potential duration at higher frequencies. Further S140G-I_{Ks} demonstrated frequency dependent APD abbreviation not noted in WT-I_{Ks}. These data are consistent with the AP effects predicted from the electrophysiological properties of S140G-I_{Ks} observed in heterologous system experiments. The constitutively active channel would contribute to hyperpolarizing the membrane, activation during the short atrial AP, and current accumulation during more rapid activation given the very delayed deactivation kinetics. WT-I_{Ks} is hypothesized to have a minimal role the APD of the atrial considering its slowed activation profile. Even with the prolonged atrial APD observed here at room temperature, over the course of 0.5 s WT-I_{Ks} would still be minimally activated. In heterologous systems, most activation pulses used are 2 sec long to observe WT-I_{Ks} activation with few channels open at 0.5 s time point. Moreover, without β-adrenergic stimulation, WT-I_{Ks} current density would not be predicted to increase dramatically in response to more frequent simulation. Unexpectedly, we

observed EAD and full triggered beats at lower frequency in myocytes expression S140G-I_{Ks}. A shortened action potential in an isolated myocyte is not predicted to have spontaneous triggered activity, but yield a substrate more susceptible to triggers within the atrial tissue. This unanticipated results suggests that S140G-I_{Ks} expression results in alteration of calcium dynamics that at low frequencies can results in this observed triggered activity. How this alteration might occur is not readily explained and needs further investigation.

An important limitation of this study is that while we are using a native atrial myocytes to investigate the effects of S140G-I_{Ks}, the 40+ h of cell culture, adenoviral expression levels, and electrophysiological recording conditions at room temperature introduce many non-native components that could alter the results. Nevertheless, using this system allows us to answer questions in a closer to human native atrial myocyte environment than in heterologous system or even transgenic mouse models. In summary, we demonstrate that S140G-I_{Ks} expression in rabbit atrial myocytes shortens APD and increases triggered activity while hyperpolarizing the resting membrane potential.

CHAPTER IV

SELECTIVE TARGETING OF GAIN-OF-FUNCTION KCNQ1 MUTATIONS PREDISPOSING TO ATRIAL FIBRILLATION

Introduction

Atrial fibrillation (AF) is the most common sustained cardiac arrhythmia in adults. The prevalence of AF rises exponentially with age, and because of the aging population, the number of persons with AF in the United States is projected to increase to 12 million by 2050.[1] Importantly, AF confers a 6-fold increased risk for thromboembolic disease including stroke, predisposes to heart failure and is associated with premature death.[27] The incremental healthcare costs directly related to the diagnosis and management of AF in the United States have been estimated at $6 billion.[28]

Most often, AF occurs within the context of structural heart disease with onset past the age of 65 years. However, an estimated 10-30% of AF, designated as lone AF, arises in the absence of overt heart disease and has a younger age of onset.[29-32] Genetic predisposition to AF has been demonstrated in populations[33, 34] and in families with monogenic forms of the disease.[35] AF-associated mutations have been identified in potassium channels,[2, 15, 38, 39, 73, 74] sodium channels,[41-43] and other genes.[21] The mutation KCNQ1-S140G was the first

identified mutation and remains the best-studied genetic variant associated with autosomal dominant AF.[2, 16, 17, 25]

KCNQ1 encodes a pore-forming voltage-gated potassium channel (Kv7.1 or KCNQ1) that combines with the auxiliary subunit KCNE1 to generate the slow component of the delayed rectifier potassium current (I_{Ks}), critical for cardiac action potential repolarization. Co-expression of KCNQ1-S140G with KCNE1 (S140G-I_{Ks}) demonstrated a gain-of-function with larger and more instantaneous current activation.[2, 17] A similar gain-of-function effect occurs with the AF-associated mutation KCNQ1-V141M.[15] These *in vitro* data are consistent with the notion that increased repolarizing potassium current evoked by these mutations cause shortening of atrial action potentials in myocytes and an abbreviated effective refractory period in atrial tissues, resulting in an increased probability of reentry circuits and AF.[17]

We hypothesized that KCNQ1 gain-of-function mutations have pharmacological properties distinct from the WT channel that may enable selective inhibition of mutant channel complexes. Pharmacological targeting of this gain-of-function behavior would be predicted to decrease AF susceptibility in persons with this dominant mutant allele. We tested this hypothesis using the chromanol 293B derivative HMR-1556, a highly specific I_{Ks} blocker when used at low concentrations.[71, 75] Here we present evidence that S140G-I_{Ks} and V141M-I_{Ks} exhibit enhanced sensitivity to HMR-1556 due to an additional high affinity state.

Using a concentration that predominantly inhibits the high affinity state, HMR-1556 effectively suppressed S140G-I_{Ks} amplitudes to levels not different from WT-I_{Ks}, attenuated the use-dependent accumulation of current without significant effects on WT-I_{Ks}, and mitigated action potential shortening in cultured adult rabbit left atrial myocytes without affecting WT-I_{Ks} action potential duration. These data suggest a potential opportunity for genotype-specific treatment of familial AF.

Methods

Plasmids and heterologous expression

Human KCNQ1 and KCNE1 cDNAs were generated as described previously.[3] The S140G and V141M mutations were engineered in KCNQ1 using QuikChange mutagenesis (Stratagene Corp, La Jolla, CA). For experiments comparing heteromeric channel complexes consisting of only one KCNQ1 allele, cells were transiently transfected with KCNE1-IRES2-eGFP and either KCNQ1-IRES2-DsRedMST (WT-I_{Ks}) or S140G-IRES2-DsRedMST (S140G-I_{Ks}). For expression of V141M-I_{Ks}, cells were co-transfected with KCNE1-IRES2-DsRedMST and V141M-IRES2-eGFP plasmids. To study heteromeric channel complexes with both WT and mutant (S140G) KCNQ1 subunits, WT-I_{Ks} was expressed in cells transfected with KCNE1-IRES2-CD8, KCNQ1-IRES2-eGFP and KCNQ1-IRES2-DsRedMST whereas HET-I_{Ks} was reconstituted by transfecting cells with KCNE1-IRES2-CD8, KCNQ1-IRES2-eGFP and S140G-

IRES2-DsRedMST. The efficiency of triple transfection was approximately 1-5%. All constructs were verified by sequencing of the entire open reading frames.

Chinese hamster ovary cells (CHO-K1, American Type Culture Collection, Manassas, VA) were grown at 37°C with 5% CO_2 in F-12 nutrient mixture medium supplemented with 10% fetal bovine serum (FBS, Atlanta Biologicals, Atlanta, GA), penicillin (50 units/ml), streptomycin (50 µg/ml), and L-glutamine (2 mM). Unless otherwise stated, all tissue culture media were obtained from Life Technologies (Grand Island, NY). CHO cells were transiently transfected using FuGENE 6 (Roche Applied Sciences, Indianapolis, IN) at a ratio of 3:1.

Adenovirus generation

Adenovirus vectors, pAd5-CMVK-NpA and pAd5-(9.2-100)delta1.6KbE3, were obtained from the University of Iowa Gene Transfer Vector Core (supported in part by the NIH and the Roy J. Carver Foundation). Using the pAd5-CMVK-NpA vector, we created shuttle vectors for KCNQ1-IRES2-DsRedMST, S140G-IRES2-DsRedMST, and KCNE1-IRES2-eGFP. A modified CMV promoter was used for all shuttle vectors. This modified promoter consisted of the CMV immediate early promoter sequence immediately followed by last 358 nucleotides of IRES2. This modification was hypothesized to attenuate promoter efficiency and enabled more efficient generation of KCNQ1 encoding adenovirus.

Adenovirus was generated using the RAPAd^{TM} system as previously described.[54] In brief, each shuttle vector and the backbone vector pAd5-(9.2-100)delta1.6KbE3 were co-precipitated with calcium-chloride into human embryonic kidney (HEK) 293 cells in 60 mm Petri dishes. When 60% of cells had detached (12-14 days for KCNE1 and vector-only viruses; 17-25 days for KCNQ1 and S140G), the cells and media were harvested, lysed through repeated freezing/thawing cycles, and amplified in HEK cells (typically using 5-10 150 mm Petri dishes). After 60% of cells detached from the large dishes (1-3 days), cells were pelleted by centrifugation and resuspended 5 ml of viral storage solution (10 mM Tris, 2 mM $MgCl_2$, 4% sucrose, pH 8.0). Cells were then lysed and centrifuged. The supernatant was stored at −80°C in single use aliquots and the virus was used within 5 months.

Viral titer was determined using the tissue culture infective dose 50 ($TCID_{50}$) method as described for the AdenoVator^{TM} Vector System (QBioGene, Carlsband, CA). For multiplicity of infection (MOI) calculations, titers were converted to plaque forming units (PFU) by the following equation: PFU = 0.69*$TCID_{50}$. The titers achieved ranged from 10^9 to 10^{10} PFU/ml. Activity of each virus prep was confirmed for fluorescent marker and potassium channel expression by transduction and subsequent whole cell patch clamp of CHO cells stably expressing the coxsackie adenovirus receptor (CHO-CAR cells), generously provided by Dr. Jeffrey Bergelson at the University of Pennsylvania.[70]

Rabbit atrial myocyte isolation

Left atrial myocytes were isolated from hearts of male New Zealand White rabbits (6-7 lbs from Charles River Canada), using the method of Bassani, *et al*.[50] with modifications. Briefly, rabbits were sedated with intramuscular acepromazine and then anesthetized with intravenous pentobarbital sodium. Hearts were excised quickly and arrested on ice for 5 minutes in nominally calcium-free minimum essential medium solution (MEM, Joklik modification). Hearts were Langendorf perfused at 37°C for 10-15 min in the same MEM solution gassed with 95% O_2 and 5% CO_2. During initial perfusion, the pulmonary vessels were closed with microvessel clips to perfuse both atrial chambers at high pressure, and the atrial chambers were punctured twice at their apex to facilitate flow-through. Then the perfusion was switched to MEM solution containing 0.05 mg/ml Liberase TH (Roche Applied Sciences, Indianapolis, IN). After 5 min of enzymatic digestion, a small incision was made in the left ventricle in an area between major coronary vessels. Serial tissue samples (30 s - 1 min) were taken from this incision with fine tweezers and inspected immediately by light microscopy. When the majority of ventricular myocytes released were quiescent rods (7-20 min), the left atrium was removed from the heart, the remaining heart was removed from the Langendorrf apparatus, and left atrium was recannulated on the Langendorff apparatus. Serial samples were taken from the perfused atrium until the sample edges contained packets of rod-shaped atrial myocytes and the majority of released atrial myocytes were quiescent rods (5-20 minutes). The left atrium was removed and placed in MEM solution containing 1% bovine serum albumin

(BSA). The tissue was minced, gently triturated with a wide-bore pipette, and filtered through a 100 µm cell strainer (BD Biosciences, San Jose, CA) into a 50 ml conical tube. The myocytes were allowed to settle into a soft pellet by gravity for 30 – 60 min at room temperature. Then the supernatant was aspirated, and atrial myocytes were resuspended in fresh BSA solution. Myocytes were plated on laminin-coated glass coverslips, and incubated at 37°C with 5% CO_2. The experimental procedure for isolating rabbit cardiac myocytes was approved by Vanderbilt University Institutional Animal Care and Use Committee.

Atrial myocyte culture and adenoviral transduction

Three hours after termination of enzymatic digestion, myocytes were placed into culture media consisting of MEM supplemented with Hank's salts, 2 mM L-glutamine (Gibco-Invitrogen, Life Technologies, Grand Island, NY), insulin-transferrin-selenium-X supplement (Gibco-Invitrogen, Life Technologies, Grand Island, NY), penicillin (50 units/ml), streptomycin (50 µg/ml), 1% bovine serum albumin, 5 µM blebbistatin at pH 7.4 (modified from Kabaeva, *et al*.[52]). Virus was added to the myocytes at a MOI of 2,000 immediately after plating in culture media. To express WT-I_{Ks}, adenoviruses Ad5-KCNQ1-DsRedMST and Ad5-KCNE1-eGFP were used to co-infect myocytes, whereas S140G-I_{Ks} was generated by co-infecting myocytes with adenoviruses Ad5-S140G-DsRedMST and Ad5-KCNE1-eGFP. Infected myocytes were cultured at 37°C in 5% CO_2 and used for electrophysiology experiments 48-72 hours post-isolation. The efficiency

of dual transduction of healthy-appearing (striated, rod-shaped) myocytes was approximately 15-20%.

Voltage clamp recording

Potassium currents were recorded from CHO cells using the whole-cell configuration of the patch clamp technique.[55] In dual transfection experiments examining channels composed of KCNE1 with just one KCNQ1 allele, only cells exhibiting yellow fluorescence (co-expression of dsRed-MST and eGFP) were studied. In triple transfection experiments designed to examine heteromeric channels composed of KCNE1 with both WT and mutant KCNQ1 subunits, yellow fluorescent cells with at least 3 adhered anti-CD8 Dynabeads® (Life Technologies, Grand Island, NY) were studied. The extracellular solution contained in mM: 132 NaCl, 4.8 KCl, 1.2 $MgCl_2$, 1 $CaCl_2$, 5 glucose, and 10 HEPES, pH 7.4. In experiments with drug application, bath solution containing vehicle (<0.01% dimethyl sulfoxide) or HMR-1556 (1 nM - 2 μM) was applied by pencil perfusion using the Automate Valve-link perfusion system. HMR-1556 ((3R,4S)-(+)-N-[-3-hydroxy-2,2-dimethyl-6-(4,4,4-trifluorobutoxy)chroman-4-yl]-N-methyl-ethanesulfon-amide) was synthesized by the Vanderbilt Institute of Chemical Biology Synthesis Core using a published method.[71] The standard intracellular solution contained in mM: 110 potassium aspartate, 1 $CaCl_2$, 10 HEPES, 11 EGTA, 1 $MgCl_2$, and 5 K_2ATP, pH 7.35. Pipette solution was diluted 5-10% to prevent activation of swelling-activated currents. Patch pipettes were pulled from thick wall borosilicate glass (World Precision Instruments, Inc.) with a

multistage P-97 Flaming-Brown micropipette puller (Sutter Instrument Co., Novato, CA) and heat-polished with a Micro Forge MF 830 (Narashige International USA, Inc., East Meadow, NY). After heat polishing, the resistance of the patch pipettes was 2-4 megaohms in the standard solutions. A 2% agar bridge with composition similar to the control bath solution was used as a reference electrode. Unless otherwise stated, all chemicals were obtained from Sigma-Aldrich (St. Louis, MO).

Whole-cell currents were recorded at room temperature (20–23°C) using an Axopatch 200B amplifier (MDS Analytical Technologies, Sunnyvale, CA). Test pulses were generated using Clampex 8.1 (MDS Analytical Technologies), and whole-cell currents were acquired at 5 kHz and filtered at 1 kHz. The access resistance and apparent membrane capacitance were estimated as described previously.[56] Whole-cell currents were not leak subtracted. Junction potentials were zeroed with the filled pipette in the bath solution. All recordings were started 4 min after achieving a whole cell patch. For concentration-response experiments, a single 2 s pulse to +40mV from a holding potential of −80 mV followed by a 1 s voltage step to −30mV was repeated every 10 s. Following 30 s of stable current levels, HMR-1556 was applied until 1 min of steady-state current was observed. For activation protocols, whole-cell currents were measured during a series of 2 s voltage steps from a holding potential of −80 mV to test potentials ranging from −80 to +60 mV (in 10 mV increments) followed by a 1 s step to −30 mV to record tail currents with a 20 s interpulse duration. For

current accumulation experiments, a single 2 s pulse to +40 mV followed by a 1 s step to −30mV was repeated for 1 minute with a 1 s interpulse duration.

Voltage clamp data analysis

Data were collected for each experimental condition from at least three separate transfections and analyzed using a combination of Clampfit (MDS Analytical Technologies), OriginPro 7 (OriginLab Corp., Northhampton, MA), and SigmaPlot 2000 (Systat Software, Inc., Chicago, IL). To determine the kinetics of onset of and recovery from inhibition, fractional current remaining over time after 1 µM HMR-1556 application or after wash with bath solution was fitted with a monoexponential function ($f(t) = \sum_{i=1}^{n} A_i e^{-\frac{t}{\tau_i}} + C$) where t indicates time, τ is a time constant, A is an amplitude term and *C* is the fraction of unblocked current. The IC_{50} for inhibition of WT-I_{Ks} was determined by fitting the percent inhibition from 1 nM to 2 µM HMR-1556 with $\mathrm{y} = \mathrm{Imin} + (\mathrm{Imax} - \mathrm{Imin})/(1 + 10^{\log(\mathrm{IC_{50}})-\mathrm{x}} * \mathrm{k})$ for monophasic fits where Imin is the minimal current inhibition, Imax is the maximal current inhibition, IC_{50} is the concentration producing half maximal inhibition, x is log of concentration, and k is the Hill slope factor. For biphasic fits required for S140G-$I_{Ks,}$ V141M-I_{Ks} and HET-I_{Ks}, we used $\mathrm{y} = \mathrm{Imin} + (\mathrm{ImaxA} - \mathrm{Imin})/(1 + 10^{(\mathrm{x}-\mathrm{IC_{50A}})*\mathrm{kA}}) + (\mathrm{ImaxB} - \mathrm{Imin})/(1 + 10^{(\mathrm{IC_{50B}}-\mathrm{x})*\mathrm{kB}})$ where ImaxA and ImaxB are the maximal current inhibition for the high and the low affinity states, respectively, IC_{50A} and IC_{50B} are the concentrations that produce half maximal inhibition of the high or low affinity states, respectively, kA and kB are the Hill slope factors for the high and low affinity states, respectively.

Instantaneous current was measured 100 ms following a voltage step and steady-state current was measured at 1900 ms. Current density was obtained by normalizing current level to cell capacitance. Voltage dependence of activation was determined by plotting normalized peak tail current *versus* voltage, then fitting curves with a Boltzmann function to determine the voltage for half-maximal activation ($V_{½}$) and the slope factor (k). Deactivation time constants were determined by fitting tail current decay with the monoexponential function shown above.

Differences between two groups were assessed using unpaired Student's *t* test. One-way ANOVA followed by a Tukey *post hoc* test was performed when comparing more than two groups. Statistical tests were performed using SigmaStat 2.03 (Systat Software, Inc., Chicago, IL).

Current clamp recording

Action potentials were elicited from atrial myocytes using the whole-cell configuration of the patch clamp technique.[55] Yellow, striated atrial myocytes were used for patch clamp experiments using previously described solutions.[58] The extracellular solution contained in mM: 140 NaCl, 5.4 KCl, 1 $MgCl_2$, 1 $CaCl_2$, 7.5 glucose, 0.33 NaH_2PO_4, and 5 HEPES, pH 7.4. The intracellular solution contained in mM: 120 KCl, 10.25 NaCl, 5 $MgCl_2$, 0.36 $CaCl_2$, 5 HEPES, 5 EGTA, 5 creatine phosphate (Tris), 5 glucose, and 5 K_2ATP, pH 7.2. For drug application, bath solution containing vehicle (<0.01% dimethyl sulfoxide) or HMR-

1556 (1 μM) was applied by pencil perfusion using the Automate Valve-link perfusion system. Patch pipettes were pulled from thick wall borosilicate glass (World Precision Instruments, Inc., Sarasota, FL) with a multistage P-97 Flaming-Brown micropipette puller (Sutter Instrument Co., Novato, CA) and heat-polished with a Micro Forge MF 830 (Narashige International USA, Inc., East Meadow, NY). After heat polishing, the resistance of the patch pipettes was 1.5-2.5 megaohms in the above solutions. A 2% agar bridge with composition similar to the control bath solution was used as a reference electrode.

Action potentials were elicited at room temperature (20–23°C) using an Axopatch 700B amplifier (MDS Analytical Technologies, Sunnyvale, CA). Pulses were generated using Clampex 9.1 (MDS Analytical Technologies), and action potentials were acquired at 10 kHz. No current was injected to maintain resting membrane potentials. To elicit action potentials, a stimulus threshold was determined for each myocyte, using a protocol of 0.1 nA steps of 3-4 ms duration. For experiments, 1.25 times stimulus threshold was used. Action potentials were elicited at 0.1 Hz for 5 min initially to achieve equilibration, and then at 1 Hz for experiments. HMR-1556 was applied after steady state action potential duration (APD) was achieved.

Current clamp data analysis

Data were collected for each experimental condition from at least three separate myocyte isolations and analyzed using a combination of Clampfit 9.1 (MDS Analytical Technologies) and Excel 2010 (Microsoft). Data were transferred from Clampfit to Excel with each 1 Hz recording period contained in a separate file. A Visual Basic for Applications (VBA) program in Excel was written to read each file and to determine the resting membrane potential and atrial action potential duration at 90% (APD_{90}) for each recorded action potential. The resting membrane potential (RMP) in mV was defined as the average value observed 10 ms prior to the stimulus. APD_{90} was defined as time from the action potential overshoot to the return to 90% RMP. The overshoot was defined as the highest value after the current stimulus. All parameters determined were placed in a new Excel file organized by recording file name and trace number. To assess accuracy, parameters for randomly selected action potentials in each recording were verified manually using Clampfit. For each experimental condition, the parameters were averaged for the last 10 recorded action potentials. Differences between two groups were assessed using unpaired Student's *t* test. Statistical tests were performed using SigmaStat 2.03 (Systat Software, Inc.).

Results

S140G-I_{Ks} exhibits enhanced sensitivity to HMR-1556

We tested whether heterologously expressed I_{Ks} channel complexes consisting of either wildtype (WT) or mutant (S140G) KCNQ1 subunits in combination with the auxiliary subunit KCNE1 are inhibited by HMR-1556. Whole-cell recordings of CHO cells transfected with S140G and KCNE1 (S140G-I_{Ks}) demonstrated nearly instantaneous activation of outward current in contrast to the slowly activating current observed in cells expressing WT-I_{Ks} (Figure 47 A, B). Because KCNQ1-S140G mutation-positive subjects were reported to be heterozygous in familial AF and because WT and mutant KCNQ1 subunits can co-assemble in heteromeric channels, we examined channel complexes consisting of both WT and mutant subunits co-expressed with KCNE1 (HET-I_{Ks}), which exhibited larger amplitudes with a large fraction of instantaneous current (Figure 47 C). Superfusion of 1 µM HMR-1556 completely and rapidly inhibited all channel complexes activated by low frequency pulsing (10 s interpulse duration) to +40 mV (Figure 47 D-F). However, inhibition of S140G-I_{Ks} and HET-I_{Ks} was more pronounced than WT-I_{Ks} at lower concentrations.

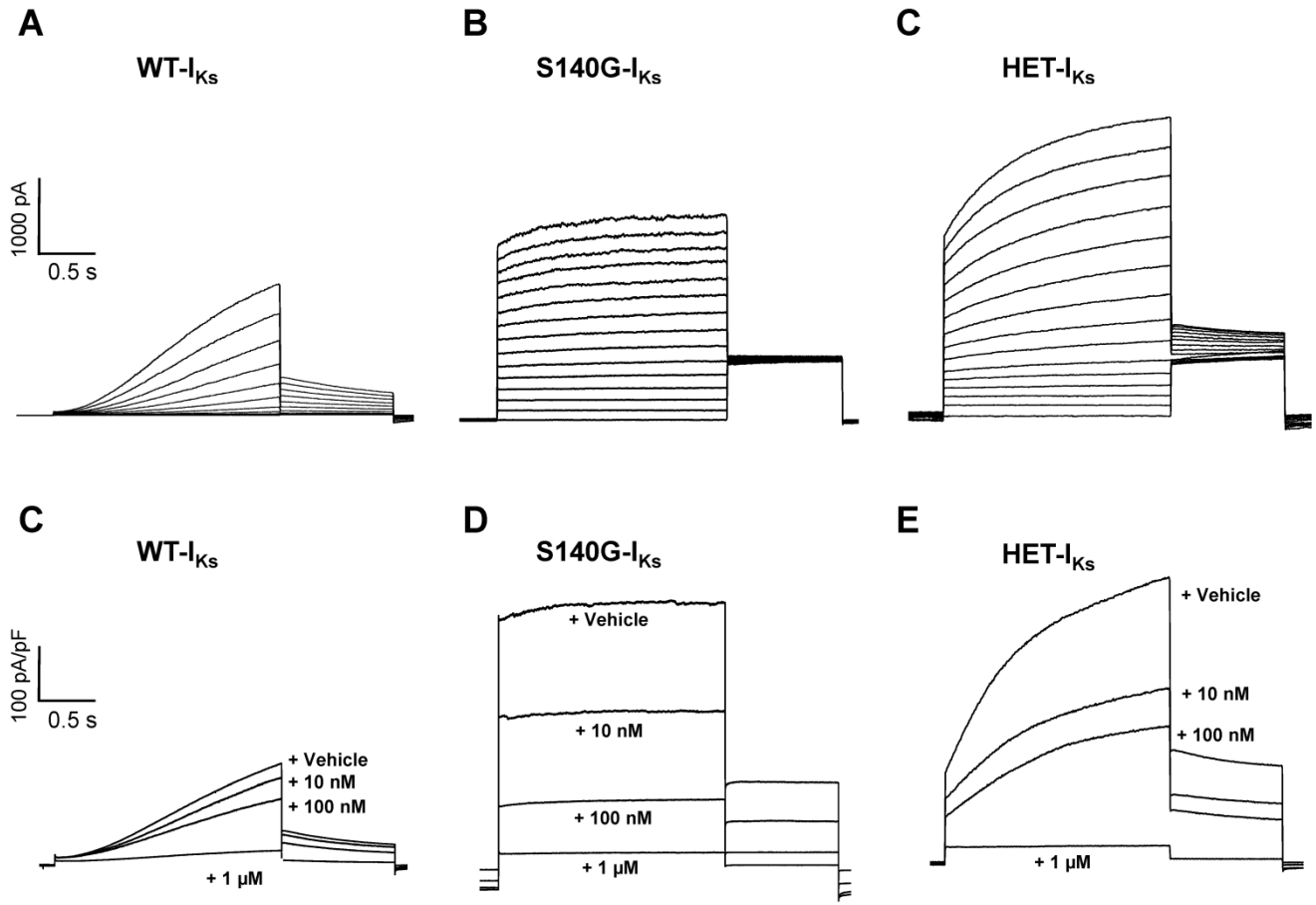

Figure 47. S140G-I_{Ks} and HET-I_{Ks} exhibit enhanced sensitivity to HMR-1556. **A, B and C,** Representative current recordings from cells expressing WT-I_{Ks} (**A**), S140G-I_{Ks} (**B**), or HET-I_{Ks} (**C**). Recordings illustrated in **A**, **B and C** were obtained using the activation protocol described in the Methods. **D, E, and F,** Average current densities (current normalized to cell capacitance) elicited by a 2 s voltage step to +40 mV followed by a 10 s interpulse during application of vehicle or various concentration of HMR-1556 from cells expressing WT-I_{Ks} (**D**), S140G-I_{Ks} (**E**), or HET-I_{Ks} (**F**). Current density traces in D, E, and F are averages from 9-11 cells.

We assessed concentration-response relationships for WT-I_{Ks}, S140G-I_{Ks}, and HET-I_{Ks} to determine whether the channel complexes have different affinities for HMR-1556 (Figure 48). Cells expressing WT-I_{Ks} exhibited a concentration-response curve that was fit by the Hill equation yielding an IC_{50} of 214nM and Hill coefficient of 1.2. By contrast, S140G-I_{Ks} exhibited a complex concentration-response that suggested two affinity states. The IC_{50} of the high affinity state was 3.7nM, whereas the lower affinity state had an IC_{50} of 97.7nM. Both states were significantly different from the IC_{50} for WT-I_{Ks} ($p<0.001$). Hill coefficients for the high (2.2) and low (2.5) affinity states on S140G-I_{Ks} suggested positive cooperative binding of the drug. The gating kinetics of the current sensitive to 30nM HMR-1556, a concentration near the crux between the two affinity states on the concentration-response curve, was not overtly different than drug-insensitive current (Figure 49) suggesting that the two affinity states do not emerge from distinct populations of channels. The HET-I_{Ks} complex demonstrated an intermediate pharmacologic phenotype with a complex concentration-response curve. The high affinity state had an IC_{50} of 5.1nM (Hill coefficient 1.7) whereas the low affinity state IC_{50} was 240nM (Hill coefficient 2.4).

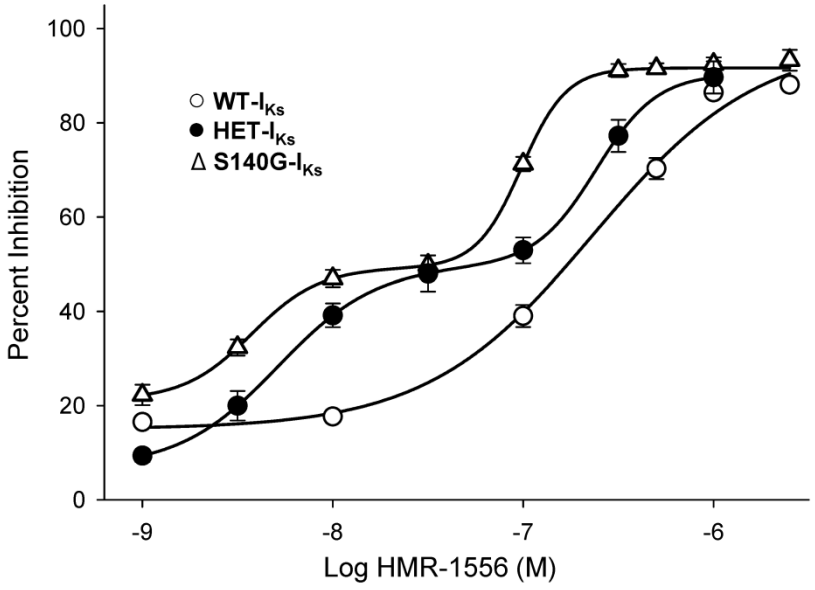

Figure 48. HMR-1556 concentration-response curves for WT-I_{Ks}, S140G-I_{Ks}, and HET-I_{Ks}. HMR-1556 (1 nM - 2 µM) applied to WT-I_{Ks} (○), S140G-I_{Ks} (Δ), and HET-I_{Ks} (●). Solid lines represents fits of the averaged data to either monophasic (WT-I_{Ks}) or biphasic (S140G-I_{Ks} and HET-I_{Ks}) Hill function (see Supplemental Material). IC_{50} values and Hill coefficients are provided in the text.

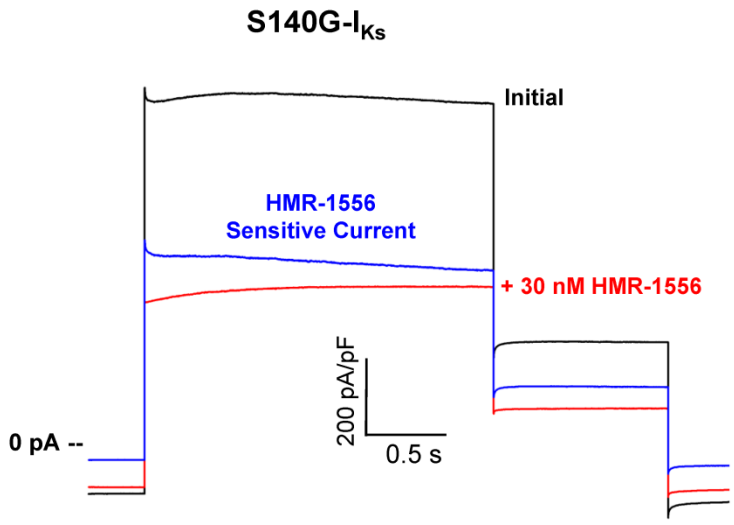

Figure 49. HMR-1556 sensitive and insensitive current for S140G-I_{Ks}. Average current densities for S140G-I_{Ks} recorded in the absence (black trace) or presence (red trace) of 30 nM HMR-1556. HMR-1556 sensitive current (blue trace) was determined by digitally subtracting the residual current (red trace) from the total current (black trace).

There were also substantial differences in the kinetics of HMR-1556 inhibition. Specifically, on- and off-rates observed for suppression of S140G-I_{Ks} were significantly slower than WT-I_{Ks} (Figure 50 A, B). The dramatically slower off-rate for S140G-I_{Ks} suggested a stronger interaction between HMR-1556 and the channel consistent with our finding that the mutant subunit confers an enhanced affinity for the drug. The intermediate phenotype of HET-I_{Ks} exhibited an on-rate comparable to WT-I_{Ks} but a significantly slower off-rate that was more similar to S140G-I_{Ks}. This enhanced sensitivity suggested an opportunity to selectively suppress the mutant current with minimal effects on WT-I_{Ks}.

V141M-I_{Ks} exhibits enhanced sensitivity to HMR-1556

We also determined the pharmacologic effects of HMR-1556 on another previously reported gain-of-function KCNQ1 mutation, V141M, associated with early onset AF.[15] V141M-I_{Ks} exhibited enhanced sensitivity to HMR-1556 and a complex IC_{50} binding curve with values similar to S140G-I_{Ks} (Figure 51). The off-rate was significantly slower than WT-I_{Ks} (Figure 50 C, D). These data demonstrate that increased HMR-1556 sensitivity was not specific to S140G-I_{Ks}. All further experiments were conducted with S140G-I_{Ks} as a prototypic familial AF mutation.

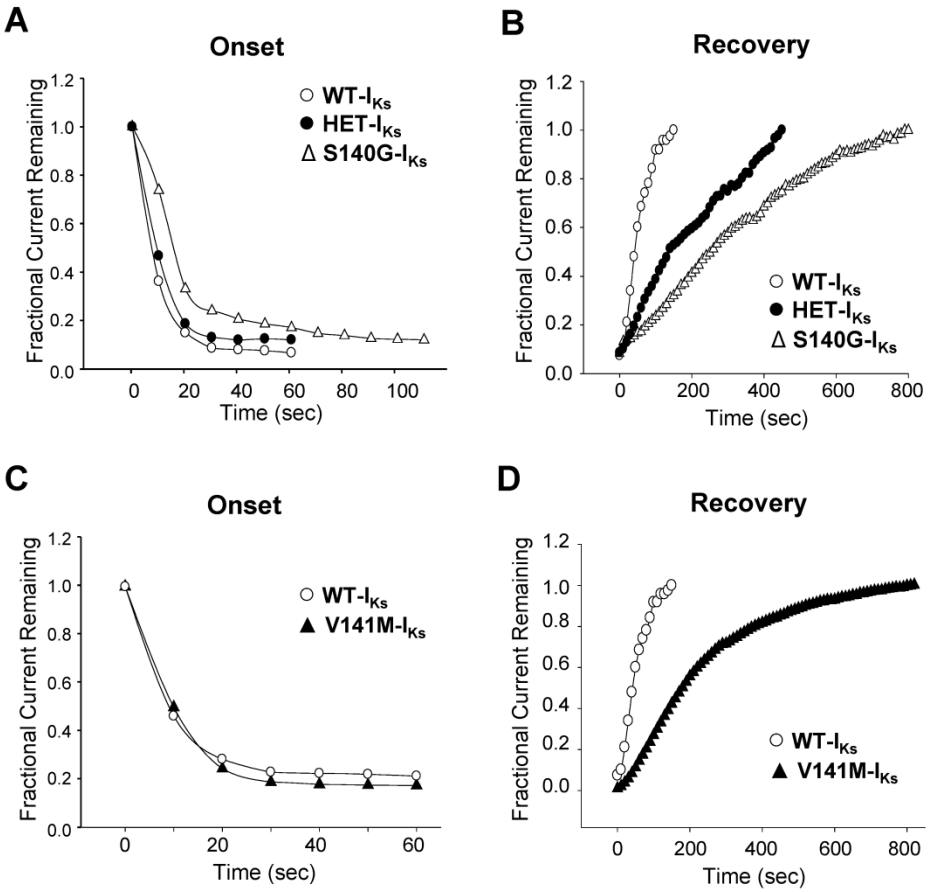

Figure 50. Kinetics of inhibition by HMR-1556. **A**, Onset of inhibition elicited by application of 1 µM HMR-1556 for WT-I_{Ks} (○), S140G-I_{Ks} (Δ), and HET-I_{Ks} (●) illustrated for representative cells. On rates: WT-I_{Ks}, 0.10 ± 0.01 sec^{-1}; S140G-I_{Ks}, 0.032 ± 0.005 sec^{-1}; HET-I_{Ks}, 0.12 ± 0.01 sec^{-1}, p<0.001 for S140G-I_{Ks} compared to HET-I_{Ks} and WT-I_{Ks}; **B**, Recovery from inhibition by 1 µM HMR-1556 for WT-I_{Ks} (○), S140G-I_{Ks} (Δ) and HET-I_{Ks} (●) illustrated for representative cells. Off rates: WT-I_{Ks}, 0.018 ± 0.001 sec^{-1}; S140G-I_{Ks}, 0.0020 ± 0.0001 sec^{-1}; HET-I_{Ks}, 0.0048 ± 0.0009 sec^{-1}; p<0.001 for HET-I_{Ks} and S140G-I_{Ks} compared to WT-I_{Ks}; **C**, Onset of inhibition elicited by application of 1 µM HMR-1556 for V141M-I_{Ks} (▲) illustrated for representative cells. WT-I_{Ks} (○) shown for reference. On rate: V141M-I_{Ks}, 0.09 ± 0.02 sec^{-1} (not statistically significant versus WT-I_{Ks}). **D,** Recovery from inhibition by 1 µM HMR-1556 for V141M-I_{Ks} (▲) illustrated for representative cells with WT-I_{Ks} (○) shown for reference. Off rate: V141M-I_{Ks}, 0.004 ± 0.002 sec^{-1} (p<0.001 versus WT-I_{Ks}). In **A-D**, the data represent the current amplitude recorded at 1990 ms after a test pulse to +40 mV and normalized to current recorded at the initial pulse (n = 4-7).

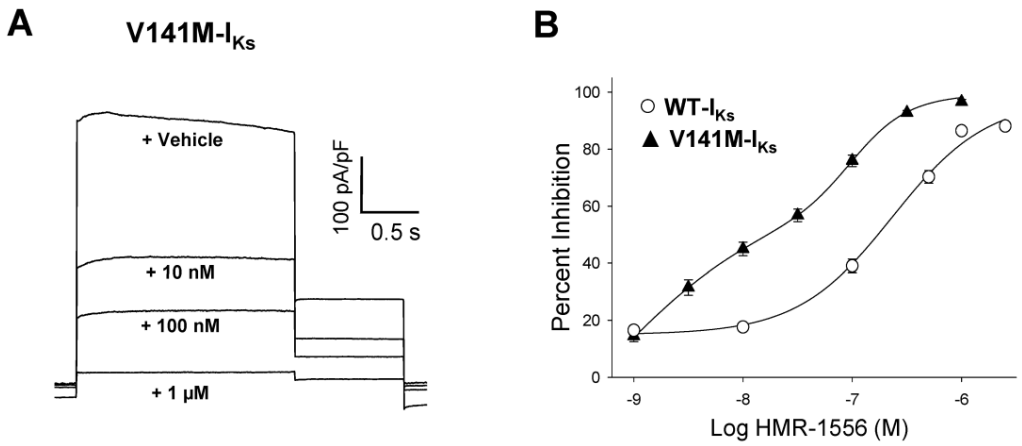

Figure 51. V141M-I_{Ks} exhibits enhanced sensitivity to HMR-1556. **A,** Representative current densities (current normalized to cell capacitance) recorded from cells expressing WT-I_{Ks} that were elicited by a 2 s voltage step to +40 mV followed by a 10 s interpulse during application of vehicle or various concentration of HMR-1556. **B,** HMR-1556 concentration-response curves for V141M-I_{Ks} (▲) and WT-I_{Ks} (○). Solid lines represents fits of the averaged data (9-11 cells) to a biphasic Hill function (see Supplemental Material). For V141M-I_{Ks}, the high affinity state had an IC_{50} of 0.72 nM and Hill coefficient of 0.6; the low affinity state had an IC_{50} of 204 nM and Hill coefficient of 1.7.

Properties of heteromeric S140G-I_{Ks} and WT-I_{Ks}

We elucidated the functional properties of HET-I_{Ks}. Compared to WT-I_{Ks}, cells expressing HET-I_{Ks} exhibited larger amplitudes with a large fraction of instantaneous current between −80 and −20 mV (Figure 52). At more positive voltage steps (−20 to +60 mV), HET-I_{Ks} exhibits both time-dependent and constitutive activation with significantly greater current density than WT-I_{Ks} (Figure 52). The voltage dependence of activation was shifted significantly in the hyperpolarized direction for HET-I_{Ks} ($V_{1/2}$: HET-I_{Ks}, 1.4±8.1 mV; WT-I_{Ks}, 30.1±9.3 mV; $p<0.001$) without any difference in slope factor (Figure 52). The time course of deactivation was extremely slow for HET-I_{Ks} as compared to WT-I_{Ks} (Figure 52).

During repetitive depolarization to +40 mV with a short recovery period, both WT-I_{Ks} and HET-I_{Ks} exhibited a use-dependent accumulation of instantaneous and steady-state current over time, but HET-I_{Ks} current density was significantly greater than WT-I_{Ks} at each successive pulse (Figure 53). The ratio of instantaneous to steady-state current at the end of this protocol, a proxy for the degree of constitutive activation, was much greater for HET-I_{Ks} (84±3%) than WT-I_{Ks} (38±4%; $p<0.001$). These findings illustrate the dynamic nature of I_{Ks} and further emphasize the biophysical consequences of the gain-of-function mutation, KCNQ1-S140G.

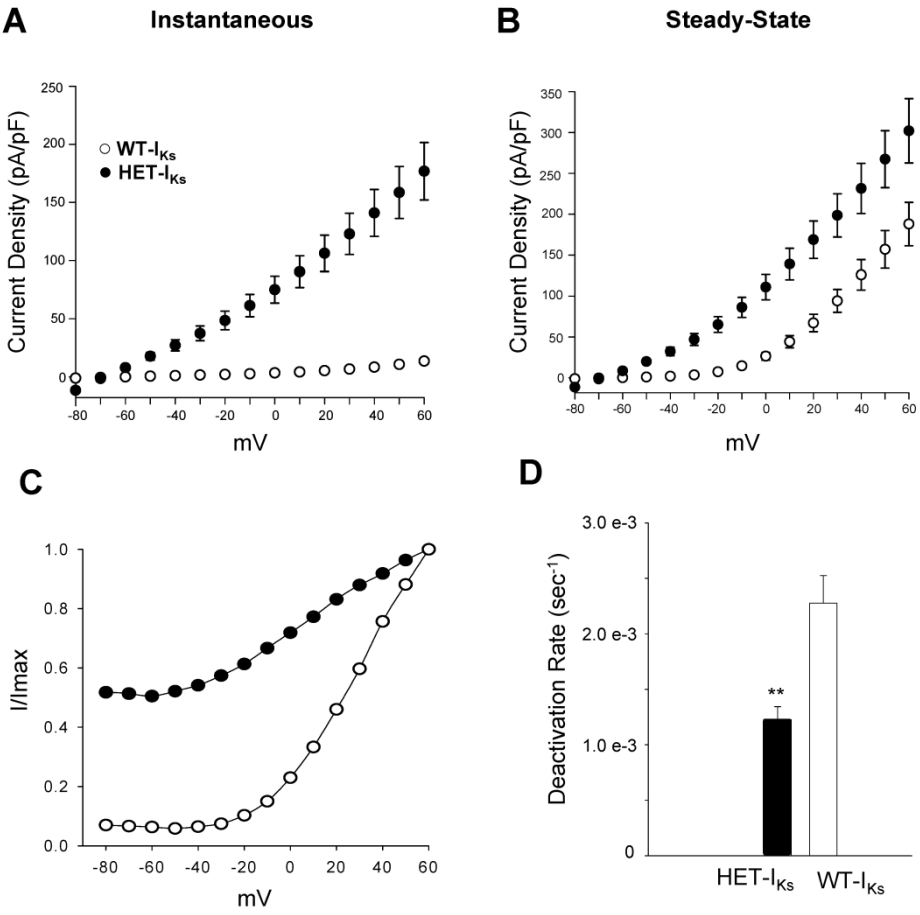

Figure 52. Functional properties of Het-I_{Ks}. **A**, Voltage dependence of instantaneous current density recorded 100 ms after onset of the voltage step for WT-I_{Ks} (○, n = 19) and HET-I_{Ks} (●, n = 19). Differences were significant at the p<0.001 level for voltages between –60 and +60 mV. **B**, Voltage dependence of steady-state current density recorded 1990 ms after onset of the voltage step for WT-I_{Ks} (○) and HET-I_{Ks} (●). Current densities are significantly different (p<0.02) between WT-I_{Ks} and HET-I_{Ks} at all voltages except −70 mV (reversal potential). **C**, Voltage dependence of activation for WT-I_{Ks} (○, n = 16) and HET-I_{Ks} (●, n = 13). Solid lines represent average of Boltzmann fits to data from individual cells. Values for slope factor were not different between WT-I_{Ks} (16.9 ± 0.6) and HET-I_{Ks} (20.9 ± 3). Values for $V_{1/2}$ are provided in the text. **D**, Deactivation kinetics illustrated for WT-I_{Ks} (n = 9) and HET-I_{Ks} (n = 11). Tail currents were elicited by a 2 s test pulse to +40 mV from a holding potential of −80 mV followed by sequential 2 s test pulses from −40 mV to −100 mV in 10 mV increments. At −100mV, HET-I_{Ks} has a significantly slower deactivation rate than WT-I_{Ks} (1.22e-3 ± 0.11e-3, *vs.* 2.28e-3 ± 0.25e-3; p<0.02).

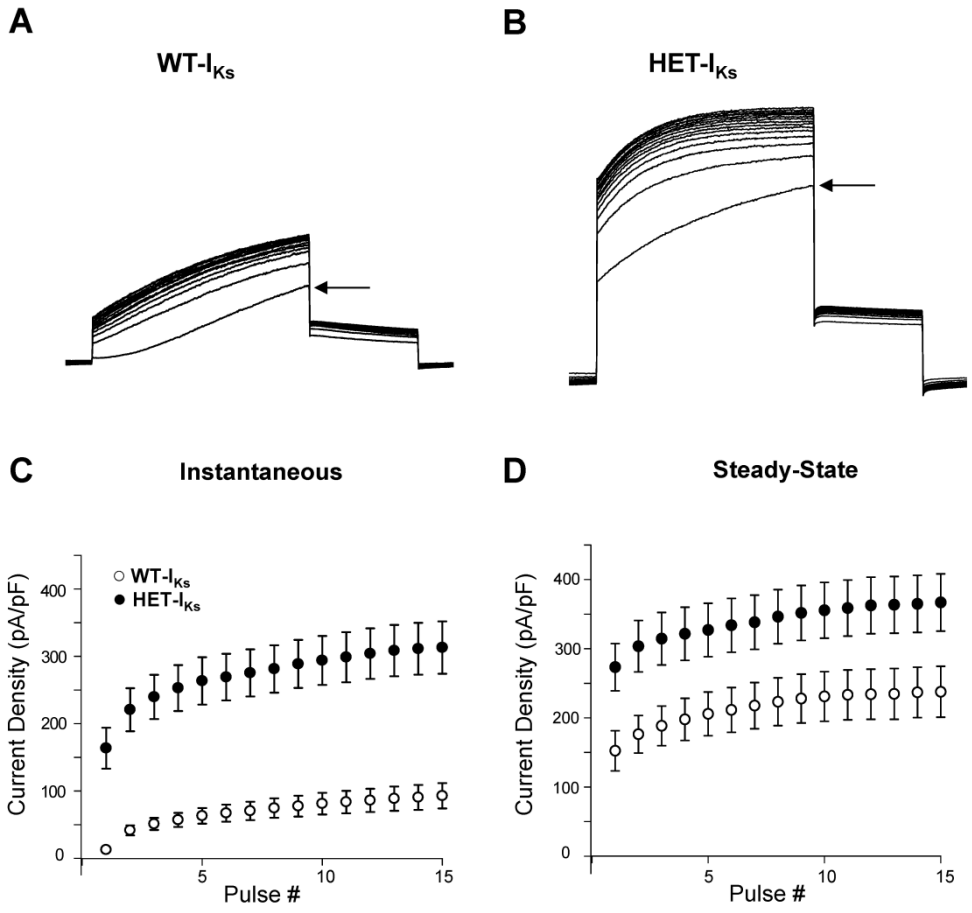

Figure 53. HET-I_{Ks} exhibits use-dependent current accumulation. **A and B**, Representative current recordings during repetitive pulsing from cells expressing WT-I_{Ks} (**A**) or HET-I_{Ks} (**B**). For **A** and **B**, cells were repetitively depolarized to +40 mV for 2 s and then to −30 mV for 1 s followed by a 1 s interpulse interval at the holding potential. The first pulse is indicated by the arrow. **C**, Use dependence of instantaneous current density for cells expressing WT-I_{Ks} (○, n = 13) and HET-I_{Ks} (●, n = 14). Differences were significant at the $p<0.001$ level for all pulses. **D**, Use dependence of steady-state current density for WT-I_{Ks} (○) and HET-I_{Ks} (●) expressing cells. Differences were significant at the $p<0.03$ level for all pulses.

Selective inhibition of HET-I_{Ks} with HMR-1556

Given the enhanced sensitivity of S140G-I_{Ks} to HMR-1556, we hypothesized that HET-I_{Ks} could be selectively suppressed by using a concentration HMR-1556 that predominantly inhibits the high affinity state. To test this hypothesis, we applied 20nM HMR-1556 or vehicle to heterologously expressed channels and assessed the effects of drug on gating kinetics and current amplitudes.

Vehicle had no effects on the behavior of WT-I_{Ks} and HET-I_{Ks} (Figure 54 A,B). Further, 20nM HMR-1556 had no appreciable effect on current levels or gating behavior of WT-I_{Ks} (Figure 54 C), but the drug exerted notable effects on HET-I_{Ks} including suppression of both instantaneous and steady-state current amplitude and attenuation of use-dependent current accumulation (Figure 54 D). The effects of 20nM HMR-1556 on WT-I_{Ks} and HET-I_{Ks} are quantified in Figure 55. Importantly, 20nM HMR-1556 did not inhibit WT-I_{Ks}, but did reduce the amplitude of HET-I_{Ks} to levels that were not significantly different from WT-I_{Ks}. Additionally, the ratio of instantaneous to steady-state current for HET-I_{Ks} was also modified by the drug to a value that was not significantly different from WT-I_{Ks} (Figure 55). These findings demonstrated the selective suppression of HET-I_{Ks} and the normalization of this mutant current to WT-I_{Ks} levels.

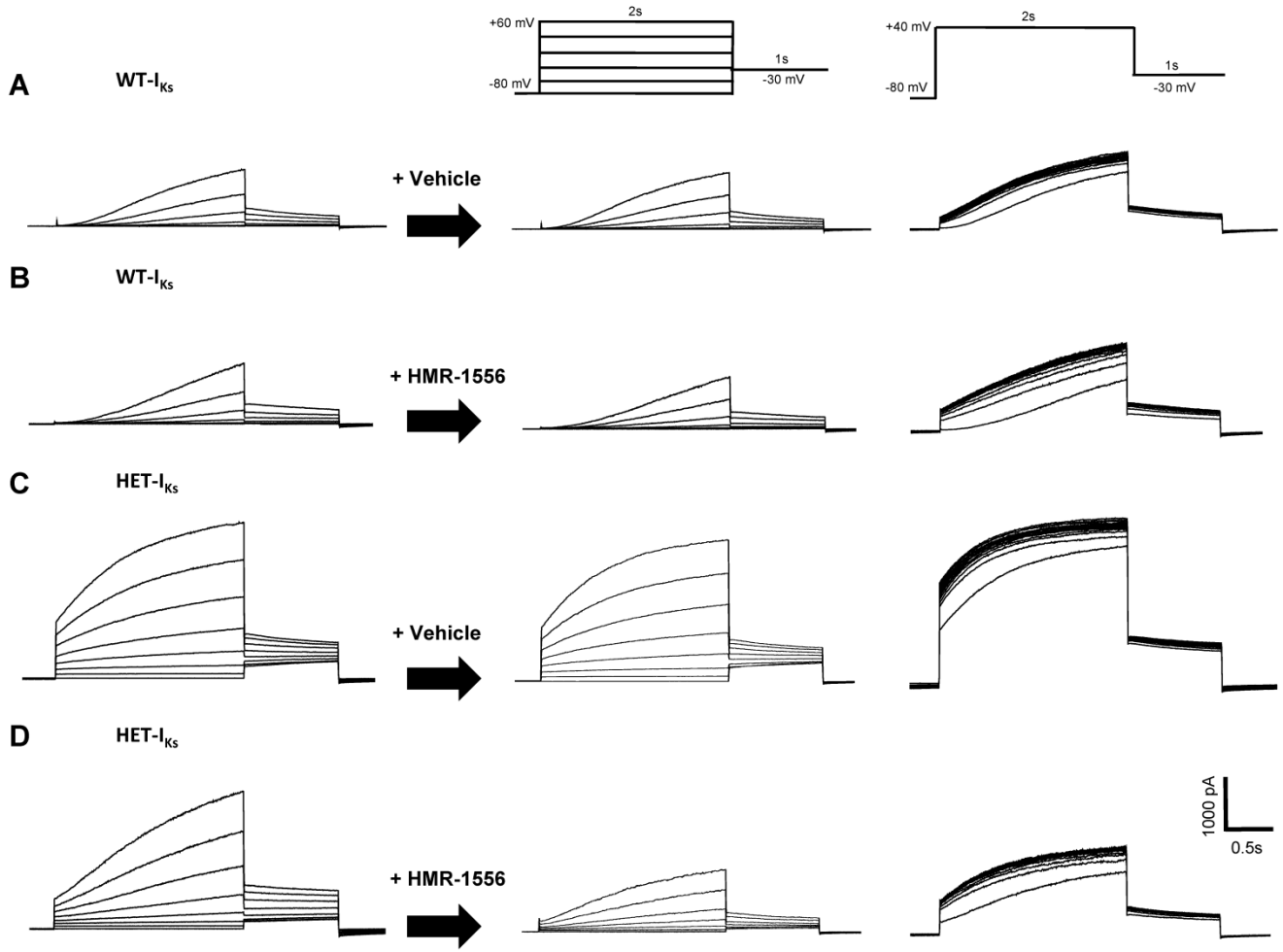

Figure 54. Representative traces of selective inhibition of HET-I_{Ks} by HMR-1556. **A and B,** Effects of vehicle on whole-cell currents during an activation voltage clamp protocol (middle panel) and during repetitive stimulation (right panel) from cells expressing WT-I_{Ks} (**A**) or HET-I_{Ks} (**B**). **C and D**, Effect of HMR-1556 (20 nM) on whole-cell currents during activation (middle panel) and repetitive stimulation (right panel) protocols from cells expressing WT-I_{Ks} (**C**) or HET-I_{Ks} (**D**). In **A-D**, traces in each row

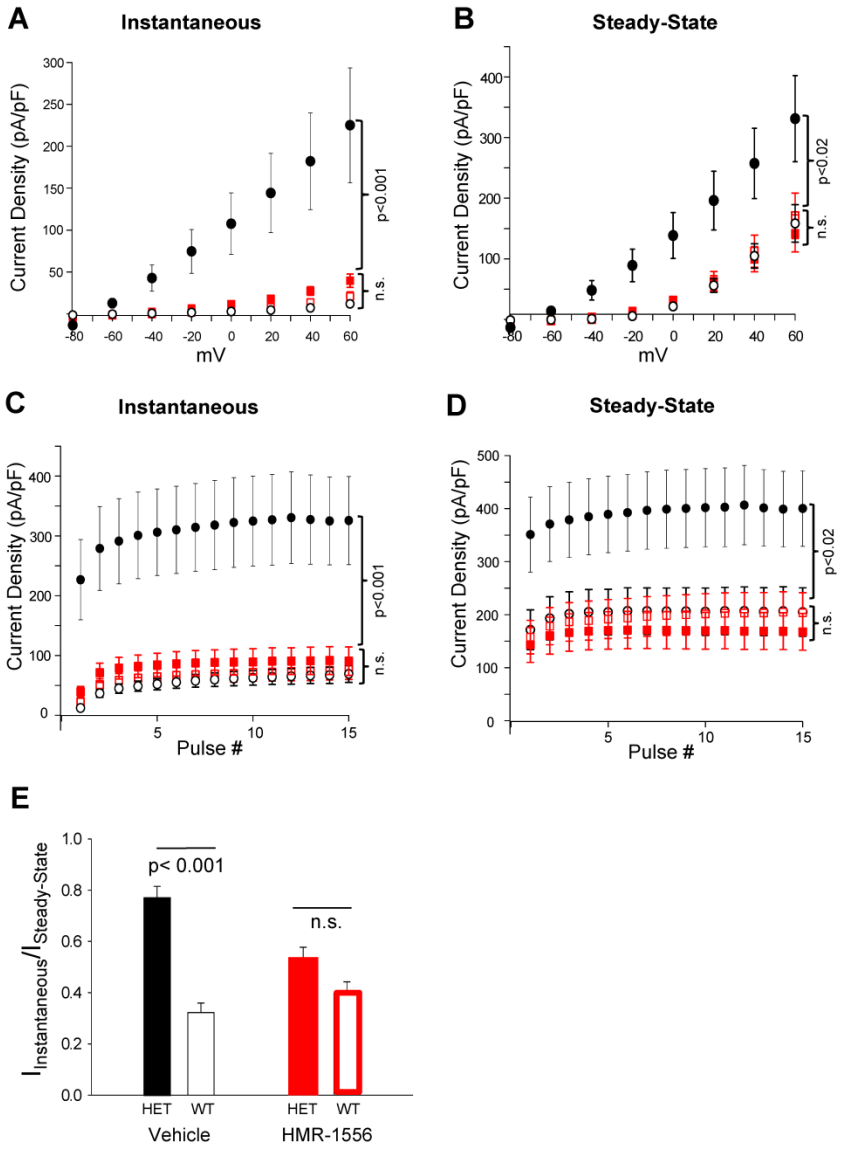

Figure 55. Selective inhibition of HET-I_{Ks} by HMR-1556. **A**, Voltage dependence of instantaneous current density for vehicle-treated WT-I_{Ks} (○, n = 10), vehicle-treated HET-I_{Ks} (●, n = 11), HMR-1556 (20 nM) treated WT-I_{Ks} (□, n = 10), and HMR-1556 (20 nM) treated HET-I_{Ks} (■, n = 9). Differences between vehicle-treated HET-I_{Ks} and other groups were significant at the p<0.001 level for voltages between –20 and +60 mV. **B**, Voltage dependence of steady-state current density for vehicle or HEM-1556 treated WT-I_{Ks} or HET-I_{Ks} (symbols defined in **A**). Differences between vehicle-treated HET-I_{Ks} and other groups were significant at the p<0.02 level for voltages between –40 and +60 mV. **C**, Use dependence of instantaneous current density for vehicle or HEM-1556 treated WT-I_{Ks} or HET-I_{Ks} (symbols defined in **A**). Differences between vehicle-treated HET-I_{Ks} and other groups were significant at the p<0.001 level at all tested potentials. **D**, Use dependence of steady-state current density for vehicle or HEM-1556 treated WT-I_{Ks} or HET-I_{Ks} (symbols defined in **A**). Differences between vehicle-treated HET-I_{Ks} and other groups were significant at the p<0.02 level at all tested potentials. In **A-D**, there were no differences among vehicle-treated WT-I_{Ks}, HMR-1556 treated WT-I_{Ks}, and HMR-1556 treated HET-I_{Ks}. **E**, Ratios of instantaneous current density to steady-state current density. Differences between vehicle-treated WT-I_{Ks} (open black bar) or HET-I_{Ks} (solid black bar) was significant at p<0.001, whereas there was no significant difference between HMR-1556 treated WT-I_{Ks} (open red bar) and HET-I_{Ks} (solid red bar).

HMR-1556 mitigates S140G-I_{Ks}-induced atrial action potential duration shortening

We examined the effects of HMR-1556 on action potentials in cultured adult rabbit left atrial myocytes expressing WT-I_{Ks} or S140G-I_{Ks} channel complexes. Action potentials were elicited at 1 Hz during whole-cell current clamp recording of adenovirus transduced atrial myocytes. Expression of S140G-I_{Ks} in left atrial myocytes hyperpolarized the resting membrane potential and significantly reduced 90% action potential duration (APD_{90}) compared to WT-I_{Ks} expression (APD_{90}: WT-I_{Ks}, 177.4 ± 21.0 msec; S140G-I_{Ks}, 68.9 ± 19.2 msec; $p<0.001$) (Figure 56 A). Application of 1µM HMR-1556 did not alter APD_{90} of WT-I_{Ks} expressing myocytes (185.2 ± 27.3 msec, $p>0.4$), whereas application of 1µM HMR-1556 significantly lengthened APD_{90} of S140G-I_{Ks} expressing myocytes (117.1 ± 12.7 msec, $p<0.04$) (Figure 56 B). These findings illustrate that HMR-1556 can selectively suppress S140G-I_{Ks} effects on atrial action potential duration without altering action potentials in myocytes expressing WT-I_{Ks}.

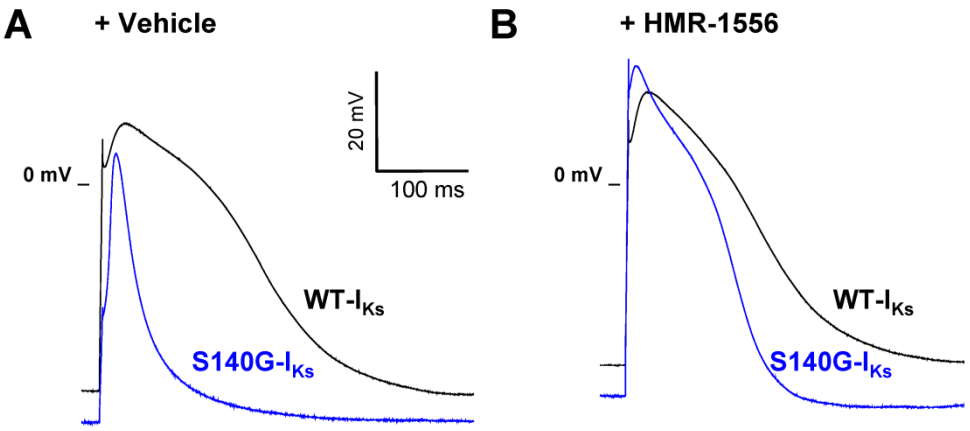

Figure 56. HMR-1556 mitigates atrial action potential shortening by S140G-I_{Ks}. Representative averages of 10 sequential action potentials from cultured rabbit left atrial myocytes expressing either WT-I_{Ks} (black line, n=6) or S140G-I_{Ks} (blue line, n=6). **A**, Action potentials elicited after application of vehicle. **B,** Action potentials elicited after application of 1 µM HMR-1556. APD_{90} values are provided in the text.

Discussion

The discovery of mutations in familial AF illustrated the contribution of specific genetic factors to AF susceptibility and suggested molecular mechanisms for some heritable forms of this common arrhythmia. For gain-of-function KCNQ1 mutations in particular, we sought to exploit this knowledge to explore a potential targeted therapy. Specifically, we hypothesized that KCNQ1 mutations predisposing to AF encode potassium channels with distinct pharmacological properties that could render them susceptible to selective inhibition. Genotype-specific therapies for inherited arrhythmia syndromes such as congenital long-QT syndrome and catecholaminergic polymorphic ventricular tachycardia are emerging.[76, 77] Further, a precedent for mutation-specific pharmacology of a rare, inherited disorder was established by the approval of ivacaftor for treatment of cystic fibrosis caused by CFTR-G551D.[78]

In this study, we investigated the utility of the selective and high affinity I_{Ks} blocker HMR-1556 to inhibit gain-of-function KCNQ1 mutations S140G and V141M. Chromanol 293B was the first identified selective I_{Ks} blocker, which exerts its effect at low micromolar concentrations.[79] The chromanol derivative HMR-1556 was developed to increase potency and improve the selectivity of I_{Ks} inhibition.[75] This derivative was initially demonstrated to have an IC_{50} of 120 nM against I_{Ks} expressed in *Xenopus* oocytes with little effect on other recombinant potassium channels at 10 µM consistent with a high level of specificity.[75] In isolated canine ventricular myocytes, HMR-1556 inhibits I_{Ks} with a nanomolar

IC_{50} whereas inhibition of other ionic currents (e.g., I_{Kr}, I_{K1}, I_{to}, $I_{Ca,L}$) required much higher concentrations.[80]

Consistent with our hypothesis, we observed that S140G-I_{Ks} exhibits enhanced sensitivity to HMR-1556. This enhancement was correlated with the emergence of an additional high affinity state, which was also observed with V141M-$I_{Ks.}$ Importantly, using a concentration that predominantly inhibits the high affinity state, we demonstrated that HMR-1556 effectively suppressed HET-I_{Ks} amplitude to a level that was not significantly different from WT-I_{Ks}. Further, this drug concentration attenuated the use-dependent accumulation of HET-I_{Ks} that occurs during repetitive pulsing. Significantly, we demonstrated that HMR-1556 can mitigate the S140G-I_{Ks} induced APD shortening in cultured adult rabbit atrial myocytes without affecting action potentials in myocytes expressing WT-I_{Ks}. These findings offer evidence supporting the potential for genotype-specific therapy of familial AF.

The potential utility of HMR-1556 or a similarly acting drug in the setting of familial AF should be considered in the context of the liabilities of inhibiting I_{Ks} in tissues other than atria. Reduction of I_{Ks} in ventricular muscle carries the risk of reduced repolarization reserve and predisposition to reentrant arrhythmia as in type 1 congenital long-QT syndrome. In anesthetized dogs receiving continuous intravenous infusions of HMR-1556, there was significant QTc prolongation and reproducible triggering of torsades de points with an isoproterenol bolus.[81]

Prolongation of QTc during HMR-1556 exposure is accentuated in dogs by co-administration of the I_{Kr} blocker dofetilide.[82] In Langendorff-perfused rabbit hearts, HMR-1556 alone was not sufficient to prolong monophasic action potential duration (APD) but co-administration of either dofetilide alone or dofetilide with veratridine caused significant lengthening of APD.[83, 84] These reports emphasize the potential proarrhythmic effects of high concentration HMR-1556 or of concurrent I_{Ks} and I_{Kr} inhibition. Fortunately, our data indicate that selective inhibition of S140G-I_{Ks} can be achieved at HMR-1556 concentrations that do not suppress WT-I_{Ks}.

Ototoxicity is another potential concern with HMR-1556. Because I_{Ks} expressed in the stria vascularis of inner ear is important in the generation of the K^+ rich cochlear endolymph, disruption of I_{Ks} has the potential to impair hearing as observed in autosomal recessive Jervell-Lange-Nielson syndrome associated with KCNQ1 or KCNE1 mutations.[85-87] Indeed, high concentrations of HMR-1556 exert a reversible ototoxicity in cats.[88] Again, our data suggest that there is a potential concentration range that may be free of inner ear adverse effects.

In summary, the AF-associated mutations KCNQ1-S140G and KCNQ1-V141M confer enhanced sensitivity to HMR-1556 in the context of the I_{Ks} channel complex. At a concentration that predominantly suppresses current by interacting with a novel high affinity state expressed by the S140G mutant, HMR-1556 normalized current amplitudes to levels that are not significantly different from WT-I_{Ks}, and attenuated the use-dependent accumulation of current. In cultured adult rabbit atrial myocytes, HMR-1556 mitigated the shortened APD induced by S140G-I_{Ks} expression. Our demonstration of selective targeting of this gain-of-function mutation provides a potential proof-of-principal for genotype-specific treatment of familial AF.

CHAPTER V

SUMMARY AND FUTURE DIRECTIONS

Summary

Atrial fibrillation (AF) is the most common sustained cardiac arrhythmia in adults. With a rising incidence in the aging population and association with significant morbidity and increased mortality, AF is a major public health burden. The discovery of mutations in familial AF illustrated the contribution of specific genetic factors to AF susceptibility and suggested molecular mechanisms for some heritable forms of this common arrhythmia. This dissertation focused on the first identified causative familial AF mutation (S140G) in the voltage gated potassium channel gene KCNQ1. Together with the auxiliary subunit KCNE1, KCNQ1 forms the slow component of the delayed rectifier potassium current, I_{Ks}. In the heart, I_{Ks} is critical to myocardial repolarization and action potential shortening in response to β adrenergic stimulation. We used S140G-I_{Ks} to explore AF mechanisms and therapeutic opportunities in familial AF.

Because transgenic S140G mouse models were inadequate for reproducing an AF-prone substrate, we first developed methods for high yield isolation, extended culture, and transfection of adult atrial myocytes suitable for electrophysiological experiments from more human-like cardiac model organisms, guinea pigs and rabbits. While guinea pig atrial and ventricular myocytes could be isolated

simultaneous, multi-chamber isolation of adult rabbit myocytes required more extensive modifications to the traditional Langendorf methods. Using a novel serial sampling technique, we were able to achieve reproducible high yields of both ventricular and atrial myocytes. After ventricular digestion, sequential recannulation and digestion of the left and right atria was critical for individual myocyte isolation. Yields of calcium tolerant cardiomyocytes were further enriched by gravity pelleting between wash steps, plating on laminin-coated coverslips, and at least a 2 h recovery time before exposure to physiological levels of calcium in culture media. The culture of adult cardiac myocytes with preserved morphology for 5 days was optimized through the use of laminin as an extracellular matrix to promote cell adherence, the identification of MEM as a base for culture media, the addition of pH buffering capacity, and the use of a low concentration of the E/C-uncoupler, blebbistatin. For the transfection of adult cardiac myocytes, biolistics and viral methods were successful. Adenovirus-mediated transduction proved most efficient in guinea pig and rabbit myocyte preparations with high titers and robust expression of transgenes. Electrophysiology confirmed the utility of these isolated cultured myocytes for future experiments.

Using this rabbit adult atrial myocyte model system, we advanced the insights garnered from characterization of monogenic AF mutations in heterologous systems and mathematical model by investigating the impact of S140G-I_{Ks} expression in native atrial myocytes. We presented evidence that under our

recording conditions I_{Ks} is not endogenously expressed in rabbit atrial myocytes. In addition, to exogenously express I_{Ks} in rabbit atrial myocytes, a modified adenoviral promoter must be used to generate the potassium channel virus and a very high MOI is necessary to generate expression. Further, we created a program to facilitate the high throughput analysis of action potentials. In S140G-I_{Ks} expressing myocytes, we revealed evidence of triggered activity at low frequency stimulation and a shorter action potential duration at higher frequency with hyperpolarized resting membrane potential compared to WT-I_{Ks} expressing myocytes. Overall, we illustrated effects of the FAF-associated mutation S140G-I_{Ks} in a native albeit cultured adult atrial myocyte supporting the hypothesis that a shortened APD likely underlies substrate susceptibility.

Springing from these observations, we sought to explore potential targeted therapeutic opportunities to ameliorate the physiological consequences of a KCNQ1 gain-of-function mutation. Specifically, we hypothesized that KCNQ1 mutations predisposing to AF encode potassium channels with distinct pharmacological properties that could render them susceptible to selective inhibition. Consistent with our hypothesis, we observed that S140G-I_{Ks} exhibits enhanced sensitivity to the I_{Ks}-selective blocker, HMR-1556. This enhancement was correlated with the emergence of an additional high affinity state, which was also observed with V141M-$I_{Ks,}$ a neighboring gain-of-function AF-associated mutation. Because KCNQ1-S140G mutation-positive subjects were reported to be heterozygous in familial AF and because WT and mutant KCNQ1 subunits

can co-assemble in heteromeric channels, we examined channel complexes consisting of both WT and mutant subunits co-expressed with KCNE1 (HET-I_{Ks}), which exhibited larger amplitudes with a large fraction of instantaneous current. Importantly, using a concentration that predominantly inhibits the high affinity state, we demonstrated that HMR-1556 effectively suppressed HET-I_{Ks} amplitude to a level that was not significantly different from WT-I_{Ks}. Further, this drug concentration attenuated the use-dependent accumulation of HET-I_{Ks} that occurs during repetitive pulsing. Significantly, we demonstrated that HMR-1556 can mitigate the S140G-I_{Ks} induced APD shortening in cultured adult rabbit atrial myocytes without affecting action potentials in myocytes expressing WT-I_{Ks}. These findings offer evidence supporting the potential for genotype-specific therapy of familial AF.

Future directions

The work discussed in this dissertation provides multiple avenues for the further scrutiny of AF substrate susceptibility and the possible therapeutic value of HMR-1556. The establishment of the adult rabbit atrial myocyte model system with exogenous ion channel expression enables further investigation into the genesis of FAF substrate susceptibility as related to S140G-I_{Ks} and other gain-of-function mutations in combination with other known acquired AF susceptibility factors. The intriguing increased sensitivity of S140G-I_{Ks} to HMR-1556 provokes questions about the biophysical determinants of HMR-1556 specificity to I_{Ks}. Further the increased sensitivity of V141M-I_{Ks} evokes a broader possible role for

HMR-1556 with additional KCNQ1 FAF mutations and encourages further consideration of HMR-1556 as a possible therapeutic. Each of these intriguing experimental possibilities will be reflected upon in turn.

AF susceptibility in the cultured rabbit atrial myocyte model

The model system developed for investigating S140G-I_{Ks} expression effect on rabbit atrial myocytes can be further used to determine the effects of acquired AF susceptibility factors, to explore the possible differential effects of other KCNQ1 FAF-associated mutations on atrial APD, and to investigate the pleiotropy with LQTS observed in some patients. Further, a native atrial myocyte system can be exploited to dissect pharmacologically the effect of familial AF-associated KCNE mutations on the atrial action potential and atrial potassium currents.

Effect of acquired AF factors on S140G-I_{Ks} expressing rabbit atrial myocytes

Although we elucidated the effects of S140G-I_{Ks} on rabbit atrial myocytes, this effect alone is not enough for the clinical manifestation of AF as this arrhythmia does not present in childhood. Unknown are what factors acquired during life are needed for AF manifestation. How S140G-I_{Ks} genetic susceptibility interacts, potentially additively or synergistically, with known acquired AF susceptibility factors needs to be explored. Considered here are AF contributing factors of oxidative stress and electrical remodeling.

Oxidative stress has been implicated in the pathogenesis of AF by several studies and is an established factor that increases with aging.[89] Oxidative stress also profoundly affects gating properties of ion channels.[90] Yet the mechanism or mechanisms by which ROS could promote AF are not well understood. Although we determined that oxidative stress mimicked by application of tert-butyl hydroperoxide (t-BHP) does not directly potentiate the activity of S140G-I_{Ks} (data not shown), how oxidative stress alters native myocyte predisposition to AF and whether S140G-I_{Ks} exert additive or synergistic in this circumstance is unknown. Analysis of the current and action potential alterations in S140G-I_{Ks} expressing myocytes under acute or prolonged exposure to tBHP will provide insight into the effects of oxidative stress on this genetically-encoded AF risk factor.

AF itself can induce substrate vulnerability through electrical remodeling induced by tachypacing. These changes include shortened APD, increased outward potassium current, DAD predisposition, and downregulation of calcium and sodium currents. Future studies can test the hypothesis that S140G-I_{Ks} affects atrial myocyte adaptation to conditions that promote electrical remodeling in a manner that potentiates the effects of these factors to produce an AF-prone cellular substrate. These myocyte studies could elucidate electrophysiological changes that occur in the context of electrically remodeled cells. During culture of S140G-I_{Ks} expressing rabbit atrial myocytes, the culture can be paced rapidly to induce remodeling. Recorded potassium currents and action potentials may help elucidate how S140G-I_{Ks} adapts to tachypacing compared to WT-I_{Ks} controls.

Anticipated results: These studies might reveal how S140G-I_{Ks} could work synergistically or additively to promote AF vulnerability in the context of oxidative stress or electrical remodeling. Given that we observed triggered activity in S140G-I_{Ks} at low frequency, this predisposition may be augmented with exposure to t-BHP and the threshold for triggered activity may be lower. Further high frequency stimulus of action potentials exacerbated the shortened APD induced by S140G-I_{Ks}. Because electrical remodeling shortens APD, this tachypacing in culture may have an additive effect on APD abbreviation and further augment potassium channel current. In the context of a electrical remodeled myocyte, the predisposition of S140G-I_{Ks} expressing myocytes to triggered activity likely may be enhanced. Together, these experiments could elucidate the interaction between genetic and acquired AF susceptibility factors.

Effect of other familial AF-associated mutations in rabbit atrial myocytes

With an established model system for expressing and analyzing the effects of S140G-I_{Ks} on rabbit atrial myocytes, this system can be used to further explore the effects of other atrial fibrillation associated mutations in a native atrial cardiac myocyte environment. The initial candidates would be the KCNQ1 mutations V141M, R231C, and R231H, which all have some constitutive activity in heterologous experiments. In addition, familial AF associated mutation, KCNQ1-IAP54-56 demonstrates gain-of-function in current density but does not have a constitutively active component. Whether this mutation effects the rabbit atrial myocyte in a similar fashion to S140G-I_{Ks} would be intriguing. Adenovirus can be

created to express each of these mutations and used to transduce rabbit atrial myocytes. The potassium currents and the action potentials can be elicited through whole cell patch clamp and analyzed. In addition to response to increased stimulus frequency, the response to adrenergic stimulation such as isoproterenol could be revealing.

Anticipated results: Expression of the other familial AF mutations could shorten rabbit atrial potential duration and augment potassium current density. However, we anticipate variability in the degree of shortening. Given the earliest AF onset was with V141M, we anticipate the shortest APD from myocytes expression V141M-I_{Ks}. Further, without constitutive activity component, we anticipate a smaller effect on APD with IAP-54-56-I_{Ks} and possibly less APD shortening in response to increased stimulation frequency. Further these myocytes may have differential sensitive to adrenergic stimulation that could augment their contribution to AF susceptibility. These experiments would reveal commonalities between gain-of-function KCNQ1 mutation and their contribution to AF susceptibility. A common mechanism between genetic causes of AF would provide a larger target for therapeutic intervention.

Examine AF and LQT1-associated mutation pleiotropy in rabbit myocytes

Although S140G-I_{Ks} was identified as the causative mutation in familial AF, many affected familial members also had a prolonged QT interval. Similarly, the related KCNQ1 mutation, R231C, was first associated with LQT1 and only recently has

been implicated in familial AF. This observed pleiotropy in individuals and between families provokes the hypothesis that these mutations have differential effects in atrial myocytes than in ventricular myocytes. Both S140G-I_{Ks} and R231C-I_{Ks} have a constitutively active component; yet R231C-I_{Ks} has been shown to have a decrease in current density. How these attributes may alter ventricular myocytes is not known. To address, this hypothesis adenovirus expressing either S140G-I_{Ks} or R231C-I_{Ks} can be used to transduce rabbit ventricular myocytes. The potassium current and action potential can be recorded.

Anticipated results:. We anticipate a prolongation of APD in R231C-I_{Ks} expressing ventricular myocytes due to its decrease in current density. We predict a shortening in ventricular APD in S140G-I_{Ks}. Yet we anticipate altered or diminished responses to β-adrenergic stimulation which may promote APD prolongation characteristic of a prolonged QT interval, or increased triggered activity which may reflect altered calcium dynamics. These experiments would illustrate whether these mutations have differential effects on ventricular myocytes that might clarify the observed pleiotropy in AF and prolonged QT interval.

Impact of familial AF-associated KCNE mutations on rabbit atrial myocytes

In addition to familial AF associated mutations in the pore-forming potassium channel KCNQ1, familial AF associated mutations in auxiliary single transmembrane KCNE subunits have also been reported: KCNE2-R27C,[22] KCNE2-X124N,[23] and KCNE3-V17M.[24] Initial heterologous experiments have illustrated that these mutation increase currents when co-expressed with KCNQ1. However, KCNEs are promiscuous and interact with multiple voltage-gated potassium channels. How these interactions contribute to the cardiac action potential and how mutations might perturb these interactions are unknown. We hypothesize that these mutations would shorten overall APD though alternation of many different potassium currents. Adenoviral expression of these mutations or the respective wild-type KCNE in rabbit atrial myocytes and analysis of potassium currents and action potentials would address this hypothesis.

Anticipated results: We predict that expression of these familial AF-associated mutations may shorten the atrial action potential and overall increase the potassium current in atrial myocytes. Application of specific potassium channel blockers would reveal the relative contribution of the KCNEs to specific channels expression. Given the known interactions of KCNE2 and KCNE3 with I_{Ks}, I_{TO}, I_{Kr}, we predict that these experiments might demonstrate alteration to each current and augment our understanding of KCNEs in action potential determination.

Biophysics of HMR-1556 inhibition

Beyond the experiment opportunities provided by cultured rabbit atrial myocyte model, the increased sensitivity of S140G-I_{Ks} and V141M-I_{Ks} to HMR-1556 provokes some fundamental biophysical questions about the mechanism of HMR-1556 inhibition and of HMR-1556 to I_{Ks}. The importance of the abnormal gating properties of the mutant channels to HMR-1556 sensitivity and the complex binding curve of HMR-1556 inhibition of these mutants suggest further exploration.

HMR-1556 inhibition requires KCNE1 coexpression with KCNQ1. Yet previous work demonstrated that point mutations in KCNE1 were unsuccessful in abolishing or diminishing I_{Ks} chromanol sensitivity[91] suggesting that KCNE1 acts allosterically to promote drug sensitivity. The additive sensitivity noted with S140G and V141M mutations, which notably require KCNE1 to reveal their gain-of-function, is provocative. Our studies have demonstrated no enhanced sensitivity to HMR-1556 when S140G-Q1 is expressed without KCNE1 (data not shown) suggesting that the residue change itself is not sufficient. To address whether the abnormal channel gating properties conferred by these mutations is responsible for increased sensitivity, experiments can be conducted with channels having similar gating properties. In particular, the non-disease linked mutation, Q1-R237A, has a similar phenotype of ultraslow deactivation yet does not require KCNE1 co-expression.[18] Moreover, R237 is predicted to interact with V141 and S140 in the open state. Experiments with R237A could determine if the

constitutively activity conferred by disruption of this residue interaction is sufficient for HMR-1556 sensitivity. Furthermore, the KCNE3 co-expression with KCNQ1 results in a similar increased current density and had a near instantaneous activation rate. Whether KCNQ1-KCNE3 complex has increased sensitivity would be intriguing and would further suggest that KCNQ1 with these gating properties promotes for HMR-1556 sensitivity. In addition to the potassium channel gating properties, the complex HMR-1556 inhibition curve of S140G-I_{Ks} and V141M-I_{Ks} suggests either a second binding affinity state or a second binding affinity site for HMR-1556. Previous work with chromanol 293B, structurally similar to HMR-1556, demonstrated a slight preferential open channel block mechanism. The binding site was predicted to be in the inner pore of vestibule containing the ion selectivity filter of Q1, but the open state alone did not enhance sensitivity.[91, 92] We attempted to apply HMR-1556 to a closed S140G-I_{Ks}, but the degree of hyperpolarization and time (>4 mins) required to close the channel completely was not commensurate with CHO cell viability. Computational modeling of drug docking could provide insights into the differential blockade observed in mutant and wild-type channels.

Anticipate results: Future work with R237A and KCNQ1-KCNE3 might reveal whether the gating dynamics of KCNQ1 are critical to enhanced sensitive of HMR-1556 or whether the disruption of the R231-V141/S140-E160 is important for increased sensitivity. Computational modeling and drug docking studies might help determine whether the mutations expose a second binding site or provide a

second affinity state for the drug to preferentially bind. These data could be used to design site-directed mutagenesis to further probe the nature of HMR-1556 specific to I_{Ks} inhibition.

HMR-1556 as a potential therapeutic agent

The increased sensitivity of S140G-I_{Ks} and V141M-I_{Ks} to HMR-1556 compared to WT-I_{Ks} suggested a potential therapeutic opportunity, to inhibit these gain-of-function mutations AF predisposing mutations without deleterious effects on the WT channel. Indeed in a heterologous system and in rabbit atrial myocytes, we demonstrated that HMR-1556 could mitigate the effect of S140G-I_{Ks} on potassium currents and action potential duration without WT channel blockade. These data suggest further exploration of HMR-1556 as a potential therapeutic agent for familial AF. Considering the similar increased sensitivity of V141M-I_{Ks}, whether other familial AF associated mutations had enhanced sensitivity to HMR-1556 would expand the possible candidates and further promote a broader mechanistic approach to treating familial AF.

HMR-1556 sensitivity of other familial AF-associated KCNQ1 mutations

The physiologic constitutive activity S140G- I_{Ks} is caused by ultraslowed deactivation of the channel, hypothesized to be due to the salt bridge disruption between the V141/S140-R231-E160 residues in the closed state or stabilization between residues V141/S140-R237-E160 in the open state.[17] The disruption or stabilization of the salt bridge and the S140G mutation itself may independently

or together confer increased sensitivity through an additional high affinity state. If the salt bridge perturbation is critical for enhanced sensitivity, then other gain-of-function FAF-linked mutations in KCNQ1, R231C and R231H, may be similarly selectively inhibited. A concentration-response curve could be completed in a heterologous system to determine whether these mutations have similar enhanced sensitive to HMR-1556. Other potassium channel gain-of-function familial AF mutations include KCNQ1-IAP54-56 NPPA-S64R, and KCNEs: KCNE2-R27C, KCNE2-X124N, and KCNE3-V17M. Although the mechanism for I_{Ks} enhancement is not as well articulated with these mutations, whether they have increased sensitivity to HMR-1556 would be intriguing.

Anticipated results: We predicted that mutations in R231 with slowed deactivation may have similar enhanced sensitivity to HMR-1556. Given that we do not know the effects of HMR-1556 on KCNQ1-KCNE2 or KCNQ1-KCNE3 channel complex, it is more difficult to anticipate the sensitivity of these mutations. However, because KCNE3-V17M does not increase KCNQ1 current (instead, increases HERG), it is less likely to have enhanced sensitivity to HMR-1556. The gain-of-function I_{Ks} AF-associated mutations may have enhanced sensitivity.

REFERENCES

1. Go AS, Mozaffarian D, Roger VL, Benjamin EJ, Berry JD, Borden WB, Bravata DM, Dai S, Ford ES, Fox CS, Franco S, Fullerton HJ, Gillespie C, Hailpern SM, Heit JA, Howard VJ, Huffman MD, Kissela BM, Kittner SJ, Lackland DT, Lichtman JH, Lisabeth LD, Magid D, Marcus GM, Marelli A, Matchar DB, McGuire DK, Mohler ER, Moy CS, Mussolino ME, Nichol G, Paynter NP, Schreiner PJ, Sorlie PD, Stein J, Turan TN, Virani SS, Wong ND, Woo D, Turner MB. Executive summary: heart disease and stroke statistics--2013 update: a report from the American Heart Association. *Circulation.* 2013;127(1):143-152.

2. Chen YH, Xu SJ, Bendahhou S, Wang XL, Wang Y, Xu WY, Jin HW, Sun H, Su XY, Zhuang QN, Yang YQ, Li YB, Liu Y, Xu HJ, Li XF, Ma N, Mou CP, Chen Z, Barhanin J, Huang W. KCNQ1 gain-of-function mutation in familial atrial fibrillation. *Science.* 2003;299(5604):251-254.

3. Lundquist AL, Manderfield LJ, Vanoye CG, Rogers CS, Donahue BS, Chang PA, Drinkwater DC, Murray KT, George AL, Jr. Expression of multiple KCNE genes in human heart may enable variable modulation of I(Ks). *J Mol Cell Cardiol.* 2005;38(2):277-287.

4. Lundquist AL, Turner CL, Ballester LY, George AL, Jr. Expression and transcriptional control of human KCNE genes. *Genomics.* 2006;87(1):119-128.

5. Ciampa E. *Investigating the function of KCNE4 in cardiac physiology*: Pharmacology, Vanderbilt University; 2011.

6. Marx SO, Kurokawa J, Reiken S, Motoike H, D'Armiento J, Marks AR, Kass RS. Requirement of a macromolecular signaling complex for beta adrenergic receptor modulation of the KCNQ1-KCNE1 potassium channel. *Science.* 2002;295(5554):496-499.

7. Loussouarn G, Park KH, Bellocq C, Baro I, Charpentier F, Escande D. Phosphatidylinositol-4,5-bisphosphate, PIP2, controls KCNQ1/KCNE1 voltage-gated potassium channels: a functional homology between voltage-gated and inward rectifier K+ channels. *Embo J.* 2003;22(20):5412-5421.

8. Park KH, Piron J, Dahimene S, Merot J, Baro I, Escande D, Loussouarn G. Impaired KCNQ1-KCNE1 and phosphatidylinositol-4,5-bisphosphate interaction underlies the long QT syndrome. *Circ Res.* 2005;96(7):730-739.

9. Jespersen T, Grunnet M, Olesen SP. The KCNQ1 potassium channel: from gene to physiological function. *Physiology (Bethesda).* 2005;20:408-416.

10. Darbar D, Roden DM. Genetic mechanisms of atrial fibrillation: impact on response to treatment. *Nat Rev Cardiol.* 2013;10(6):317-329.

11. Barhanin J, Lesage F, Guillemare E, Fink M, Lazdunski M, Romey G. K(V)LQT1 and lsK (minK) proteins associate to form the I(Ks) cardiac potassium current. *Nature.* 1996;384(6604):78-80.

12. Sanguinetti MC, Curran ME, Zou A, Shen J, Spector PS, Atkinson DL, Keating MT. Coassembly of K(V)LQT1 and minK (IsK) proteins to form cardiac I(Ks) potassium channel. *Nature.* 1996;384(6604):80-83.

13. Splawski I, Timothy KW, Vincent GM, Atkinson DL, Keating MT. Molecular basis of the long-QT syndrome associated with deafness. *N Engl J Med.* 1997;336(22):1562-1567.

14. Wang Z, Tristani-Firouzi M, Xu Q, Lin M, Keating MT, Sanguinetti MC. Functional effects of mutations in KvLQT1 that cause long QT syndrome. *J Cardiovasc Electrophysiol.* 1999;10(6):817-826.

15. Hong K, Piper DR, Diaz-Valdecantos A, Brugada J, Oliva A, Burashnikov E, Santos-de-Soto J, Grueso-Montero J, Diaz-Enfante E, Brugada P, Sachse F, Sanguinetti MC, Brugada R. De novo KCNQ1 mutation responsible for atrial fibrillation and short QT syndrome in utero. *Cardiovasc Res.* 2005;68(3):433-440.

16. Bendahhou S, Marionneau C, Haurogne K, Larroque MM, Derand R, Szuts V, Escande D, Demolombe S, Barhanin J. In vitro molecular interactions and distribution of KCNE family with KCNQ1 in the human heart. *Cardiovasc Res.* 2005;67(3):529-538.

17. Restier L, Cheng L, Sanguinetti MC. Mechanisms by which atrial fibrillation-associated mutations in the S1 domain of KCNQ1 slow deactivation of IKs channels. *J Physiol.* 2008;586(Pt 17):4179-4191.

18. Panaghie G, Abbott GW. The role of S4 charges in voltage-dependent and voltage-independent KCNQ1 potassium channel complexes. *J Gen Physiol.* 2007;129(2):121-133.

19. Bartos DC, Duchatelet S, Burgess DE, Klug D, Denjoy I, Peat R, Lupoglazoff JM, Fressart V, Berthet M, Ackerman MJ, January CT, Guicheney P, Delisle BP. R231C mutation in KCNQ1 causes long QT syndrome type 1 and familial atrial fibrillation. *Heart Rhythm.* 2011;8(1):48-55.

20. Bartos DC, Anderson JB, Bastiaenen R, Johnson JN, Gollob MH, Tester DJ, Burgess DE, Homfray T, Behr ER, Ackerman MJ, Guicheney P, Delisle BP. A KCNQ1 Mutation Causes a High Penetrance for Familial Atrial Fibrillation. *J Cardiovasc Electrophysiol.* 2013;24(5):562-569.

21. Abraham RL, Yang T, Blair M, Roden DM, Darbar D. Augmented potassium current is a shared phenotype for two genetic defects associated with familial atrial fibrillation. *J Mol Cell Cardiol.* 2010;48(1):181-190.

22. Yang Y, Xia M, Jin Q, Bendahhou S, Shi J, Chen Y, Liang B, Lin J, Liu Y, Liu B, Zhou Q, Zhang D, Wang R, Ma N, Su X, Niu K, Pei Y, Xu W, Chen Z, Wan H, Cui J, Barhanin J, Chen Y. Identification of a KCNE2 gain-of-function mutation in patients with familial atrial fibrillation. *Am J Hum Genet.* 2004;75(5):899-905.

23. George AL, Jr. Unpublished.

24. Lundby A, Ravn LS, Svendsen JH, Hauns S, Olesen SP, Schmitt N. KCNE3 mutation V17M identified in a patient with lone atrial fibrillation. *Cell Physiol Biochem.* 2008;21(1-3):47-54.

25. Yang Y, Liu Y, Dong X, Kuang Y, Lin J, Su X, Peng L, Jin Q, He Y, Liu B, Pan Z, Li L, Zhu Q, Lin X, Zhou Q, Pan Q, Eurlings PM, Fei J, Wang Z, Chen YH. Human KCNQ1 S140G mutation is associated with atrioventricular blocks. *Heart Rhythm.* 2007;4(5):611-618.

26. Miyasaka Y, Barnes ME, Gersh BJ, Cha SS, Bailey KR, Abhayaratna WP, Seward JB, Tsang TS. Secular trends in incidence of atrial fibrillation in Olmsted County, Minnesota, 1980 to 2000, and implications on the projections for future prevalence. *Circulation.* 2006;114(2):119-125.

27. Benjamin EJ, Wolf PA, D'Agostino RB, Silbershatz H, Kannel WB, Levy D. Impact of atrial fibrillation on the risk of death: the Framingham Heart Study. *Circulation.* 1998;98(10):946-952.

28. Kim MH, Johnston SS, Chu BC, Dalal MR, Schulman KL. Estimation of total incremental health care costs in patients with atrial fibrillation in the United States. *Circ Cardiovasc Qual Outcomes.* 2011;4(3):313-320.

29. Chugh SS, Blackshear JL, Shen WK, Hammill SC, Gersh BJ. Epidemiology and natural history of atrial fibrillation: clinical implications. *J Am Coll Cardiol.* 2001;37(2):371-378.

30. Kopecky SL, Gersh BJ, McGoon MD, Whisnant JP, Holmes DR, Jr., Ilstrup DM, Frye RL. The natural history of lone atrial fibrillation. A

population-based study over three decades. *N Engl J Med.* 1987;317(11):669-674.

31. Brand FN, Abbott RD, Kannel WB, Wolf PA. Characteristics and prognosis of lone atrial fibrillation. 30-year follow-up in the Framingham Study. *Jama.* 1985;254(24):3449-3453.

32. Scardi S, Mazzone C, Pandullo C, Goldstein D, Poletti A, Humar F. Lone atrial fibrillation: prognostic differences between paroxysmal and chronic forms after 10 years of follow-up. *Am Heart J.* 1999;137(4 Pt 1):686-691.

33. Fox CS, Parise H, D'Agostino RB, Sr., Lloyd-Jones DM, Vasan RS, Wang TJ, Levy D, Wolf PA, Benjamin EJ. Parental atrial fibrillation as a risk factor for atrial fibrillation in offspring. *Jama.* 2004;291(23):2851-2855.

34. Gudbjartsson DF, Arnar DO, Helgadottir A, Gretarsdottir S, Holm H, Sigurdsson A, Jonasdottir A, Baker A, Thorleifsson G, Kristjansson K, Palsson A, Blondal T, Sulem P, Backman VM, Hardarson GA, Palsdottir E, Helgason A, Sigurjonsdottir R, Sverrisson JT, Kostulas K, Ng MC, Baum L, So WY, Wong KS, Chan JC, Furie KL, Greenberg SM, Sale M, Kelly P, MacRae CA, Smith EE, Rosand J, Hillert J, Ma RC, Ellinor PT, Thorgeirsson G, Gulcher JR, Kong A, Thorsteinsdottir U, Stefansson K. Variants conferring risk of atrial fibrillation on chromosome 4q25. *Nature.* 2007;448(7151):353-357.

35. Roberts R. Mechanisms of disease: Genetic mechanisms of atrial fibrillation. *Nat Clin Pract Cardiovasc Med.* 2006;3(5):276-282.

36. Ma KJ, Li N, Teng SY, Zhang YH, Sun Q, Gu DF, Pu JL. Modulation of KCNQ1 current by atrial fibrillation-associated KCNE4 (145E/D) gene polymorphism. *Chin Med J (Engl).* 2007;120(2):150-154.

37. Olson TM, Alekseev AE, Moreau C, Liu XK, Zingman LV, Miki T, Seino S, Asirvatham SJ, Jahangir A, Terzic A. KATP channel mutation confers risk for vein of Marshall adrenergic atrial fibrillation. *Nat Clin Pract Cardiovasc Med.* 2007;4(2):110-116.

38. Sinner MF, Pfeufer A, Akyol M, Beckmann BM, Hinterseer M, Wacker A, Perz S, Sauter W, Illig T, Nabauer M, Schmitt C, Wichmann HE, Schomig A, Steinbeck G, Meitinger T, Kaab S. The non-synonymous coding IKr-channel variant KCNH2-K897T is associated with atrial fibrillation: results from a systematic candidate gene-based analysis of KCNH2 (HERG). *Eur Heart J.* 2008;29(7):907-914.

39. Xia M, Jin Q, Bendahhou S, He Y, Larroque MM, Chen Y, Zhou Q, Yang Y, Liu Y, Liu B, Zhu Q, Zhou Y, Lin J, Liang B, Li L, Dong X, Pan Z, Wang R, Wan H, Qiu W, Xu W, Eurlings P, Barhanin J, Chen Y. A Kir2.1 gain-of-function mutation underlies familial atrial fibrillation. *Biochem Biophys Res Commun.* 2005;332(4):1012-1019.

40. Das S, Makino S, Melman YF, Shea MA, Goyal SB, Rosenzweig A, Macrae CA, Ellinor PT. Mutation in the S3 segment of KCNQ1 results in familial lone atrial fibrillation. *Heart Rhythm.* 2009;6(8):1146-1153.

41. Watanabe H, Darbar D, Kaiser DW, Jiramongkolchai K, Chopra S, Donahue BS, Kannankeril PJ, Roden DM. Mutations in sodium channel

beta1- and beta2-subunits associated with atrial fibrillation. *Circ Arrhythm Electrophysiol.* 2009;2(3):268-275.

42. Makiyama T, Akao M, Shizuta S, Doi T, Nishiyama K, Oka Y, Ohno S, Nishio Y, Tsuji K, Itoh H, Kimura T, Kita T, Horie M. A novel SCN5A gain-of-function mutation M1875T associated with familial atrial fibrillation. *J Am Coll Cardiol.* 2008;52(16):1326-1334.

43. Darbar D, Kannankeril PJ, Donahue BS, Kucera G, Stubblefield T, Haines JL, George AL, Jr., Roden DM. Cardiac sodium channel (SCN5A) variants associated with atrial fibrillation. *Circulation.* 2008;117(15):1927-1935.

44. Wyse DG, Waldo AL, DiMarco JP, Domanski MJ, Rosenberg Y, Schron EB, Kellen JC, Greene HL, Mickel MC, Dalquist JE, Corley SD. A comparison of rate control and rhythm control in patients with atrial fibrillation. *N Engl J Med.* 2002;347(23):1825-1833.

45. Van Gelder IC, Hagens VE, Bosker HA, Kingma JH, Kamp O, Kingma T, Said SA, Darmanata JI, Timmermans AJ, Tijssen JG, Crijns HJ. A comparison of rate control and rhythm control in patients with recurrent persistent atrial fibrillation. *N Engl J Med.* 2002;347(23):1834-1840.

46. Opolski G, Torbicki A, Kosior DA, Szulc M, Wozakowska-Kaplon B, Kolodziej P, Achremczyk P. Rate control vs rhythm control in patients with nonvalvular persistent atrial fibrillation: the results of the Polish How to Treat Chronic Atrial Fibrillation (HOT CAFE) Study. *Chest.* 2004;126(2):476-486.

47. Fuster V, Ryden LE, Cannom DS, Crijns HJ, Curtis AB, Ellenbogen KA, Halperin JL, Le Heuzey JY, Kay GN, Lowe JE, Olsson SB, Prystowsky EN, Tamargo JL, Wann S, Smith SC, Jr., Jacobs AK, Adams CD, Anderson JL, Antman EM, Halperin JL, Hunt SA, Nishimura R, Ornato JP, Page RL, Riegel B, Priori SG, Blanc JJ, Budaj A, Camm AJ, Dean V, Deckers JW, Despres C, Dickstein K, Lekakis J, McGregor K, Metra M, Morais J, Osterspey A, Tamargo JL, Zamorano JL. ACC/AHA/ESC 2006 Guidelines for the Management of Patients with Atrial Fibrillation: a report of the American College of Cardiology/American Heart Association Task Force on Practice Guidelines and the European Society of Cardiology Committee for Practice Guidelines (Writing Committee to Revise the 2001 Guidelines for the Management of Patients With Atrial Fibrillation): developed in collaboration with the European Heart Rhythm Association and the Heart Rhythm Society. *Circulation.* 2006;114(7):e257-354.

48. Itzhaki I, Maizels L, Huber I, Zwi-Dantsis L, Caspi O, Winterstern A, Feldman O, Gepstein A, Arbel G, Hammerman H, Boulos M, Gepstein L. Modelling the long QT syndrome with induced pluripotent stem cells. *Nature.*471(7337):225-229.

49. Belevych AE, Nulton-Persson A, Sims C, Harvey RD. Role of tyrosine kinase activity in alpha-adrenergic inhibition of the beta-adrenergically regulated L-type Ca(2+) current in guinea-pig ventricular myocytes. *J Physiol.* 2001;537(Pt 3):779-792.

50. Bassani JW, Bassani RA, Bers DM. Calibration of indo-1 and resting intracellular [Ca]i in intact rabbit cardiac myocytes. *Biophys J.* 1995;68(4):1453-1460.

51. Savio-Galimberti E, Frank J, Inoue M, Goldhaber JI, Cannell MB, Bridge JH, Sachse FB. Novel features of the rabbit transverse tubular system revealed by quantitative analysis of three-dimensional reconstructions from confocal images. *Biophys J.* 2008;95(4):2053-2062.

52. Kabaeva Z, Zhao M, Michele DE. Blebbistatin extends culture life of adult mouse cardiac myocytes and allows efficient and stable transgene expression. *Am J Physiol Heart Circ Physiol.* 2008;294(4):H1667-1674.

53. Dou Y, Balse E, Dehghani Zadeh A, Wang T, Goonasekara CL, Noble GP, Eldstrom J, Steele DF, Hatem SN, Fedida D. Normal targeting of a tagged Kv1.5 channel acutely transfected into fresh adult cardiac myocytes by a biolistic method. *Am J Physiol Cell Physiol.* 2010;298(6):C1343-1352.

54. Anderson RD, Haskell RE, Xia H, Roessler BJ, Davidson BL. A simple method for the rapid generation of recombinant adenovirus vectors. *Gene Ther.* 2000;7(12):1034-1038.

55. Hamill OP, Marty A, Neher E, Sakmann B, Sigworth FJ. Improved patch-clamp techniques for high-resolution current recording from cells and cell-free membrane patches. *Pflugers Arch.* 1981;391(2):85-100.

56. Lindau M, Neher E. Patch-clamp techniques for time-resolved capacitance measurements in single cells. *Pflugers Arch.* 1988;411(2):137-146.

57. Benavides-Haro DE, Sanchez-Chapula JA. Chloroquine blocks the background potassium current in guinea pig atrial myocytes. *Naunyn Schmiedebergs Arch Pharmacol.* 2000;361(3):311-318.

58. Liu GX, Choi BR, Ziv O, Li W, de Lange E, Qu Z, Koren G. Differential conditions for early after-depolarizations and triggered activity in cardiomyocytes derived from transgenic LQT1 and LQT2 rabbits. *J Physiol.* 2012;590(Pt 5):1171-1180.

59. Lundgren E, Terracio L, Mardh S, Borg TK. Extracellular matrix components influence the survival of adult cardiac myocytes in vitro. *Exp Cell Res.* 1985;158(2):371-381.

60. Gwathmey JK, Hajjar RJ, Solaro RJ. Contractile deactivation and uncoupling of crossbridges. Effects of 2,3-butanedione monoxime on mammalian myocardium. *Circ Res.* 1991;69(5):1280-1292.

61. Ostap EM. 2,3-Butanedione monoxime (BDM) as a myosin inhibitor. *J Muscle Res Cell Motil.* 2002;23(4):305-308.

62. Kovacs M, Toth J, Hetenyi C, Malnasi-Csizmadia A, Sellers JR. Mechanism of blebbistatin inhibition of myosin II. *J Biol Chem.* 2004;279(34):35557-35563.

63. Ferreira G, Artigas P, Pizarro G, Brum G. Butanedione monoxime promotes voltage-dependent inactivation of L-type calcium channels in heart. Effects on gating currents. *J Mol Cell Cardiol.* 1997;29(2):777-787.

64. Coulombe A, Lefevre IA, Deroubaix E, Thuringer D, Coraboeuf E. Effect of 2,3-butanedione 2-monoxime on slow inward and transient outward

currents in rat ventricular myocytes. *J Mol Cell Cardiol.* 1990;22(8):921-932.

65. Watanabe Y, Iwamoto T, Matsuoka I, Ohkubo S, Ono T, Watano T, Shigekawa M, Kimura J. Inhibitory effect of 2,3-butanedione monoxime (BDM) on Na(+)/Ca(2+) exchange current in guinea-pig cardiac ventricular myocytes. *Br J Pharmacol.* 2001;132(6):1317-1325.

66. Verrecchia F, Herve JC. Reversible blockade of gap junctional communication by 2,3-butanedione monoxime in rat cardiac myocytes. *Am J Physiol.* 1997;272(3 Pt 1):C875-885.

67. Straight AF, Cheung A, Limouze J, Chen I, Westwood NJ, Sellers JR, Mitchison TJ. Dissecting temporal and spatial control of cytokinesis with a myosin II Inhibitor. *Science.* 2003;299(5613):1743-1747.

68. Fedorov VV, Lozinsky IT, Sosunov EA, Anyukhovsky EP, Rosen MR, Balke CW, Efimov IR. Application of blebbistatin as an excitation-contraction uncoupler for electrophysiologic study of rat and rabbit hearts. *Heart Rhythm.* 2007;4(5):619-626.

69. Dou Y, Arlock P, Arner A. Blebbistatin specifically inhibits actin-myosin interaction in mouse cardiac muscle. *Am J Physiol Cell Physiol.* 2007;293(3):C1148-1153.

70. Bergelson JM, Cunningham JA, Droguett G, Kurt-Jones EA, Krithivas A, Hong JS, Horwitz MS, Crowell RL, Finberg RW. Isolation of a common receptor for Coxsackie B viruses and adenoviruses 2 and 5. *Science.* 1997;275(5304):1320-1323.

71. Gerlach U, Brendel J, Lang HJ, Paulus EF, Weidmann K, Bruggemann A, Busch AE, Suessbrich H, Bleich M, Greger R. Synthesis and activity of novel and selective I(Ks)-channel blockers. *J Med Chem.* 2001;44(23):3831-3837.

72. Cheng J, Kamiya K, Liu W, Tsuji Y, Toyama J, Kodama I. Heterogeneous distribution of the two components of delayed rectifier K+ current: a potential mechanism of the proarrhythmic effects of methanesulfonanilideclass III agents. *Cardiovasc Res.* 1999;43(1):135-147.

73. Olson TM, Alekseev AE, Liu XK, Park S, Zingman LV, Bienengraeber M, Sattiraju S, Ballew JD, Jahangir A, Terzic A. Kv1.5 channelopathy due to KCNA5 loss-of-function mutation causes human atrial fibrillation. *Hum Mol Genet.* 2006;15(14):2185-2191.

74. Yang Y, Li J, Lin X, Yang Y, Hong K, Wang L, Liu J, Li L, Yan D, Liang D, Xiao J, Jin H, Wu J, Zhang Y, Chen YH. Novel KCNA5 loss-of-function mutations responsible for atrial fibrillation. *J Hum Genet.* 2009;54(5):277-283.

75. Gogelein H, Bruggemann A, Gerlach U, Brendel J, Busch AE. Inhibition of IKs channels by HMR 1556. *Naunyn Schmiedebergs Arch Pharmacol.* 2000;362(6):480-488.

76. Watanabe H, Chopra N, Laver D, Hwang HS, Davies SS, Roach DE, Duff HJ, Roden DM, Wilde AA, Knollmann BC. Flecainide prevents

catecholaminergic polymorphic ventricular tachycardia in mice and humans. *Nat Med.* 2009;15(4):380-383.

77. Moss AJ, Zareba W, Schwarz KQ, Rosero S, McNitt S, Robinson JL. Ranolazine shortens repolarization in patients with sustained inward sodium current due to type-3 long-QT syndrome. *J Cardiovasc Electrophysiol.* 2008;19(12):1289-1293.

78. Ramsey BW, Davies J, McElvaney NG, Tullis E, Bell SC, Drevinek P, Griese M, McKone EF, Wainwright CE, Konstan MW, Moss R, Ratjen F, Sermet-Gaudelus I, Rowe SM, Dong Q, Rodriguez S, Yen K, Ordonez C, Elborn JS. A CFTR potentiator in patients with cystic fibrosis and the G551D mutation. *N Engl J Med.* 2011;365(18):1663-1672.

79. Bosch RF, Gaspo R, Busch AE, Lang HJ, Li GR, Nattel S. Effects of the chromanol 293B, a selective blocker of the slow, component of the delayed rectifier K+ current, on repolarization in human and guinea pig ventricular myocytes. *Cardiovasc Res.* 1998;38(2):441-450.

80. Thomas GP, Gerlach U, Antzelevitch C. HMR 1556, a potent and selective blocker of slowly activating delayed rectifier potassium current. *J Cardiovasc Pharmacol.* 2003;41(1):140-147.

81. Gallacher DJ, Van de Water A, van der Linde H, Hermans AN, Lu HR, Towart R, Volders PG. In vivo mechanisms precipitating torsades de pointes in a canine model of drug-induced long-QT1 syndrome. *Cardiovasc Res.* 2007;76(2):247-256.

82. Nakashima H, Gerlach U, Schmidt D, Nattel S. In vivo electrophysiological effects of a selective slow delayed-rectifier potassium channel blocker in anesthetized dogs: potential insights into class III actions. *Cardiovasc Res.* 2004;61(4):705-714.

83. So PP, Hu XD, Backx PH, Puglisi JL, Dorian P. Blockade of IKs by HMR 1556 increases the reverse rate-dependence of refractoriness prolongation by dofetilide in isolated rabbit ventricles. *Br J Pharmacol.* 2006;148(3):255-263.

84. So PP, Backx PH, Dorian P. Slow delayed rectifier K+ current block by HMR 1556 increases dispersion of repolarization and promotes Torsades de Pointes in rabbit ventricles. *Br J Pharmacol.* 2008;155(8):1185-1194.

85. Neyroud N, Tesson F, Denjoy I, Leibovici M, Donger C, Barhanin J, Faure S, Gary F, Coumel P, Petit C, Schwartz K, Guicheney P. A novel mutation in the potassium channel gene KVLQT1 causes the Jervell and Lange-Nielsen cardioauditory syndrome. *Nat Genet.* 1997;15(2):186-189.

86. Tyson J, Tranebjaerg L, Bellman S, Wren C, Taylor JF, Bathen J, Aslaksen B, Sorland SJ, Lund O, Malcolm S, Pembrey M, Bhattacharya S, Bitner-Glindzicz M. IsK and KvLQT1: mutation in either of the two subunits of the slow component of the delayed rectifier potassium channel can cause Jervell and Lange-Nielsen syndrome. *Hum Mol Genet.* 1997;6(12):2179-2185.

87. Schulze-Bahr E, Wang Q, Wedekind H, Haverkamp W, Chen Q, Sun Y, Rubie C, Hordt M, Towbin JA, Borggrefe M, Assmann G, Qu X, Somberg

JC, Breithardt G, Oberti C, Funke H. KCNE1 mutations cause jervell and Lange-Nielsen syndrome. *Nat Genet.* 1997;17(3):267-268.

88. Hartmann R, Gerlach U, Klinke R. Ototoxic side-effects of the I(Ks)-channel blocker HMR1556. *Hear Res.* 2002;172(1-2):145-150.

89. Kregel KC, Zhang HJ. An integrated view of oxidative stress in aging: basic mechanisms, functional effects, and pathological considerations. *Am J Physiol Regul Integr Comp Physiol.* 2007;292(1):R18-36.

90. Annunziato L, Pannaccione A, Cataldi M, Secondo A, Castaldo P, Di Renzo G, Taglialatela M. Modulation of ion channels by reactive oxygen and nitrogen species: a pathophysiological role in brain aging? *Neurobiol Aging.* 2002;23(5):819-834.

91. Lerche C, Seebohm G, Wagner CI, Scherer CR, Dehmelt L, Abitbol I, Gerlach U, Brendel J, Attali B, Busch AE. Molecular impact of MinK on the enantiospecific block of I(Ks) by chromanols. *Br J Pharmacol.* 2000;131(8):1503-1506.

92. Seebohm G, Lerche C, Pusch M, Steinmeyer K, Bruggemann A, Busch AE. A kinetic study on the stereospecific inhibition of KCNQ1 and I(Ks) by the chromanol 293B. *Br J Pharmacol.* 2001;134(8):1647-1654.